

# Along-strike diachroneity in deposition of the Kailas Formation in central southern Tibet: Implications for Indian slab dynamics

Ryan Leary<sup>1\*</sup>, Devon A. Orme<sup>1\*\*</sup>, Andrew Laskowski<sup>1</sup>, Peter G. DeCelles<sup>1</sup>, Paul Kapp<sup>1</sup>, Barbara Carrapa<sup>1</sup>, Matt Dettinger<sup>1</sup>

<sup>1</sup>*Department of Geosciences, University of Arizona, Tucson, AZ 85721*

*\*now at School of Earth Sciences and Environmental Sustainability, Northern Arizona University, Flagstaff, AZ, 86011*

*\*\*now at Department of Geological Sciences, Stanford University, Stanford, CA 94305*

## **ABSTRACT**

The Oligo-Miocene Kailas Formation is exposed along strike for ~1,300 km within the southernmost Lhasa terrane. In this study, we document the sedimentology, structure, and age of this unit exposed between 87° and 90° E. Within this region, the Kailas Formation is composed of continental deposits dominated by conglomerate and sandstone, with lesser volumes of siltstone and paleosols. These rocks were deposited nonconformably on Gangdese Batholith and related volcanic rocks along their northern boundary, whereas to the south, the south-dipping Great Counter Thrust places them in contact with Xigaze Forearc and mélangé units. We interpret the Kailas Formation to have been deposited in alluvial fan and fluvial environments with sediment principally derived from the north. Based on sedimentology and structural relationships, we interpret these rocks to have formed in a north-south extensional setting. New zircon U-Pb ages from volcanic tuffs and flows show that Kailas Formation deposition younged to the east: deposition in western Tibet (81°E) occurred between 26-24 Ma, 25-23 Ma north of Lazi (87.8°E), 23-22 Ma near Dazhuka (89.8°E), and as late as 18 Ma southwest of Lhasa (92°E). Overall, basin development propagated eastward at a rate of ~300 mm/yr. This pattern and rate

of propagation are similar to that of the temporal-spatial distribution of adakitic and ultrapotassic magmatism within the Lhasa terrane to the north, which has been interpreted as a record of slab breakoff. Magmatism lags several million years behind Kailas basin development at most locations. We interpret the Kailas basin to have formed as the result of Indian slab shearing and breakoff, which began in western Tibet around 26 Ma and reached eastern Tibet by ~18 Ma.

## **INTRODUCTION**

The rocks of the India-Asia suture zone preserve a record of processes related to the India-Asia collision and the subsequent evolution of southern Tibet. Much work has focused on the timing and nature of the India-Asia collision (Besse et al., 1984; Garzanti et al., 1987; Leech et al., 2005; Green et al., 2008; Najman et al., 2010; van Hinsbergen et al., 2011; DeCelles et al., 2014; Hu et al., 2015). In contrast, fewer studies have investigated the evolution of this area following initial collision (e.g., Ratschbacher et al., 1994; Wang et al., 2010; DeCelles et al., 2011; Carrapa et al., 2014; Li et al., 2015), and the geodynamics driving this evolution remain enigmatic. In particular, the geodynamic origin of the thick (> 4 km in some localities), continental Kailas Formation, deposited in the center of the largest Cenozoic continent-continent collision zone is still debated (Aitchison et al., 2002; 2007; DeCelles et al., 2011; Li et al., 2015; Wang et al., 2015). However, more significant than the thickness of these deposits is their along-strike continuity: the Kailas Formation is exposed, with some variation in facies, for over 1,300 km in Tibet and has been correlated to rocks within the Indus Group several hundred kilometers farther west (Searle et al., 1990). Although initially thought to represent syn-contractual deposits related to a flexural basin associated with the late stage of India-Asia collision (Aitchison et al., 2007) or deformation related to the Great Counter Thrust (GCT) (Yin et al.,

1999; Wang et al., 2015), recent investigation in western Tibet (~81° E) indicates that these rocks were deposited in an extensional basin, possibly resulting from Indian slab rollback (DeCelles et al., 2011). Precise dating of the Kailas Formation along the entire India-Asia suture zone is critical to understanding the geodynamic drivers of collisional basin formation and can shed light on the along-strike variations in collision zone evolution. In this study, we present the results of field mapping, sedimentology, and stratigraphy, as well as new U-Pb zircon ages from interbedded tuffs and volcanic rocks for the Kailas Formation preserved between 87° and 90° E. We show that deposition of the Kailas Formation began in western Tibet around 26 Ma and became progressively younger to the east, arriving at 90° E by 23 Ma.

## **GEOLOGIC SETTING**

The Tibetan Plateau (Fig. 1) formed through the successive accretion of continental fragments to the southern margin of Asia and the closure of their previously intervening oceanic basins (Allégre et al., 1984; Yin and Harrison, 2000). The southernmost of these continental fragments is the Lhasa Terrane, which collided with Asia during early Cretaceous time (Kapp et al., 2007). The appearance of Asian detritus in Tethyan Himalayan (Indian passive margin) strata beginning at ca. 60 Ma has been interpreted to represent the initiation of India-Asia collision after the Neo-Tethyan ocean basin was completely consumed by northward subduction beneath the Lhasa Terrane (Ding et al., 2005; DeCelles et al., 2014; Orme et al., 2014; Hu et al., 2015). The record of the pre-collisional Asian margin, continental collision, and subsequent evolution of the southern Tibetan Plateau is preserved in four major litho-tectonic zones within southern Tibet, Nepal, and northern India. From north to south, these are the Gangdese magmatic arc, the Xigaze Forearc, the India-Asia suture zone, and the Tethyan Himalayan thrust belt. The

Gangdese magmatic arc formed initially as an Andean style arc produced by northward subduction of the Neo-Tethyan slab beneath the Lhasa Terrane, and it is dominated by calc-alkaline intrusive and volcanic rocks (e.g. He et al., 2007; Ji et al., 2009; Zhu et al., 2011). The arc was most active between ca. 200 Ma and 40 Ma with low volume magmatism continuing as late as 8 Ma (Zhu et al., 2011; Zhang et al., 2014); the highest apparent magmatic flux occurred ca. 52 Ma (Zhu et al., 2011). To the south of the Gangdese arc, the Xigaze Forearc represents the remnants of an originally much wider forearc basin which formed on the southern margin of Asia prior to collision (Einsele et al., 1994; Dürr et al., 1996; Wang et al., 2012; Orme et al., 2014). Sedimentation in the Xigaze Forearc basin began as early as Barremian time and continued until the early Eocene (51 Ma) (Einsele et al., 1994; Dürr, 1996; Ziabrev et al., 2003; Orme et al., 2014; An et al., 2014; Hu et al., 2015a; Huang et al., 2015). South of the forearc basin, the India-Asia suture zone (IASZ on Fig. 1) is defined by of ophiolitic slivers, radiolarian chert, and sedimentary- and serpentinite-matrix mélangé complexes (Cai et al., 2012; Huang et al., 2015; Maffione et al., 2015; An et al., 2015). The ophiolites, where dated, are Jurassic-Early Cretaceous and were accreted onto the southern side of the forearc domain before India-Asia collision (Guilmette, et al., 2009; 2012; Cai et al., 2012). Mélangé complexes formed structurally below ophiolites and have been proposed to represent the accretionary complex and subduction channel associated with Tethyan oceanic subduction (Tapponier et al., 1981; Burg and Chen 1984; Searle et al., 1987; Cai et al., 2012; An et al., 2015). To the south, the Tethyan Himalayan thrust belt is made up of northward dipping thrust sheets of sedimentary rocks originally deposited on the northern Indian passive margin (Ratschbacher et al., 1994). These rocks represent the northernmost extent of Himalayan thrust belt deformation.

The India-Asia suture zone and the Xigaze forearc basin are cut and deformed by a series of north-vergent thrust faults collectively referred to as the Great Counter Thrust system (GCT) (Heim and Gansser, 1939; Ratschbacher et al., 1994; Yin et al., 1994, 1999; Murphy et al., 2010; Sanchez et al., 2010). The GCT is the northern-most fault system in the Tethyan Himalayan thrust belt; movement along this fault began as early as ~25 Ma and continued until ~16 Ma based on structural relationships and thermochronometric ages (Ratschbacher et al., 1994; Harrison et al., 2000; Yin, 2006; Murphy et al., 2010; Sanchez et al., 2010a). In various localities along strike, the GCT places Tethyan Himalayan rocks over suture zone rocks, Xigaze forearc rocks above the Kailas Formation, or ophiolitic and Tethyan rocks over other Cenozoic conglomerates within the suture zone such as the Liuqu Conglomerate. Displacement estimates for the GCT are >38 km in western Tibet (Murphy and Yin, 2003) and between >12 km and 60 km in eastern Tibet (Yin, 2006).

The Kailas Formation is exposed for ~1300 km along strike (Fig 1). To the west, it has been correlated with lithologically similar rocks of the Indus Group in the northwestern Himalaya (Searle et al., 1990; Sinclair and Jaffey, 2001). These rocks have been referred to by numerous local names along strike such as the Kailas Conglomerate (Heim and Gansser, 1939; Gansser, 1964) and the Kailas Formation (Cheng and Xu, 1986; DeCelles et al., 2011) in western Tibet; and the Qiuwu (Wang et al., 2013), Dazhuka (Aitchison et al., 2009), and Luobusa (Yin et al., 1999) Formations in the central segment of the suture zone. Aitchison et al. (2002) grouped all of these units into the Gangrinboche Conglomerate, whereas Li et al. (2015) referred to this group of rocks as the Gangdese Conglomerate. In this study, we use the name “Kailas Formation” (Cheng and Xu, 1986; DeCelles et al., 2011) to refer to the entire east-west extent of these lithologically and structurally similar sedimentary rocks.

## STRUCTURAL SETTING AND SECTION LOCALITIES

For this study, we examined the Kailas Formation in three separate localities (Fig. 2). The westernmost of these, referred to as the “Lazi locality,” is located ~30 km northeast of the town of Lazi (Fig. 3); the central locality, referred as the “Xigaze locality,” is exposed ~20 km northwest of the city of Xigaze (Fig. 4); and the easternmost section, the “Dazhuka locality,” is exposed ~15 km east of the town of Dazhuka in the Yarlung Zangpo gorge (Fig. 2). The structural boundaries of the Kailas Formation are all generally similar. Along its northern boundary, the Kailas Formation was deposited in buttress unconformity on Gangdese arc rocks. To the south, the Kailas Formation is disrupted by folds and faults attributed to the southward dipping Great Counter Thrust system (Fig. 2), which in some places juxtapose Xigaze forearc deposits against the Kailas Formation. At the Dazhuka locality, the southern thrust contact of the Kailas Formation is with the Triassic Renbu mélangé (Cai et al., 2011; Li et al., 2010) (the Bainang Terrane of Aitchison et al. (2000)). Bedding within all Kailas sections studied here dips generally to the south.

The deformation experienced by the Kailas Formation varies considerably along strike. In the Lazi section, most of the section is not folded, although a few, ~30 m wavelength recumbent folds are present. In the upper (southern) portion of the Lazi section, a ~100 m thick, vertical to south-dipping ductile shear zone cuts through the Kailas Formation. Granitic cobbles deformed as sigma and delta clasts within this zone indicate top-to-the-north sense of shear (Fig. 3).

At the Xigaze locality, the Kailas Formation is extensively deformed. Folds are slightly north vergent and have wavelengths of 100-500 m (Fig. 5); ~500 m wavelength isoclinal folds are present in some places. This deformation, in addition to faulting between and within individual

members of the Kailas Formation, makes stratigraphic correlation difficult over distances of <1 km.

The Dazhuka section is only slightly deformed. This section dips 40° south and contains a ~100 m wide footwall syncline below a south dipping thrust contact with Triassic *mélange* rocks (Cai et al., 2011).

## **SEDIMENTOLOGY**

The depositional environment of the Kailas Formation was documented through facies analysis of ~3200 m of measured stratigraphic section at three localities (Figs. 6-9). In the following we use the facies classification scheme after Miall (1978) (Table 1). Paleocurrent directions were determined by measurement of clast imbrications ( $\geq 10$  individual measurements per site) and analyses of trough-cross bedded sandstones (method I in DeCelles et al., 1983).

The Kailas Formation in western Tibet has been divided into four major lithologic divisions: a lower conglomeratic interval, a fluvial sandstone interval, a fine-grained lacustrine interval, and an upper conglomeratic red-bed interval (DeCelles et al., 2011). This general stratigraphy is not maintained in the field areas of this study. This along strike variation could have arisen because of poor preservation in the current study area or could be due to differing basin and depositional conditions along strike. Here we examine the sedimentology of each major locality individually, from west to east.

### **Lazi Locality**

At the Lazi locality (figs. 2, 6, and 7), the Kailas Formation is ~1000 m thick. This section is divided into three different lithologic members: a basal conglomerate, a middle sandstone

member, and an upper conglomerate. The basal conglomerate (section 1KS) was deposited nonconformably on Gangdese arc granite and is approximately 690 m thick. The lower ~400 m of this section is characterized by massive, matrix-supported cobble to boulder conglomerates (Gmm) and massive, clast-supported pebble to cobble conglomerate (Gcm). Above the 400 m level, these facies transition into horizontally stratified, clast-supported (Gch) and imbricated (Gci) conglomerates (Fig. 10B). In the upper portion of this member, horizontally stratified, clast-supported cobble conglomerates (Gch) are interbedded with massive and horizontally stratified sandstones (Sm and Sh) and fine-grained intervals; fine-grained intervals consist primarily of horizontally laminated siltstone (Fsh) and paleosols (Fp). Conglomerate beds in this member range from ~1 to ~12 m thick with an average thickness of ~8 m. Clast-supported conglomerates typically show erosion and channelization at their bases. Paleocurrent directions within the lower member are dominantly northward (Fig. 6).

The middle member at this location (1KS and 2KS) is >120 m thick and is dominated by thinly bedded (< 10 cm) laterally extensive horizontally stratified sandstone (Sh) beds separated by horizontally laminated red siltstone (Fsl). Sandstone beds generally show fining upward trends. Trough-cross bedded (St) and horizontally stratified (Sh) sandstone beds between 1 and 5 m thick are also occasionally present. Sparse clast-supported, horizontally stratified conglomerate beds are present, and one thick (~15 m) trough cross-stratified sandstone (St) showing numerous lateral accretion elements was documented (Fig. 10A). Paleocurrent measurements from this sandstone unit are southward and are perpendicular to the dip of the accretion elements.

The upper conglomeratic member is ~210 m thick. It consists of 1-6 m thick clast-supported, horizontally stratified pebble conglomerates (Gch) interbedded with red paleosols (Fp) and red

horizontally laminated siltstones (Fig. 10C). Minor volumes of trough cross-stratified (St) and horizontally stratified (Sh) sandstone are also present. The bases of most conglomeratic intervals are scoured and channelized. Paleocurrent indicators from this section show eastward sediment transport (Figs. 6 and 7). One tuffaceous bed containing volcanic ash, biotite grains, and reworked sand is present in the upper portion of this member. Dating of this layer provides the best constraint on the age of this section (see below).

The dominance of Gmm facies at the base of the lower member suggests deposition by sediment-gravity flows in the proximal portion of an alluvial fan (Shultz, 1984; Blair and McPherson, 1994; Singh et al., 2001). The facies association within the upper portion of this member (Gch, Gcm, Sh, St, Fsl, Fp) suggests deposition by fluvial processes in a more distal alluvial fan setting (Rust, 1977; Allen, 1981; Ridgway and DeCelles, 1993). The shift in lithofacies and likely environment of deposition most likely reflects initial rapid deposition adjacent to high relief topography, followed by slower, more distal deposition as initial topography was denuded and the basin filled in.

The facies within in the middle member of the Kailas Formation at this location suggest deposition in a fluvial setting. Thick, trough cross-stratified sandstone (St) bodies represent deposition by strong, unidirectional currents in major channels (Ashley, 1990; Ashworth et al., 2011); lateral accretion elements in one of these bodies that dip perpendicular to measured paleocurrent indicators suggest that channels in this interval were of moderate to high sinuosity (Miall, 1985; Miall and Turner-Peterson, 1989). Fine-grained intervals within this member likely represent floodplain and overbank deposits, whereas thin, tabular sandstone bodies are interpreted as crevasse splay deposits (Miall, 1985; Smith et al., 1989; Bristow et al., 1999).

We interpret the coarse, channelized conglomerate beds (Gch) in the upper member to represent fluvial channels on a stream dominated alluvial fan (Rust, 1977; Allen, 1981; Ori, 1982; Nemeč and Steel, 1988; Ridgway and DeCelles, 1993). Horizontally stratified sandstone (Sh) intervals within this member likely represent deposition in upper flow-regime conditions during floods (Cant and Walker, 1976; Allen, 1981). Paleosols most likely represent weathering in the interfluvial regions of the fan, whereas laminated siltstone (Fsl) likely represents suspension settling in marshy overbank environments (Allen, 1981; Evans, 1991).

### **Xigaze Locality**

The Kailas Formation at the Xigaze locality is structurally disrupted by folds and faults making correlation of members and interpretation of stratigraphic position difficult (Fig. 5; Wang et al., 2013). In this study, we follow the stratigraphic divisions of Wang et al. (2013) who divided the Kailas Formation into two formations: the Qiuwu Formation (lower) and the Dazhuka Formation (upper). The Qiuwu Formation is ~400 m thick and is made up of sandstone, coal, and carbonaceous shale (Wang et al., 2013). Based on sedimentology and paleocurrents, Wang et al. (2013) interpreted this to represent a lacustrine depositional environment that drained southward away from rocks of the Gangdese Batholith.

Because the Qiuwu Formation is poorly exposed over a very limited area, we focus here on the Dazhuka Formation. The Dazhuka Formation is divided into the Jiangqingze (lower), Deri (middle), and Tunqiong Members (upper). The Jiangqingze Member (Fig 8) is 685 m thick and is exposed in a series of east plunging folds (Fig. 5). It is dominated by thick (~10 m) horizontally stratified sandstone (Sh) bodies separated by red, bioturbated paleosols (Fp) and red laminated siltstones (Fsl). Many of these sandstone bodies have scoured bases. Trough cross-

stratified sandstones (St) are also present, although they make up only a small volume of this member. Thinner (< 1 m thick), horizontally stratified upward fining sandstone beds are commonly interbedded with fine-grained intervals.

The Deri Member is up to 1800 m thick (Wang et al., 2013), although numerous thrust faults within this section make this a maximum estimate. We documented part of the Deri Member by measuring 440 m of un-faulted strata along the north limb of an east-plunging, ~500 m wavelength anticline. This section is dominated by thick (10-20 m) clast-supported horizontally stratified (Gch) and imbricated (Gchi) pebble-cobble conglomerates (Fig. 10E). Clasts are well-rounded and well-sorted. These beds are separated by trough cross-stratified (St) and horizontally stratified (Sh) sandstones and sparse paleosols (Fp).

The entire Tunqiong Member where it was measured for this study is 185 m thick and exposed in an east-plunging, ~400 m wide syncline structurally beneath the GCT. Wang et al. (2013) reported that this member is as thick as 750 m to the east. This member is dominated by thinly bedded rippled sandstone (Sr) interbedded with red paleosols (Fp) and sparse laminated siltstone (Fsl). The thinnest of these sandstone beds are often laterally discontinuous, whereas thicker intervals are laterally extensive over several hundred meters. Paleosols are bioturbated, rooted, and contain sparse carbonate nodules; 5-10 m thick rippled sandstone bodies are present in the upper portion of this section, and two ~2 m thick clast-supported massive pebble conglomerates (Gch) are present in the upper portion of this member.

We interpret the lithofacies assemblage of the Jiangqingze Member as representing deposition in a fluvial system. Thick (5- 10 m) horizontally stratified (Sh) and trough cross-stratified (St) sandstone bodies with erosional bases are interpreted to have been deposited by strong, unidirectional currents within fluvial channels (Cant and Walker, 1978; Bridge and Lunt,

2006; Ashworth et al., 2011). Paleosols (Fp), massive siltstone (Fsm), and laminated siltstone (Fsl) are interpreted as overbank deposits. Thin (<1 m), fining upward sandstone beds are interpreted to have been deposited within crevasse splays during splay abandonment (Miall, 1985; Smith et al., 1989; Bristow et al., 1999). This overall interpretation is consistent with that of Wang et al. (2013).

Also consistent with the conclusions of Wang et al. (2013), we interpret the lithofacies preserved in the Deri Member as representing a high-energy fluvial system. Clast-supported horizontally stratified (Gch) and imbricated conglomerates (Gchi) likely represent deposition by gravel bars within main channels (Rust, 1977; Allen, 1981; Wooldridge and Hickin, 2005). Trough cross-stratified sandstones (St) are interpreted as deposits of subaqueous dune forms in sandy channels (Rust, 1977; Ashley, 1990; Bridge and Lunt, 2006; Ashworth et al., 2011). Sparse fine-grained material is interpreted as overbank deposits.

The lithofacies assemblage of the Tunqiong Member is interpreted to represent distal overbank deposits of a fluvial system. Tabular, laterally continuous rippled sandstone beds are interpreted as crevasse splay deposits formed during avulsion events (Miall, 1985; Smith et al., 1989; Bristow et al., 1999). Rippled, lenticular sandstone bodies are interpreted as the toes of crevasse splays and levees (Allen, 1964; Bristow et al., 1999). Abundant red paleosols are interpreted to have developed on exposed overbank areas between major floods (Allen, 1964; Miall, 1985). This assemblage of geomorphic elements (paleosols, crevasse splays, levees) is typical of fluvial floodplain environments, rather than alluvial fans (as suggested by Wang et al., 2013).

## **Dazhuka Locality**

The Kailas Formation exposed at the Dazhuka locality was previously referred to locally as the Dazhuka Conglomerate (Aitchison et al., 2007). This section includes ~740 m of strata, which we divide into informal upper and lower members (Fig. 9). The lower member rests nonconformably on Gangdese granite, although the contact is covered by Quaternary colluvium.

The lower member at this location is composed almost entirely of massive, disorganized, and poorly sorted clast-supported boulder conglomerate (Gcm) (Fig. 10F). Beds range in thickness between 1 and 25 m, and largest clast sizes are up to 3 m in diameter. The matrix is primarily poorly sorted sandstone. Clasts range from subangular to subrounded with more resistant lithologies such as volcanic rocks making up the bulk of the subangular clasts, and less resistant lithologies such as limestone and marble forming the more rounded clasts. Some beds are inversely graded. Several porphyritic trachy-andesite flows containing abundant subangular to rounded clasts of varying lithologies (Gma) are preserved in this section (Fig. 10G). Very little fine-grained material is preserved in this section; however, several weakly developed paleosols (Fp) were observed.

The upper member is finer-grained and dominated by horizontally stratified sandstone (Sh) in beds ranging in thickness from 10 cm to 10 m; typical bed thickness is ~1-2 m. Many of these sandstones are interbedded with ~10 cm thick intervals of massive, clast-clast-supported granule to pebble conglomerate. Massive, clast-supported pebble to cobble conglomerate (Gcm) is also preserved in occasional 1-10 m thick beds. This member lacks siltstone and paleosol intervals.

We interpret the abundance of massive, clast-supported (Gcm) intervals within the lower member as representing deposition by hyperconcentrated flood-flows (e.g. Smith, 1986) or high density traction carpets (e.g. Todd, 1989) in a proximal alluvial fan. Sparse massive or coarsening upward, matrix-supported conglomerates (Gmm) are interpreted as typical high

viscosity debris flow deposits (Pierson, 1980; Shultz, 1984). Trachy-Andesite flows (Gma) are interpreted to represent deposits of pyroclastic density currents from Gangdese volcanic centers that incorporated accidental clasts while travelling across the alluvial landscape (e.g. Bryan et al., 1998). The presence of these deposits, the coarseness of this member, and the dominance of volcanic clasts all indicate that this locality was proximal to the active Gangdese arc at the time of deposition.

The upper member is interpreted to represent deposition in the medial to distal portions of an alluvial fan system. Horizontally stratified sandstone (Sh) is interpreted to represent upper flow regime conditions during sheet floods (Bull, 1972; Blair and McPherson, 1994; Blair, 2000), and the clast-supported conglomerates (Gcm) are interpreted to represent basal sheetflood deposits (Blair and McPherson, 1994; Blair, 2000) or hyperconcentrated flow deposits (Smith, 1986) because of their poorly organized structure.

## **CHRONOSTRATIGRAPHIC CONTROL**

U-Pb geochronology provides chronostratigraphic control for the Kailas Formation. Samples were collected from one tuff, a trachy-andesite flow, and seven medium- to coarse-grained sandstone beds. Zircon crystals were extracted following standard methods of crushing, panning, magnetic separation with a Frantz machine, and heavy liquids. Grains were then mounted in epoxy pucks and analyzed at the University of Arizona LaserChron Center. All samples from section 1KS were analyzed on an Element single collector mass spectrometer, whereas all other samples were analyzed using a Nu laser-ablation multicollector inductively coupled plasma-mass spectrometer following the methods of Gehrels et al. (2006, 2008) and Gehrels and Pecha (2014).

At the Lazi locality, a detritally contaminated tuff from the upper portion of section 3KS (3KS-105) provides tight constraint on the age of the Kailas Formation (Fig. 11). Although this sample contained significant numbers of older detrital grains, the youngest population of grains at  $22.8 \pm 0.3$  Ma (n=43) provides an age that is likely very close to the eruptive age of the tuffaceous material and the depositional age of this sample. Additional samples from the Lazi section (1KS-408, 1KS-754, 2KS-188) each contain one young grain between 21 and 23 Ma; the youngest statistically significant population is ~50 Ma in each of these samples and does not provide a useful maximum depositional age. There are no unconformities or major faults within the Lazi section, which rules out the possibility of a ~50 Ma basal section and a much younger upper section. These ages are comparable to the results of Li et al. (2015) whose U-Pb detrital zircon data yield maximum depositional ages of 21 Ma (basal Kailas Formation) and 15 Ma (Upper Kailas Formation) from a section 20 km to the west.

Samples from the Xigaze section (1XK-10, 1XK-313, 2XK-47) contained no syn-depositional age grains. 1XK-10 contained two ~32 Ma grains with the youngest statistically significant population at 50 Ma (Fig. 11). Samples 1XK-313 and 2XK-47 contained single youngest grains at 32 Ma and 29 Ma, respectively; again, both of these samples had youngest statistically significant populations at 50 Ma. These results are consistent with the analyses of Wang et al. (2013) who report a single 31 Ma grain at the base of this section as well as palynology results suggesting that the Qiuwu Formation (stratigraphically below 1XK) was deposited during Late Oligocene time (Li et al., 2004).

In the lower portion of Dazhuka locality, zircons from a trachy-andesite flow yielded a U-Pb age of  $22.9 \pm 0.3$  Ma (n=64) (1DK-246) (Fig. 11). This age is consistent with the  $^{40}\text{Ar}/^{39}\text{Ar}$

(biotite and plagioclase) ages between  $22.3 \pm 0.7$  Ma and  $19.5 \pm 0.2$  Ma reported by Aitchison et al. (2009) from a felsic tuff in this section.

Although ages for the Kailas Formation in this study are very similar, it is important to note that the age of the lower portion of section 1DK is nearly the same age as the upper portion of section 3KS, exposed to the west. This indicates that the Kailas Formation may be slightly younger in the eastern area of this study (see below). However, it must be acknowledged that the sections considered here are all partial sections, so remains possible that they represent different parts of the Kailas Formation.

## **PROVENANCE**

### **Conglomerate Clast Composition**

Clast composition of the Kailas Formation was determined primarily by clast counts at 15 sites covering the complete geographic and stratigraphic extent of this study. At each station, at least 100 clasts were identified.

At the Lazi locality (sections 1-4KS; Fig. 12), clasts at the base of the lower member are dominated by granite with 15% volcanic clasts. The middle portion of the lower member contains nearly equal portions of granite and volcanic clasts with sparse sedimentary clasts; in the upper portion of the lower member, clasts are almost entirely volcanic. The upper member is composed entirely of volcanic clasts.

The Kailas Formation north of Xigaze (sections 1-2XK, 1YZ. Fig. 8) is far more compositionally diverse than the other sections examined in this study and includes abundant chert, sandstone, and volcanic clasts, with minor amounts of granite and siltstone. There are no significant up-section changes in clast type at this location.

At the Dazhuka locality (section 1DK, Fig. 9), the lower member is dominated by granite and volcanic clasts; chert, limestone, basalt, and sandstone are present in minor volumes. The upper member contains ~30% volcanic clasts. Chert and lithic sandstone are found in secondary amounts whereas quartzite, white sandstone, serpentinized material, and granite are found in trace amounts.

### **Modal Sandstone Petrography**

Modal framework-grain compositions of six representative sandstone samples were determined by point-counting 450 grains per thin section following a modified Gazzi-Dickinson method (Ingersoll, et al., 1984) to corroborate the clast compositional data. Standard petrographic slides were stained for Ca-plagioclase and K-feldspar to aid in their identification. Specific composition percentages are presented in the supplemental data.

Quartzose grains include monocrystalline (Qm), polycrystalline (Qp), and tectonized polycrystalline (Qpt) varieties and chert (Qch). Feldspars are primarily albite with trace amounts of K-feldspar. Lithic volcanic grains include felsic, vitric, and lathwork/trachytic (Lvf, Lvv, Lvl) types and rare mafic grains containing pyroxene and altered mafic minerals. Most volcanic grains are heavily sericitized. Sedimentary lithic grains include phyllite (Lph) and siltstone (Lsilt). Accessory minerals include muscovite, pyroxene, and serpentinite. Cement is most commonly calcium carbonate with abundant sericite alteration. Plotted in ternary diagrams (Fig. 12), Kailas Formation sandstones lie between the Transitional Arc and Dissected Arc fields of Dickinson (1985).

### **Detrital Zircon Ages**

Detrital zircon age spectra differ significantly between localities (Fig. 11). At the Lazi locality, nearly all grains are younger than 100 Ma, with only a single grain older than 200 Ma. At the Dazhuka locality, all grains except for one are < 100 Ma. Samples from both of these locations contain large peaks at 50 Ma with minor peaks at 90 Ma. Two samples contain large, near depositional age peaks at 23 Ma from tuffs or volcanic flows as mentioned above. In contrast, samples from the Xigaze locality contain large peaks around 50 Ma and 90 Ma minor peaks at 190 Ma and 360 Ma and scattered single grains between 500 and 3200 Ma.

In western Tibet (~82° E), detrital zircon spectra show peaks at 23 Ma, 50 Ma, and 90 Ma, with grains older than 100 Ma making up as much as 30% of each sample (DeCelles et al., 2011; Li et al., 2015). In this study, samples from the Lazi and Dazhuka localities contained < 4% scattered, single grains older than 100 Ma. In samples from the Xigaze locality, these grains make up ~15% of total grains. Farther east, samples from the Kailas Formation (Luobusha Conglomerate) yield a few grains at 23 Ma and high amplitude peaks at 50 Ma and 90 Ma (Li et al., 2015). Grains >100 Ma make up between 15% and 30% of these samples.

Kailas Formation U-Pb detrital zircon age spectra share major similarities to Gangdese pluton ages (Fig. 11). The southern Gangdese arc experienced four primary magmatic stages around 13-33 Ma, 45-55 Ma (the most voluminous), 80-100 Ma, and 170-190 Ma (Ji, et al., 2009, 2014; Zhu et al., 2011). The youngest documented intrusive rocks in the Lhasa terrane are 8-9 Ma (Kapp et al., 2005; Sundell et al., 2013).

### **Provenance Interpretation**

Provenance data from the Lazi locality are consistent with the sedimentology in suggesting deposition proximal to the sediment source. Abundant granite clasts at the base of the section

were likely derived from nearby Gangdese granites. Higher in the section, clasts are entirely volcanic suggesting either a change in catchment to a more volcanic rich source area or that granites in the catchment(s) of this depositional system were buried by volcanic rocks during Kailas deposition. Detrital zircon U-Pb data are consistent with this provenance interpretation; large populations at 50 Ma reflect erosion and recycling of material from Gangdese granite, and the presence of ~23 Ma grains (including the dated tuff) suggest input via airfall from active Gangdese volcanic centers to the north. Generally north directed paleocurrents in the lower member of the Kailas Formation at this site contrast with the dominantly southward indicators found elsewhere along strike (DeCelles et al., 2011; Wang et al., 2013). We interpret northward flow in this member to indicate that this portion of the Kailas Formation was deposited in a small, north facing catchment that fed a larger, south directed sediment transport system. Although no granitic rocks are currently exposed south of this locality, a localized granitic upland may have existed south of the Lazi locality during initial Kailas Basin subsidence; in this scenario, that upland would have been subsequently eroded or structurally buried. Alternatively, it is possible that the measured clast imbrications could represent apparent imbrications formed as armor on gravel bar flanks, rendering them meaningless as paleocurrent indicators. South and east directed paleocurrent indicators in the middle and upper members at this location, as well as more distal fluvial and alluvial facies, indicate that deposition at this site was integrated into a larger southward or perhaps axial drainage system. However, despite this possibility, the source for Kailas sediment at this location remained monolithologic.

Clast count data from the Xigaze section show much greater compositional variety within the Kailas Formation, and detrital zircon age spectra show a much larger range of U-Pb ages. The abundance of lithologies exposed primarily south of the India-Asia suture zone such as chert,

quartzite, and white sandstone suggest that sediment was being derived from the south. However, the presence of volcanic and granitic clasts suggests a northern, Gangdese source as well. A similar pattern is observed in the detrital zircon data where minor age peaks at 29 and 34 Ma, as well as major peaks around 50 and 90 Ma, suggest a Gangdese source; minor peaks at 190 and 360 Ma and scattered older ages may suggest a southern source in the accretionary mélangé or Tethyan Himalaya. However, these samples contain very few 130 Ma grains, which are abundant in mélangé rocks, and we interpret this low abundance of 130 Ma zircon grains to be the result of dilution by more zircon-rich Gangdese sources to the north. We suggest that this locality was integrated into the larger Kailas Formation depositional system which would have included axial transport and sediment input from both sides of the India-Asia suture zone (Wang et al., 2013). The predominance of fluvial facies at this location is consistent with this interpretation as are south-southeast (this study) and west-northwest (Wang et al., 2013) paleocurrent indicators. It is worth noting, however, that deformation in this location is strong, making it impossible to rule out vertical axis rotation of measured beds, and paleocurrent indicators from this section should be interpreted cautiously.

Abundant granite and volcanic clasts in the lower member of the Dazhuka locality show similar composition to those in the Lazi locality. The limited range of clast compositions, detrital zircon age peaks at 23 and 50 Ma, and proximal alluvial fan facies are interpreted to represent deposition in a small catchment near the sediment source. The upper member of this section however, shows clast compositions that are very similar to those found at the Xigaze location. We interpret this as the integration of a spatially confined alluvial fan system (lower member) into a larger alluvial/fluvial system with a much larger catchment that supplied some sediment

(chert, lithic sandstone, and quartzite) to the studied location. Distal alluvial/ fluvial facies in the upper member are consistent with this interpretation.

## **DISCUSSION**

### **Mechanism of subsidence and basin formation**

The basin type and mechanism of subsidence that accommodated Kailas Formation deposition is debated. Yin et al. (1999), Aitchison et al. (2002, 2009), and Davis et al. (2004) interpreted the unit to represent deposition in a contractional setting associated with uplift of rocks in the GCT hanging wall. Wang et al. (2015) interpreted the Kailas Formation as having been deposited in a flexural foreland basin formed by loading by the GCT. DeCelles et al. (2011) and Wang et al. (2013) interpreted the Kailas Basin to have formed in an extensional setting associated with rollback of the subducted Indian continental slab. Determining whether the Kailas Basin was extensional or contractional is key to a correct interpretation of the tectonic significance of the basin.

The Kailas Formation exposures examined in this study are not as stratigraphically complete, regionally extensive, or structurally intact as those in western Tibet (~81° E), from which the extensional basin interpretation was originally drawn. However, several important structural and stratigraphic features within the rocks examined for this study point to a similar extensional origin for this portion of the Kailas Formation.

Along the entirety of its ~1300 km strike, the northern boundary of the Kailas Formation is nonconformable on Gangdese granite. The only deformation associated with this contact is southward tilting. Paleocurrent indicators, clast counts, and sandstone petrography indicate that the majority of the Kailas Formation was derived from the Gangdese magmatic complex

(including both granitic and volcanic rocks) located to the north, although there is some local variation (e.g. the Lazi locality). This structural and stratigraphic geometry is not typical of syn-contractional conglomerates, which are typified by clast types different than the depositional substrate and often contain growth strata that fan away from the thrust belt (Anadon et al., 1986; Verges et al., 2002). Additionally, syn-contractional deposits (wedge-top deposits) are often typified by strata that coarsen upwards as crustal shortening closes the distance between hinterland and depositional center (DeCelles and Giles, 1996). The Kailas Formation is arranged in a 'very coarse-grained → fine-grained → coarse-grained' stratigraphic arrangement more typical of extensional basins (Schlische, 1992; DeCelles et al., 2011). Although the Xigaze locality does not exhibit this stratigraphic arrangement, the facies progression at this location is still atypical of convergent deposits and can be explained by local variation along strike or differing preservation along strike. It is also likely that the Xigaze section is equivalent only to the upper part of the Kailas Formation, based on its composition.

Large (>1km) scale growth-strata within the Kailas formation were documented by Wang et al. (2015). Wang et al. (2015) interpreted these as a result north-vergent contractional structures; however, the southward fanning stratal geometry is not consistent with structural growth to the south of the Kailas basin as envisioned by Wang et al. (2015). Instead, these growth strata are better interpreted as the result of southward increasing accommodation space in an asymmetric half graben with the main fault dipping northward along the south flank of the basin (Fig. 13). Although minor extensional features can be found in overall convergent settings, kilometer scale growth strata such as those pictured by Wang et al. (2015) (Fig. 13) indicate an extensional origin (Leeder and Gawthorpe, 1987; Schlische and Olsen, 1990; Schlische, 1992; Coogan and DeCelles, 1996; Shaw et al., 1997), and the geometries observed are atypical of growth strata

formed in contractional settings (see Anadon et al., 1986; DeCelles et al., 1987, 1991; Lawton et al., 1999; and Verges et al., 2002 for examples of contractional growth strata).

One perplexing aspect of an extensional origin for the Kailas Formation is the lack of preserved normal faults. Although some authors have interpreted this to preclude an extensional origin for the basin (Wang et al., 2015), we argue that the fault or faults bounding the basin to the south have been tectonically buried by the GCT hanging wall, which was emplaced after Kailas Formation deposition (Fig. 13). In the current study area, the north-south extent of Kailas Formation exposure is no more than 2 km, and only the northernmost portion of the basin is exposed. As such, the normal fault(s) that controlled Kailas Basin subsidence are not expected to be preserved at the surface. In western Tibet, the preserved Kailas Formation is ~10 km wide. Based on proximal facies near the southern outcrop boundary such as boulder conglomerates and Gilbert deltas, the southern basin margin is interpreted to have been within several kilometers of the southern exposure boundary (DeCelles et al., 2016). However, as in central Tibet, that boundary is buried by the GCT hanging wall, and the basin bounding normal fault(s) are not directly observed.

In addition to stratigraphic architecture and growth strata, there are several other features of the Kailas Formation that preclude deposition within a contractional or foredeep setting as suggested by Wang et al. (2015).

Wang et al. (2015) argue that Gangdese belt, which sits ~700 m higher than the Tibetan Plateau to the north, is a flexural forebulge. In this model, the Kailas Formation represents the foredeep to this system. However, the topographic amplitude of a flexural forebulge is typically an order of magnitude less than the depth of the foredeep basin (Beaumont, 1981; DeCelles and Giles, 1996; Allen and Allen, 2006). In order for the proposed Gangdese “flexural forebulge” to

have an amplitude of ~700 m, the Kailas Basin would have been up to 11 km deep and at least 80 km wide (Wang et al., 2015; Fig. 4), yet the thickest accumulation of Kailas Formation strata is only ~4 km (DeCelles et al., 2011; Wang et al., 2013). Both margins of the Kailas basin are well documented by the presence of very coarse boulder conglomerates that could not have been transported more than a few kilometers (DeCelles et al., 2011; 2016). Where these margins are documented, the basin could not have been more than ~15 km in north-south width, far less than the >80 km wide Kailas basin required by the model of Wang et al., (2015).

Wang et al. (2015) interpret 23.4 Ma to 16.4 Ma apatite fission track ages from the Gangdese arc to indicate a pulse of rapid exhumation related to forebulge uplift. Assuming a geothermal gradient of 30°C/km (Carrapa et al., 2014), these ages require at least several kilometers of exhumation to have taken place in the Gangdese arc as a result of forebulge uplift. Although this magnitude of erosion is hypothetically possible for a large forebulge, erosion associated with the development and migration of forebulges is typically very slow, ranging from 0.01 to 0.1 mm/yr (Crampton and Allen, 1995; Sinclair, 1997). These rates are far too slow to result in several kilometers of exhumation over the ~5 million year duration of proposed flexural activity (Wang et al., 2015).

### **Burial History of the Kailas Formation**

Numerous lines of evidence support the conclusion that the processes driving subsidence and sedimentation for the Kailas Formation were similar along strike; however, there is good evidence that these rocks experienced very different burial and exhumation histories subsequent to deposition. First, the physical deformation state of these rocks changes significantly along strike: in the Mt. Kailas region, the Kailas Formation is only mildly deformed by brittle faults

along its southern margin (DeCelles et al., 2011); the same is true of the Kailas Formation for as much as 500 km east of Mt Kailas and for rocks at the Dazhuka locality. However, Kailas Formation rocks in the center of the current study area depart from this trend. North of Xigaze, the Kailas Formation is folded into tight, occasionally isoclinal, folds; at the Lazi locality the southern edge of the Kailas Formation is bounded by a ductile shear zone (Figs. 3 and 10).

Similar along-strike heterogeneities are observed in the temperature histories of Kailas Formation rocks. In the Mt. Kailas region, zircon (U-Th)/He ages are a mix of reset and unreset, indicating that burial temperatures were between 120-230°C (Carrapa et al., 2014); zircon (U-Th)/He ages from the Kailas Formation exposed near Sangsang (“Geydo section” in Carrapa et al., 2014) are unreset, indicating that burial temperatures did not exceed 200-230 °C. However, in exposures north of Saga (east of the Lopukangri Range), zircon (U-Th)/He ages are reset indicating that burial temperatures exceeded 200-230 °C. Although no thermochronometric data exist for the current study area, rough temperature constraints can be supplied by the ductile behavior of granitic clasts within the mylonitic shear zone which truncates the southern Kailas exposure at the Lazi locality. In typical continental crust, the brittle-ductile transition occurs at temperatures of roughly 300-400°C (Tullis and Yund, 1977).

The majority of post depositional burial experienced by the Kailas Formation was likely driven by northward movement along the GCT. The wide discrepancies in physical deformation and temperature history along strike suggest that the amount of tectonic and/or depositional burial varied significantly along strike and suggest that displacement along the GCT and/or thickness of the hanging wall was highly variable, or that slip was partitioned differently along the India-Asia suture zone.

## **Implications for slab dynamics**

Based on comparisons with other continental rift basins, it is likely that the formation of the Kailas Basin resulted from modest (<5-10 km) horizontal extension (Morely, 1988; Ebinger, 1989; Schlische and Olsen, 1990; Schlische, 1992). Extension of this magnitude can be produced by a variety of local factors in a variety of tectonic settings. Although the magnitude of Kailas extension does not alone demand a plate-scale driving mechanism, the formation of this basin over ~1300 km suggests that subsidence was driven by plate scale processes.

Formation of the Kailas basin was attributed by DeCelles et al. (2011) to rollback of the subducted Indian slab based on several lines of evidence: 1) the along strike continuity of the Kailas Formation suggests that the mechanism driving subsidence must have been regional in scale; 2) spatio-temporal analysis of magmatic patterns north of the India-Asia suture zone reveals a 600 km southward sweep in magmatism between 32 and 25 Ma (for western Tibet), a pattern similar to slab rollback processes documented elsewhere (e.g., Humphreys, 1995); 3) a pulse of adakitic and high-K magmatism across the Lhasa terrane at 25-20 Ma suggests slab breakoff (e.g. Maheo et al., 2002; Chung et al., 2003; Williams et al., 2004; Gao et al., 2007; Zhang et al., 2014); 4) tomographic studies interpret large, high-velocity zones in the mantle beneath Tibet as representing two separate, foundered slabs, one related to initial collision, a second potentially linked to Oligo-Miocene rollback followed by slab break-off (e.g. Replumaz et al., 2010a; 2014).

Slab rollback processes beneath Tibet must be distinguished from oceanic slab rollback documented in the Mediterranean region (e.g. Jolivet and Brun, 2010; Jolivet et al., 2013) and continental slab rollback proposed to explain anomalous subsidence in the Alpine foreland basin

(Schlunegger and Kissling, 2015). In these cases, slab rollback refers to movement of a slab through the mantle opposite the direction of subduction.

In contrast, the mantle anomalies interpreted as the remnants of Oligo-Miocene breakoff in southern Tibet are currently located ~800 km south of the India-Asia suture zone (Replumaz et al., 2010a; 2014). This indicates that unlike subduction zones in the eastern Mediterranean, the India-Asia subduction zone has experienced overall trench advance relative to the mantle. As such, slab processes within the India-Asia system should be viewed as subducted slabs anchored in the mantle being ‘peeled’ or ‘sheared’ southward and broken off as both India and Asia moved northward relative to the mantle (van der Meer et al., 2010; Doubrovine et al., 2012; GPlate reconstructions by Douwe van Hinsbergen, <http://www.geologist.nl/>). The implication of this is that slab ‘shearing’ would not necessarily alter the net post collision north-south contractional regime within Tibet, and slab shearing would not be expected to produce a large (>100 km) zone of extension behind the shearing slab as is observed in traditional slab rollback systems (Wortel and Spakman, 2000; Brun and Faccenna, 2008; Jolivet et al., 2013). However, we propose that just prior to final slab breakoff, the shearing Indian slab would have caused a short-lived episode of trench retreat as the slab exerted a downward and southward pull on the unsubducted Indian continent (Fig 15). This episode would have lasted no more than a few million years but could have resulted in enough extension in southern Tibet to drive Kailas Basin subsidence. After slab breakoff, the trench would have returned to an advancing state, and an overall contractional deformation regime would have been re-established within the India-Asia suture zone.

If the subsidence that accommodated Kailas Formation sedimentation was driven by Indian slab rollback and breakoff, the timing of Kailas Formation deposition should provide an independent record of where and when this process occurred. Data presented in this study show

that Kailas Formation sedimentation in western Tibet is several million years older than in central Tibet (Fig 14A): the Kailas Formation was deposited between ~26 and ~23 Ma in the Mt. Kailas region (DeCelles et al., 2011; Li et al., 2015); the lower member of the Kailas Formation was deposited at ~24 Ma in the Yagra Valley (Carrapa et al., 2014); the upper member of the Kailas Formation was deposited at ~23 Ma near Lazi; and the lower member of the Kailas Formation was deposited at ~23 Ma near the town of Dazhuka, the easternmost site in this study. Based on these age constraints and on the average rate of Kailas sedimentation documented near Mt. Kailas of 0.5 mm/yr (DeCelles et al., 2011), the onset of Kailas deposition migrated eastward along the India-Asia suture zone at ~ 300 mm/yr (Fig. 14).

The magmatic record also shows an eastward younging trend. High-K and adakitic magmatism, which have been interpreted to follow slab breakoff, is older in western Tibet than in central and eastern Tibet (Ding et al., 2003; Williams et al., 2004; Liu et al., 2014). The onset of ultrapotassic magmatic activity propagated eastward at a rate comparable to that of Kailas basin sedimentation (Fig. 14). The rate of propagation is well within the rates of lateral propagation for slab tearing documented in other collisional settings (Meulenkamp et al., 1996; van der Meulen et al., 1999). The onset of adakitic and ultrapotassic magmatism lags behind basin initiation by several million years, consistent with an expected delay between slab rollback and tearing.

That slab breakoff occurred earlier in western Tibet is also supported by tomographic studies beneath the India-Asia suture zone. These show a high velocity zone below modern India that has been interpreted as remnant of a foundering Indian continental slab (van der Voo et al., 1999; DeCelles et al., 2002; Li et al., 2008; Replumaz et al., 2010a, 2010b). Beginning around 75° E,

this high velocity zone shallows eastward, which Replumaz et al. (2010a) interpreted as evidence for eastward progression of slab tearing.

Tearing of the Indian slab would likely have resulted in a change from extensional deformation (“soft collision” of DeCelles et al., 2011) to north-south convergent deformation (“hard collision”) within the India-Asia suture zone and southernmost Lhasa terrane as trench advanced resumed. DeCelles et al. (2011) interpreted a shift in paleocurrent directions and provenance in the upper Kailas Formation in western Tibet to reflect this change through displacement along the GCT. In the central suture zone, the syn-convergent Liuqu Conglomerate, deposited at ca. 20 Ma (Leary et al., 2012; Li et al., 2015) indicates that the India-Asia suture zone and southernmost Lhasa terrane had returned to a north-south convergent regime by at least 20 Ma (Fig. 15).

Beginning at ~16 Ma in southwestern Tibet (83.5°E) and ~11 Ma near Lhasa (90°E), east-west extensional deformation rapidly accelerated (Styron et al., 2015). This is interpreted to have been driven by thickening of the lower crust in response to underthrusting of the Indian slab (Styron et al., 2015). The cessation of high-K and adakitic magmatism in southern Tibet roughly coincides with this pattern: near Mount Kailas, magmatism began around 25 Ma and shut off around 15 Ma; north of the Lazi locality, magmatism initiated around 18 Ma and ceased around 9 Ma. This shut off was likely driven by Indian plate underthrusting cutting off the asthenospheric heat source that drove melting (Chung et al., 2003). Together, the Kailas sedimentary record, magmatic record, east-west extensional record, and tomography data all support the hypothesis that the Oligo-Miocene tectonic evolution of southern Tibet was driven by Indian slab dynamics.

## **Regional Implications**

Based on the younging of adakitic magmatism from the eastern syntaxis to the central India-Asia suture zone, Zhang et al. (2014) proposed that slab tearing (and initial 'rollback') proceeded the opposite direction, from east to west (Fig. 14). Zhang et al. (2014) also showed the younging trend from west to east observed in this study, but they did not interpret it. When all available data are presented (Fig. 14), it is evident that the onset of adakitic and ultrapotassic magmatism was earliest near the syntaxes and latest around 90°E. The onset of adakitic and ultrapotassic magmatism near the edges of the India-Asia suture zone and the progressive movement of that activity inward along strike raises the possibility that slab rollback and tearing could have proceeded inward from both edges of the Indian slab.

If slab rollback and tearing commenced near the eastern and western syntaxes and progressed toward the central India-Asia suture zone, we would expect the age of the Kailas basin to match the magmatic pattern that was the basis of the Zhang et al. (2014) interpretation. New age constraints reported by Li et al. (2015) and Kong et al. (2015) for the eastern Kailas Formation (locally the Luobusa Conglomerate) provide a preliminary test of this idea: detrital zircon U-Pb data reported by Li et al. (2015) yield maximum depositional ages of  $23 \pm 1$  Ma (5 grains; sample 2013LBS17) and  $24 \pm 3$  Ma (3 grains; sample 2013LBS19). U-Pb analyses of zircons from an interbedded tuff in the upper portion of the Kailas Formation ~50 km east yielded an age of  $18.7 \pm 2.0$  Ma (Kong et al., 2015). These data leave open the possibility that the basal Kailas Formation in this area may be slightly older than in the central suture zone; however, testing this hypothesis will require much more detailed age constraints.

## **CONCLUSIONS**

The Oligo-Miocene Kailas Formation exposed along the southern margin of the Lhasa terrane was deposited in alluvial fan and fluvial environments within an extensional basin setting. This study provides new constraints on the depositional age of the Kailas Formation in this region and shows that deposition younged to the east between 81°E and 90°E. The Kailas Formation near Mt. Kailas was deposited between 26 Ma and 23 Ma; deposition near Lazi occurred between ca. 25 Ma and 23 Ma; and deposition near Dazhuka occurred between 23 Ma and 22 Ma.

Based on similarities between the temporal-spatial patterns of Kailas sedimentation and ultrapotassic and adakitic magmatism in southern Tibet, we suggest that Kailas Basin formation was driven by Indian slab shearing and breakoff that initiated in western Tibet and proceeded eastward.

An east-to-west younging trend in adakitic magmatism between 91°E and 95°E and preliminary geochronologic constraints on the age of the Kailas Formation in this region raise the possibility that slab shearing and breakoff may have also initiated near the eastern syntaxis and propagated westward. However, more geochronologic work is required to fully test this hypothesis.

## **ACKNOWLEDGMENTS**

This research was supported by NSF Continental Dynamics grant EAR-1008527. The Arizona LaserChron Center is supported in part by NSF EAR-1338583. We thank Lin Ding for assistance with logistics and Liyun Zhang, Fulong Cai, and Suoya Fan for assistance in the field. We would like to thank Douwe van Hinsbergen and Fritz Schlunegger for reviews that helped us to significantly improve this manuscript. We would also like to thank Raymond Russo for editorial handling of this manuscript.

## **REFERENCES CITED**

- Aitchison, J., Davis, A., Badengzhu, and Luo, H., 2002, New constraints on the India–Asia collision: the lower Miocene Gangrinboche conglomerates, Yarlung Tsangpo suture zone, SE Tibet: *Journal of Asian Earth Sciences*, v. 21, p. 251-263.
- Aitchison, J., Davis, A., Liu, J., Luo, H., and Malpas, J., 2000, Remnants of a Cretaceous intra-oceanic subduction system within the Yarlung–Zangbo suture (southern Tibet): *Earth and Planetary Science Letters*, v. 183, p. 231-244.
- Aitchison, J.C., Ali, J.R., Chan, A., Davis, A.M., and Lo, C., 2009, Tectonic implications of felsic tuffs within the Lower Miocene Gangrinboche conglomerates, southern Tibet: *Journal of Asian Earth Sciences*, v. 34, p. 287-297, doi: 10.1016/j.jseaes.2008.05.008.
- Aitchison, J.C., Ali, J.R., and Davis, A.M., 2007, When and where did India and Asia collide?: *Journal of Geophysical Research*, v. 112, doi: 10.1029/2006JB004706.
- Allegre, C., Courtillot, V., Tapponnier, P., Hirn, A., Tattauer, M., Coulon, C., Jaeger, J.J., Achache, J., Scharer, U., Marcoux, J., Burg, J.P., Girardeau, J., Armijo, R., Gariépy, C., et al., 1984, Structure and evolution of the Himalaya–Tibet orogenic belt: *Nature*, v. 305, p. 17-22.
- Allen, J., 1964, Studies in fluvial sedimentation: six cyclothems from the Lower Old Red Sandstone, Anglowelsh Basin: *Sedimentology*, v. 3, p. 163-198.
- Allen, P., 1981, Sediments and processes on a small stream-flow dominated, Devonian alluvial fan, Shetland Islands: *Sedimentary Geology*, v. 29, p. 31-66.
- Allen, P.A., and Allen, J.R., 2006, *Basin Analysis: Principles and Applications*: Malden, MA, Blackwell Publishing Ltd., 562 p.
- An, W., Hu, X. and Garzanti, E., 2015, Sandstone provenance and tectonic evolution of the Xiukang Mélange from Neotethyan subduction to India–Asia collision (Yarlung-Zangbo suture, south Tibet): *Gondwana Research*, doi:10.1016/j.gr.2015.08.010.
- An, W., Hu, X., Garzanti, E., BouDagher-Fadel, M.K., Wang, J., and Sun, G., 2014, Xigaze forearc basin revisited (South Tibet): Provenance changes and origin of the Xigaze Ophiolite: *Geological Society of America Bulletin*, v. 126, p. 1595-1613, doi: 10.1130/B31020.1.
- Anadón, P., Cabrera, L., Colombo, F., Marzo, M., and Riba, O., 1986, Syntectonic intraformational unconformities in alluvial fan deposits, eastern Ebro Basin margins (NE Spain): *Foreland Basins*, v. 8, p. 259-271.
- Ashley, G., 1990, Classification of large-scale subaqueous bedforms: a new look at an old problem: *Journal of Sedimentary Petrology*, v. 60, p. 160-172.
- Ashworth, P.J., Sambrook Smith, G.H., Best, J.L., Bridge, J.S., Lane, S.N., Lunt, I.A., Reesink, A.J., Simpson, C.J. and Thomas, R.E., 2011, Evolution and sedimentology of a channel fill in the sandy braided

- South Saskatchewan River and its comparison to the deposits of an adjacent compound bar. *Sedimentology*, v. 58, p. 1860-1883.
- Beaumont, C., 1981, Foreland basins: *Geophysical Journal International*, v. 65, p. 291-329.
- Besse, J., Courtillot, V., Pozzi, J., Westphal, M., and Zhou, Y., 1984, Palaeomagnetic estimates of crustal shortening in the Himalayan thrusts and Zangbo suture: *Nature*, v. 311, p. 621-626.
- Blair, T., 2000, Sedimentology and progressive tectonic unconformities of the sheetflood-dominated Hell's Gate alluvial fan, Death Valley, California: *Sedimentary Geology*, v. 132, p. 233-262.
- Blair, T.C., and McPherson, J.G., 1994, Alluvial Fans and their Natural Distinction from Rivers Based on Morphology, Hydraulic Processes, Sedimentary Processes, and Facies Assemblages: *Journal of Sedimentary Research*, v. 64 p. 450-489.
- Bridge, J., and Lunt, I., 2006, Depositional models of braided rivers *in*: Smith, G.H.S., Best, J.L., Bristow, C.S., Petts, G.E., eds., *Braided Rivers: Processes, Deposits, Ecology and Management: International Association of Sedimentologists Special Publication*, 36, p. 11-50.
- Bristow, C.S., Skelly, R.L. and Ethridge, F.G., 1999, Crevasse splays from the rapidly aggrading, sand-bed, braided Niobrara River, Nebraska: effect of base-level rise: *Sedimentology*, v. 46, p. 1029-1048.
- Brun, J.P., and Faccenna, C., 2008, Exhumation of high-pressure rocks driven by slab rollback: *Earth and Planetary Science Letters*, v. 272, p. 1-7, doi:10.1016/j.epsl.2008.02.038.
- Bryan, S., Cas, R., and Martı, J., 1998, Lithic breccias in intermediate volume phonolitic ignimbrites, Tenerife (Canary Islands): constraints on pyroclastic flow depositional processes: *Journal of volcanology and geothermal*, v. 81, p. 269-296.
- Bull, W., 1972, Recognition of alluvial fan deposits in the stratigraphic record *in*: Rigby, J., and Hamblin, W.K., *Recognition of ancient sedimentary environments: Society of Economic Paleontologists and Mineralogists Special Publication* 16, p. 63-83.
- Burg, J., and Chen, G., 1984, Tectonics and structural zonation of southern Tibet, China: *Nature*, v. 311, p. 219-223.
- Cai, F., Ding, L., Leary, R.J., Wang, H., Xu, Q., Zhang, L., and Yue, Y., 2012, Tectonostratigraphy and provenance of an accretionary complex within the Yarlung–Zangpo suture zone, southern Tibet: Insights into subduction–accretion processes in the Neo-Tethys: *Tectonophysics*, v. 574-575, p. 181-192, doi: 10.1016/j.tecto.2012.08.016.
- Cai, F., Ding, L., and Yue, Y., 2011, Provenance analysis of upper Cretaceous strata in the Tethys Himalaya, southern Tibet: Implications for timing of India–Asia collision: *Earth and Planetary Science Letters*, v. 35, p. 195-206, doi: 10.1016/j.epsl.2011.02.055.

- Cant, D., and Walker, R., 1978, Fluvial processes and facies sequences in the sandy braided South Saskatchewan River, Canada: *Sedimentology*, v. 25, p. 625-648.
- Cant, D.J., and Walker, R.G., 1976, Development of a braided-fluvial facies model for the Devonian Battery Point Sandstone, Québec: *Canadian Journal of Earth Science*, v. 13, p. 102-119.
- Carrapa, B., Orme, D.A., DeCelles, P.G., Kapp, P., Cosca, M.A., and Waldrip, R., 2014, Miocene burial and exhumation of the India-Asia collision zone in southern Tibet: Response to slab dynamics and erosion: *Geology*, v. 42, p. 443-446, doi: 10.1130/G35350.1.
- Cheng, J., and Xu, G., 1986, Geologic Map of the Gaize Region with Report: Tibetan Bureau of Geology and Mineral Resources, 369 p.
- Chung, S., Liu, D., Ji, J., Chu, M., Lee, H., Wen, D., Lo, C., Lee, T., Qian, Q., and Zhang, Q., 2003, Adakites from continental collision zones: Melting of thickened lower crust beneath southern Tibet: *Geology*, v. 31, p. 1021, doi: 10.1130/G19796.1.
- Coogan, J.C., and DeCelles, P.G., 1996, Extensional collapse along the Sevier Desert reflection, northern Sevier Desert basin, western United States: *Geology*, v. 24, p.933-936, doi:10.1130/0091-7613(1996).
- Crampton, S., and Allen, P., 1995, Recognition of forebulge unconformities associated with early stage foreland basin development: example from the North Alpine Foreland Basin: *AAPG bulletin*, v. 79, p. 1495-1514.
- Davis, A., Aitchison, J., Badengzhu, and Hui, L., 2004, Conglomerates record the tectonic evolution of the Yarlung-Tsangpo suture zone in southern Tibet, *in* Malpas, J., Fletcher, C.J., Ali, J.R., and Aitchison, J.C. tran., *Aspects of the Tectonic Evolution of China*, Geological Society of London, p. 235-246.
- DeCelles, P.G., Castañeda, I.S., Carrapa, B.C., Liu, J., Quade, J., Leary, R., Zhang, L., (in review) Oligocene-Miocene Great Lakes in the India-Asia Collision Zone, *Basin Research*.
- DeCelles, P.G., and Giles, K., 1996, Foreland basin systems: *Basin Research*, v. 8, p. 105-123.
- DeCelles, P.G., Gray, M.B., Ridgway, K.D., Cole, R.B., Srivastava, P., Pequera, N. and Pivnik, D.A., 1991, Kinematic history of a foreland uplift from Paleocene synorogenic conglomerate, Beartooth Range, Wyoming and Montana: *Geological Society of America Bulletin*, v. 103, p. 1458-1475.
- DeCelles, P.G., Kapp, P., Gehrels, G., and Ding, L., 2014, Paleocene-Eocene foreland basin evolution in the Himalaya of southern Tibet and Nepal: Implications for the age of initial India-Asia collision: *Tectonics*, v. 33, p. 824-849.
- DeCelles, P.G., Kapp, P., Quade, J., and Gehrels, G.E., 2011, Oligocene-Miocene Kailas basin, southwestern Tibet: Record of postcollisional upper-plate extension in the Indus-Yarlung suture zone: *Geological Society of America Bulletin*, v. 123, p. 1337-1362, doi: 10.1130/B30258.1.

- DeCelles, P.G., Langford, R.P., and Schwartz, R.K., 1983, Two New Methods of Paleocurrent Determination from Trough Cross-Stratification: *Journal of Sedimentary Petrology*, v. 53, p. 629-642.
- DeCelles, P.G., Robinson, D.M., and Zandt, G., 2002, Implications of shortening in the Himalayan fold-thrust belt for uplift of the Tibetan Plateau: *Tectonics*, v. 21, p. 12-1-12-25, doi: 10.1029/2001TC001322.
- Decelles, P.G., Tolson, R.B., Graham, S.A., Smith, G.A., Ingersoll, R.V., White, J., Schmidt, C.J., Rice, R., Moxon, I., Lemke, L. Handschy, J.W., Follo, M.F., Edwards, D.P., Cavazza, W., Caldwell, M., and Bargar, E., 1987, Laramide thrust-generated alluvial-fan sedimentation, Sphinx conglomerate, southwestern Montana: *AAPG Bulletin*, v. 71, p. 135-155.
- Dickinson, W., 1985, Interpreting provenance relations from detrital modes of sandstones in G. G. Zuffa, ed., *Provenance of arenites*: D. Reidel Publishing Company, p. 333-361.
- Ding, L., Kapp, P., Zhong, D., and Deng, W., 2003, Cenozoic Volcanism in Tibet: Evidence for a Transition from Oceanic to Continental Subduction: *Journal of Petrology*, v. 44, p. 1833-1865, doi: 10.1093/petrology/egg061.
- Ding, L., Kapp, P., and Wan, X., 2005, Paleocene-Eocene record of ophiolite obduction and initial India-Asia collision, south central Tibet: *Tectonics*, v. 24, doi: 10.1029/2004TC001729.
- Dürr, S., 1996, Provenance of Xigaze fore-arc basin clastic rocks (Cretaceous, south Tibet): *Geological Society of America Bulletin*, v. 108, p. 669-684.
- Ebinger, C.J., 1989, Tectonic development of the western branch of the East African rift system: *Geological Society of America Bulletin*, v. 101, p.885-903.
- Einsele, G., Liu, B., Dürr, S., Frisch, W., and Liu, G., 1994, The Xigaze forearc basin: evolution and facies architecture (Cretaceous, Tibet): *Sedimentary Geology*, v. 90, p. 1-32.
- Evans, J.E., 1991, Facies Relationships, Alluvial Architecture, and Paleohydrology of a Paleogene, Humid-tropical Alluvial-fan System: Chumstick Formation, Washington State, U.S.A.: *Journal of Sedimentary Petrology*, v. 61, p. 732-755.
- Gansser, A., 1964, *Geology of the Himalayas*: London, Interscience, 289 p.
- Gao, Y., Hou, Z., Kamber, B.S., Wei, R., Meng, X., and Zhao, R., 2007, Adakite-like porphyries from the southern Tibetan continental collision zones: evidence for slab melt metasomatism: *Contributions to Mineralogy and Petrology*, v. 153, p. 105-120, doi: 10.1007/s00410-006-0137-9.
- Garzanti, E., Baud, A., and Mascle, G., 1987, Sedimentary record of the northward flight of India and its collision with Eurasia (Ladakh Himalaya, India): *Geodinamica Acta*, v. 1, p. 297-312.

- Gehrels, G., and Pecha, M., 2014, Detrital zircon U-Pb geochronology and Hf isotope geochemistry of Paleozoic and Triassic passive margin strata of western North America: *Geosphere*, v. 10, p. 49-65.
- Gehrels, G., Valencia, V., Pullen, A., 2006, Detrital Zircon Geochronology by Laser Ablation Multicollector ICPMS at the Arizona LaserChron Center, in Olszewski, T., ed., *Geochronology: Emerging Opportunities: Paleontology Society Papers*, v. 12, p. 67-76.
- Gehrels, G., Valencia, V., and Ruiz, J., 2008, Enhanced precision, accuracy, efficiency, and spatial resolution of U-Pb ages by laser ablation–multicollector–inductively coupled plasma–mass spectrometry: *Geochemistry, Geophysics, Geosystems*, v. 9, doi: 10.1029/2007GC001805.
- Green, O.R., Searle, M.P., Corfield, R.I., and Corfield, R.M., 2008, Cretaceous-Tertiary Carbonate Platform Evolution and the Age of the India-Asia Collision along the Ladakh Himalaya (Northwest India): *The Journal of Geology*, v. 116, p. 331-353, doi: 10.1086/588831.
- Guilmette, C., Hébert, R., Dostal, J., Indares, A., Ullrich, T., Bédard, É., and Wang, C., 2012, Discovery of a dismembered metamorphic sole in the Saga ophiolitic mélange, South Tibet: Assessing an Early Cretaceous disruption of the Neo-Tethyan supra-subduction zone and consequences on basin closing: *Gondwana Research*, v. 22, p. 398-414, doi: 10.1016/j.gr.2011.10.012.
- Guilmette, C., Hébert, R., Wang, C., and Villeneuve, M., 2009, Geochemistry and geochronology of the metamorphic sole underlying the Xigaze Ophiolite, Yarlung Zangbo Suture Zone, South Tibet: *Lithos*, v. 112, p. 149-162, doi: 10.1016/j.lithos.2009.05.027.
- Guynn, J.H., Kapp, P., Pullen, A., Heizler, M., Gehrels, G., and Ding, L., 2006, Tibetan basement rocks near Amdo reveal “missing” Mesozoic tectonism along the Bangong suture, central Tibet: *Geology*, v. 34, p. 505-508, doi: 10.1130/G22453.1.
- Harrison, T.M., Yin, A., Grove, M., Lovera, O.M., Ryerson, F.J., and Zhou, X., 2000, The Zedong Window: A record of superposed Tertiary convergence in southeastern Tibet: *Journal of Geophysical Research*, v. 105, p. 19,211-19,230.
- He, S., Kapp, P., DeCelles, P., Gehrels, G., and Heizler, M., 2007, Cretaceous–Tertiary geology of the Gangdese Arc in the Linzhou area, southern Tibet: *Tectonophysics*, v. 433, p. 15-37.
- Heim, A., and Gansser, A., 1939, Central Himalaya—Geological observations of the Swiss expedition, 1936: *Mémoire Société Helvétique Science Naturelle*, v. 73, p. 1–245.
- Henderson, A., Najman, Y., Parrish, R., BouDagher-Fadel, M., Barford, D., Garzanti, E., and Ando, S., 2010, Geology of the Cenozoic Indus Basin sedimentary rocks: Paleoenvironmental interpretation of sedimentation from the western Himalaya during the early phases of India-Eurasia collision: *Tectonics*, v. 29, doi: 10.1029/2009TC002651.

- Henderson, A.L., Najman, Y., Parrish, R., Mark, D.F., and Foster, G.L., 2011, Constraints to the timing of India–Eurasia collision; a re-evaluation of evidence from the Indus Basin sedimentary rocks of the Indus–Tsangpo Suture Zone, Ladakh, India: *Earth Science Reviews*, v. 106, p. 265-295, doi: 10.1016/j.earscirev.2011.02.006.
- Hu, X., Garzanti, E., Moore, T., and Raffi, I., 2015, Direct stratigraphic dating of India-Asia collision onset at the Selandian (middle Paleocene,  $59 \pm 1$  Ma): *Geology*, v. 43, p. 859-962, doi:10.1130/G36872.1.
- Hu, X., Wang, J., Boudagher-Fadel, M., Garzanti, E., and An, W., 2015a, New insights into the timing of the India-Asia collision from the Paleogene Quxia and Jialazi formations of the Xigaze forearc basin, South Tibet: *Gondwana Research*, doi: 10.1016/j.gr.2015.02.007.
- Huang, W., Van Hinsbergen, D.J., Maffione, M., Orme, D.A., Dupont-Nivet, G., Guilmette, C., Ding, L., Guo, Z. and Kapp, P., 2015, Lower Cretaceous Xigaze ophiolites formed in the Gangdese forearc: Evidence from paleomagnetism, sediment provenance, and stratigraphy. *Earth and Planetary Science Letters*, v. 415, p.142-153.
- Ingersoll, R., Bullard, T., Ford, R., Grimm, J., Pickle, J., and Sares, S., 1984, The effect of grain size on detrital modes: a test of the Gazzi-Dickinson point-counting method: *Journal of Sedimentary*, v. 54, p. 103-116.
- Ji, W., Wu, F., Chung, S., Li, J., and Liu, C., 2009, Zircon U–Pb geochronology and Hf isotopic constraints on petrogenesis of the Gangdese batholith, southern Tibet: *Chemical Geology*, v. 262, p. 229-245, doi: 10.1016/j.chemgeo.2009.01.020.
- Ji, W., Wu, F., Chung, S., and Liu, C., 2014, The Gangdese magmatic constraints on a latest Cretaceous lithospheric delamination of the Lhasa terrane, southern Tibet: *Lithos*, v. 210-211, p. 168-180, doi: 10.1016/j.lithos.2014.10.001.
- Jolivet, L., and Brun, J.P., 2010, Cenozoic geodynamic evolution of the Aegean: *International Journal of Earth Sciences*, v. 99, p.109-138, doi:10.1007/s00531-008-0366-4.
- Jolivet, L., Faccenna, C., Huet, B., Labrousse, L., Le Pourhiet, L., Lacombe, O., Lecomte, E., Burov, E., Denèle, Y., Brun, J.P. and Philippon, M., Pauli, A., Salaüni, G., Karabulutj, H., Piromallok, C., Moniél, P., Gueydanl, F., Okaym, A.I., Oberhänslin, R., Pourteun, A., Augiero, R., Gadenneo, L., Driussio, O., 2013, Aegean tectonics: Strain localisation, slab tearing and trench retreat: *Tectonophysics*, v. 597, p. 1-33, doi:10.1016/j.tecto.2012.06.011.
- Kapp, J.L.D., Harrison, T.M., Kapp, P., Grove, M., Lovera, O.M., and Ding, L., 2005, The Nyainqentanglha Shan: A window into the tectonic, thermal, and geochemical evolution of the Lhasa block, southern Tibet: *Journal of Geophysical Research*, v. 110, p. B08413, doi:10.1029/2004JB003330.

- Kapp, P., DeCelles, P.G., Gehrels, G.E., Heizler, M., and Ding, L., 2007, Geological records of the Lhasa-Qiangtang and Indo-Asian collisions in the Nima area of central Tibet: *Geological Society of America Bulletin*, v. 119, p. 917-933, doi: 10.1130/B26033.1.
- Kong, M., Jiang, W., Liu, C., Li, X., Yang, Y., Ye, P., 2015, LA-ICP-MS zircon U-Pb age of the tuffs from the Luobusha conglomerates in southeast Tibet and its implications: *Geological Bulletin of China*, v. 34, p. 328-336.
- Lawton, T.F., Roca, E. and Guimerà, J., 1999, Kinematic-stratigraphic evolution of a growth syncline and its implications for tectonic development of the proximal foreland basin, southeastern Ebro basin, Catalunya, Spain: *Geological Society of America Bulletin*, v. 111, p. 412-431.
- Leary, R.J., DeCelles, P.G., Quade, J. (2012) Provenance, Paleotemperature, and Tectonic Significance of the Liuqu Conglomerate, Southern Tibet: Abstract T51E-2643 presented at 2012 Fall Meeting, AGU, San Francisco 3-7 December.
- Leech, M., Singh, S., Jain, A., Klemperer, S., and Manickavasagam, R., 2005, The onset of India-Asia continental collision: early, steep subduction required by the timing of UHP metamorphism in the western Himalaya: *Earth and Planetary Science Letters*, v. 234, p. 83-97.
- Leeder, M.R., and Gawthorpe, R.L., 1987, Sedimentary models for extensional tilt-block/half-graben basins: *Geological Society, London, Special Publications*, v. 28, p.139-152, doi:10.1144/GSL.SP.1987.028.01.11.
- Li, C., van der Hilst, R., Meltzer, A., and Engdahl, E., 2008, Subduction of the Indian lithosphere beneath the Tibetan Plateau and Burma: *Earth and Planetary Science Letters*, v. 274, p. 157-168.
- Li, G., Kohn, B., Sandiford, M., Xu, Z., and Wei, L., 2015, Constraining the age of Liuqu Conglomerate, southern Tibet: Implications for evolution of the India-Asia collision zone: v. 426, p. 259-266, doi: 10.1016/j.epsl.2015.06.010.
- Li., G., Liu, X., Pullen, A., Lijie, W., Liu, X., Feixin, H., & Xuejun, Z., 2010, In-situ detrital zircon geochronology and Hf isotopic analyses from Upper Triassic Tethys sequence strata: *Earth and Planetary Science Letters*, v. 297, p. 461-470.
- Li, J., 2004, Discovery and preliminary study on palynofossils from the Cenozoic Qiuwu Formation of Xizang (Tibet): *Acta Micropalaeontologica Sinica*, v. 21, p. 216-221.
- Li, S., Ding, L., Xu, Q., Wang, H., Yue, Y., and Baral, U., 2015, The evolution of Yarlung Tsangpo River: Constraints from the age and provenance of the Gangdese Conglomerates, southern Tibet: *Gondwana Research*, p. 1-18, doi: 10.1016/j.gr.2015.05.010.
- Liu, D., Zhao, Z., Zhu, D., Niu, Y., DePaolo, D.J., Harrison, T.M., Mo, X., Dong, G., Zhou, S., Sun, C., Zhang, Z., and Liu, J., 2014, Postcollisional potassic and ultrapotassic rocks in southern Tibet: *Mantle*

- and crustal origins in response to India-Asia collision and convergence: *Geochimica et Cosmochimica Acta*, v. 143, p. 207-231, doi: 10.1016/j.gca.2014.03.031.
- Ludwig, K. R., 2012, User's Manual for Isoplot 3.75, A Geochronological Toolkit for Microsoft Excel, Berkeley Geochronology Center Special Publication No. 5.
- Maffione, M., Van Hinsbergen, D.J., Koornneef, L.M., Guilmette, C., Hodges, K., Borneman, N., Huang, W., Ding, L. and Kapp, P., 2015, Forearc hyperextension dismembered the south Tibetan ophiolites: *Geology*, v. 43, p.475-478.
- Maheo, G., Guillot, S., Blichert-Toft, J., Rolland, Y., and Pecher, A., 2002, A slab breakoff model for the Neogene thermal evolution of South Karakorum and South Tibet: *Earth and Planetary Science Letters*, v. 195, p. 45-58.
- Meulenkamp, J., Kováč, M., and Cicha, I., 1996, On Late Oligocene to Pliocene depocentre migrations and the evolution of the Carpathian-Pannonian system: *Tectonophysics*, v. 266, p. 301-317.
- Miall, A.D. ,1978, Lithofacies types and vertical profile models in braided river deposits: a summary. in: Miall, A.D., ed., *Fluvial Sedimentology: Canadian Society of Petroleum Geologists, Memoir 5*, p. 597-604.
- Miall, A., 1985, Architectural-element analysis: a new method of facies analysis applied to fluvial deposits: *Earth Science Reviews*, v. 22, p. 261-308.
- Miall, A., and Turner-Peterson, C., 1989, Variations in fluvial style in the Westwater Canyon Member, Morrison Formation (Jurassic), San Juan Basin, Colorado Plateau: *Sedimentary Geology*, v. 63, p. 21-60.
- Mo, X., Zhao, Z., Deng, J., Dong, G., Zhou, S., Guo, T., Zhang, S., and Wang, L., 2003, Response of volcanism to the India-Asia collision: *Earth Science Frontiers*, v. 10, p. 135-148.
- Morley, C.K., 1988, Variable extension in Lake Tanganyika: *Tectonics*, v. 7, p. 785-801.
- Murphy, M. A., Sanchez, V., and Taylor, M. H., (2010), Syncollisional extension along the India–Asia suture zone, south-central Tibet: Implications for crustal deformation of Tibet: *Earth and Planetary Science Letters*, v. 290, p. 233–243.
- Murphy, M.A. and Yin, A., 2003. Structural evolution and sequence of thrusting in the Tethyan fold-thrust belt and Indus-Yalu suture zone, southwest Tibet. *Geological Society of America Bulletin*, v. 115, p.21-34.
- Najman, Y., Appel, E., Boudagher-Fadel, M., Bown, P., Carter, A., Garzanti, E., Godin, L., Han, J., Liebke, U., Oliver, G. and Parrish, R., 2010, Timing of India-Asia collision: Geological, biostratigraphic, and palaeomagnetic constraints: *Journal of Geophysical Research: Solid Earth*, 115 doi:10.1029/2010JB007673.

- Nemec, W., and Steel, R., 1988, What is a fan delta and how do we recognize it? *in*: Nemec, W and Steel, R.J., eds., *Fan Deltas: sedimentology and tectonic settings*: Blackie and Son, p. 3-13, doi: 10.1111/j.1365-2117.1988.tb00021.x.
- Ori, G., 1982, Braided to meandering channel patterns in humid-region alluvial fan deposits, River Reno, Po Plain (northern Italy): *Sedimentary Geology*, v. 31, p. 231-248.
- Orme, D.A., Carrapa, B., and Kapp, P., 2014, Sedimentology, provenance and geochronology of the upper Cretaceous-lower Eocene western Xigaze forearc basin, southern Tibet: *Basin Research*, p. 1-25, doi: 10.1111/bre.12080.
- Parrish, R., and Tirrul, R., 1989, U-Pb age of the Baltoro granite, northwest Himalaya, and implications for monazite U-Pb systematics: *Geology*, v. 17, p. 1076-1079.
- Pierson, T., 1980, Erosion and deposition by debris flows at Mt Thomas, north Canterbury, New Zealand: *Earth Surface Processes*, v. 5, p. 227-247.
- Quidelleur, X., Grove, M., Lovera, O., Harrison, T.M., Yin, A., and Ryerson, F.J., 1997, Thermal evolution and slip history of the Renbu Zedong Thrust, southeastern Tibet: *Journal of Geophysical Research*, v. 102, p. 2659-2679.
- Ratschbacher, L., Frisch, W., Liu, G., and Chen, C., 1994, Distributed deformation in southern and western Tibet during and after the India-Asia collision: *Journal of Geophysical Research*, v. 99, p. 19,917-19,945.
- Ravikant, V., 2006, Utility of Rb–Sr geochronology in constraining Miocene and Cretaceous events in the eastern Karakoram, Ladakh, India: *Journal of Asian Earth Sciences*, v. 27, p. 534-543.
- Replumaz, A., Capitanio, F.A., Guillot, S., Negredo, A.M., and Villaseñor, A., 2014, The coupling of Indian subduction and Asian continental tectonics: *Gondwana Research*, v. 26, p. 608-626, doi: 10.1016/j.gr.2014.04.003.
- Replumaz, A., Negredo, A., Villaseñor, A., and Guillot, S., 2010a, Indian continental subduction and slab break-off during Tertiary collision: *Terra Nova*, v. 22, p. 290-296, doi: 10.1111/j.1365-3121.2010.00945.x.
- Replumaz, A., Negredo, A.M., Guillot, S., and Villaseñor, A., 2010b, Multiple episodes of continental subduction during India/Asia convergence: Insight from seismic tomography and tectonic reconstruction: *Tectonophysics*, v. 483, p. 125-134, doi: 10.1016/j.tecto.2009.10.007.
- Rex, A., Searle, M., Tirrul, R., Crawford, M., Prior, D., Rex, D., and Barnicoat, A., 1988, The geochemical and tectonic evolution of the Central Karakoram, North Pakistan: *Philosophical Transactions of the Royal Society of London*, v. 326, p. 229-255.

- Ridgway, K., and Decelles, P., 1993, Stream-dominated alluvial fan and lacustrine depositional systems in Cenozoic strike-slip basins, Denali fault system, Yukon Territory, Canada: *Sedimentology*, v. 40, p. 645-666.
- Rust, B., 1977, Depositional models for braided alluvium: *Fluvial Sedimentology Memoir*, v. 5, p. 605-625.
- Sanchez, V.I., Murphy, M.A., Dupre, W.R., Ding, L., and Zhang, R., 2010, Structural evolution of the Neogene Gar Basin, western Tibet: Implications for releasing bend development and drainage patterns: *Geological Society of America Bulletin*, v. 122, p. 926-945.
- Sanchez, V., Murphy, M.A., Robinson, A.C., Lapen, T.J., Heizler, M.T. and Taylor, M.H., 2010a, Onset of oblique extension in south-central Tibet by 15 Ma: implications for diachronous extension of the Tibetan Plateau. Abstract T43B-2185 presented at 2010 Fall Meeting, AGU, San Francisco 13-17 December.
- Schärer, U., Copeland, P., Harrison, T., and Searle, M., 1990, Age, cooling history, and origin of post-collisional leucogranites in the Karakoram Batholith; a multi-system isotope study: *The Journal of Geology*, v. 98, p. 233-251.
- Schlische, R., 1992, Structural and stratigraphic development of the Newark extensional basin, eastern North America: Evidence for the growth of the basin and its bounding structures: *Geological Society of America Bulletin*, v. 104, p. 1246-1263.
- Schlische, R.W., and Olsen, P.E., 1990, Quantitative filling model for continental extensional basins with applications to early Mesozoic rifts of eastern North America: *The Journal of Geology*, v. 98, p.135-155.
- Schlunegger, F., and Kissling, E., 2015, Slab rollback orogeny in the Alps and evolution of the Swiss Molasse basin: *Nature communications*, v. 6, p. 1-10, doi:10.1038/ncomms9605.
- Searle, M., Pickering, K., and Cooper, D., 1990, Restoration and evolution of the intermontane Indus molasse basin, Ladakh Himalaya, India: *Tectonophysics*, v. 174, p. 301-314.
- Searle, M., Windley, B., Coward, M., Cooper, D., Rex, A., Rex, D., Tingdong, L., Xuchang, X., Jan, M., Thakur, V., and Kumar, S., 1987, The closing of Tethys and the tectonics of the Himalaya: *Geological Society of America Bulletin*, v. 98, p. 678-701.
- Shaw, J.H., Hook, S.C., and Sitohang, E.P., 1997, Extensional fault-bend folding and synrift deposition: an example from the Central Sumatra Basin, Indonesia: *AAPG bulletin*, v. 81, p.367-379.
- Shultz, A., 1984, Subaerial debris-flow deposition in the upper Paleozoic Cutler Formation, western Colorado: *Journal of Sedimentary Research*, v. 54.
- Sinclair, H.D., 1997, Tectonostratigraphic model for underfilled peripheral foreland basins: An Alpine perspective: *Geological Society of America Bulletin*, v. 109, p. 324-346.

- Sinclair, H.D. and Jaffey, N., 2001, Sedimentology of the Indus Group, Ladakh, northern India: implications for the timing of initiation of the palaeo-Indus River: *Journal of the Geological Society*, v. 158, p. 151-162, doi:10.1144/jgs.158.1.151.
- Singh, K.A., Parkash, B., Mohindra, R., Thomas, J.V. and Singhvi, A.K., 2001, Quaternary alluvial fan sedimentation in the Dehradun valley piggyback basin, NW Himalaya: tectonic and palaeoclimatic implications: *Basin Research*, v. 13, p. 449-471.
- Smith, G., 1986, Coarse-grained nonmarine volcanoclastic sediment: terminology and depositional process: *Geological Society of America Bulletin*, v. 97, p. 1-10.
- Smith, N., Cross, T., Dufficy, J., and Clough, S., 1989, Anatomy of an avulsion: *Sedimentology*, v. 36, p. 1-23.
- Styron, R., Taylor, M., and Sundell, K., 2015, Accelerated extension of Tibet linked to the northward underthrusting of Indian crust: *Nature Geoscience*, v. 8, p. 131-134, doi: 10.1038/ngeo2336.
- Sundell, K.E., Taylor, M.H., Styron, R.H., Stockli, D.F., Kapp, P., Hager, C., Liu, D., and Ding, L., 2013, Evidence for constriction and Pliocene acceleration of east-west extension in the North Lunning rift region of west central Tibet: *Tectonics*, v. 32, p. 1454-1479, doi:10.1002/tect.20086.
- Tapponnier, P., Mercier, J., Proust, F., and Andrieux, J., 1981, The Tibetan side of the India–Eurasia collision: *Nature*, v. 294, p. 405-410.
- Todd, S., 2004, Stream-driven, high-density gravelly traction carpets: possible deposits in the Trabeg Conglomerate Formation, SW Ireland and some theoretical considerations of their origin: *Sedimentology*, v. 36, p. 513-530.
- Tullis, J., and Yund, R.A., 1977, Experimental deformation of dry westerly granite: *Journal of Geophysical Research*, v. 82, p. 5705-5718.
- Van der Meulen, M.J., Kouwenhoven, T., van der Zwaan, G., Meulenkamp, J., and Wortel, M., 1999, Late Miocene uplift in the Romagnan Apennines and the detachment of subducted lithosphere: *Tectonophysics*, v. 315, p. 319-335.
- Van der Voo, R., Spakman, W., and Bijwaard, H., 1999, Tethyan subducted slabs under India: *Earth and Planetary Science Letters*, v. 171, p. 7-20.
- Van Hinsbergen, D.J.J., Kapp, P., Dupont-Nivet, G., Lippert, P.C., DeCelles, P.G., and Torsvik, T.H., 2011, Restoration of Cenozoic deformation in Asia and the size of Greater India: *Tectonics*, v. 30, doi: 10.1029/2011TC002908.
- Vergés, J., Marzo, M., and Muñoz, J., 2002, Growth strata in foreland settings: *Sedimentary Geology*, v. 146, p. 1-9.

- Volkmer, J.E., Kapp, P., Guynn, J.H., and Lai, Q., 2007, Cretaceous-Tertiary structural evolution of the north central Lhasa terrane, Tibet: *Tectonics*, v. 26, p. 1-18, doi: 10.1029/2005tc001832.
- Wang, C., Li, X., Liu, Z., Li, Y., Jansa, L., Dai, J., and Wei, Y., 2012, Revision of the Cretaceous–Paleogene stratigraphic framework, facies architecture and provenance of the Xigaze forearc basin along the Yarlung Zangbo suture zone: *Gondwana Research*, v. 22, p. 415-433, doi: 10.1016/j.gr.2011.09.014.
- Wang, E., Kamp, P.J.J., Xu, G., Hodges, K.V., Meng, K., Chen, L., Wang, G., and Luo, H., 2015, Flexural bending of southern Tibet in a retro foreland setting: *Scientific Reports*, v. 5, p. 12076, doi: 10.1038/srep12076.
- Wang, J., Hu, X., Garzanti, E., and Wu, F., 2013, Upper Oligocene–Lower Miocene Gangrinboche Conglomerate in the Xigaze Area, Southern Tibet: Implications for Himalayan Uplift and Paleo-Yarlung-Zangbo Initiation: *The Journal of Geology*, v. 121, p. 425-444, doi: 10.1086/670722.
- Wang, J., Hu, X., Wu, F., and Jansa, L., 2010, Provenance of the Liuqu Conglomerate in southern Tibet: A Paleogene erosional record of the Himalayan–Tibetan orogen: *Sedimentary Geology*, v. 231, p. 74-84, doi: 10.1016/j.sedgeo.2010.09.004.
- Wen, R., Liu, D., Chung, S., Chu, M., Ji, J., Zhang, Q., Song, B., Lee, T., Yeh, M., and Lo, C., 2008, Zircon SHRIMP U–Pb ages of the Gangdese Batholith and implications for Neotethyan subduction in southern Tibet: *Chemical Geology*, v. 252, p. 191-201.
- Williams, H., Turner, S., Pearce, J., Kelley, S., and Harris, N., 2004, Nature of the Source Regions for Post-collisional, Potassic Magmatism in Southern and Northern Tibet from Geochemical Variations and Inverse Trace Element Modelling: *Journal of Petrology*, v. 45, p. 555-607, doi: 10.1093/petrology/egg094.
- Wooldridge, C.L. and Hickin, E.J., 2005, Radar architecture and evolution of channel bars in wandering gravel-bed rivers: Fraser and Squamish rivers, British Columbia, Canada: *Journal of Sedimentary Research*, v. 75, p. 844-860.
- Wortel, M.J.R., and Spakman, W., 2000, Subduction and slab detachment in the Mediterranean-Carpathian region: *Science*, v. 290, p. 1910-1917, doi: 10.1126/science.290.5498.1910.
- Xu, W., Zhang, H., Guo, L., and Yuan, H., 2010, Miocene high Sr/Y magmatism, south Tibet: Product of partial melting of subducted Indian continental crust and its tectonic implication: *Lithos*, v. 114, p. 293-306, doi: 10.1016/j.lithos.2009.09.005.
- Yin, A., 2006, Cenozoic tectonic evolution of the Himalayan orogen as constrained by along-strike variation of structural geometry, exhumation history, and foreland sedimentation: *Earth-Science Reviews*, v. 76, p. 1-131, doi: 10.1016/j.earscirev.2005.05.004.

- Yin, A., and Harrison, T., 2000, Geologic evolution of the Himalayan-Tibetan orogen: *Annual Review of Earth and Planetary Science*, v. 28, p. 211-280.
- Yin, A., Harrison, T., Ryerson, F., Wenji, C., Kidd, W., and Copeland, P., 2006, Tertiary structural evolution of the Gangdese thrust system, southeastern Tibet: *Journal of Geophysical Research*, v. 99, p. 18,175-18,201.
- Yin, A., Harrison, T., and Murphy, M., 1999, Tertiary deformation history of southeastern and southwestern Tibet during the Indo-Asian collision: *Society of America*, v. 111, p. 1644-1664.
- Zhang, L., Ducea, M.N., Ding, L., Pullen, A., Kapp, P., and Hoffman, D., 2014, Southern Tibetan Oligocene–Miocene adakites: A record of Indian slab tearing: *Lithos*, v. 210-211, p. 209-223, doi: 10.1016/j.lithos.2014.09.029.
- Zhu, D., Mo, X., Niu, Y., Zhao, Z., Wang, L., Liu, Y., and Wu, F., 2009, Geochemical investigation of Early Cretaceous igneous rocks along an east–west traverse throughout the central Lhasa Terrane, Tibet: *Chemical Geology*, v. 268, p. 298-312, doi: 10.1016/j.chemgeo.2009.09.008.
- Zhu, D., Mo, X., Zhao, Z., Niu, Y., Wang, L., Chu, Q., Pan, G., Xu, J., and Zhou, C., 2010, Presence of Permian extension- and arc-type magmatism in southern Tibet: Paleogeographic implications: *Geological Society of America Bulletin*, v. 122, p. 979-993, doi: 10.1130/B30062.1.
- Zhu, D., Zhao, Z., Niu, Y., Mo, X., and Chung, S., 2011, The Lhasa Terrane: Record of a microcontinent and its histories of drift and growth: *Earth and Planetary Science Letters*, v. 301, p. 241-255.
- Ziabrev, S., Aitchison, J., Abrajevitch, A., Badengzhu, Davis, A., and Luo, H., 2003, Precise radiolarian age constraints on the timing of ophiolite generation and sedimentation in the Dazhuqu terrane, Yarlung–Tsangpo suture zone, Tibet: *Journal of the Geological Society, London*, v. 160, p. 591-599.

## FIGURE CAPTIONS

Figure 1. Digital elevation model and simplified geologic map (after Yin and Harrison, 2000) of the Tibetan Plateau showing The Kailas Formation and Indus Group in black. Literature study locations numbered; locations from for this study are lettered. Kailas Basin: 1-4, a, b, c; Indus Basin, 5. Specific study locations: 1. Kailas Formation, DeCelles et al. (2011); 2: Gangdese Conglomerate, Li et al. (2015); 3: Luobusa Conglomerate, Kong et al. (2015); 4: Kailas Formation, Carrapa et al., 2014; 5: Indus Group, Henderson et al. (2010; 2011). IASZ: India-Asia suture zone; ISZ: Indus suture zone; SSZ: Shyok suture zone; BNSZ: Bangong-Nujian

suture zone; STDS: South Tibetan Detachment System; AKMS: Ayimaqin-Kunlun-Mutztagh suture zone; JSZ: Jinsha suture zone; ATF: Altyn Tagh Fault; MBT: Main Boundary Thrust.

Figure. 2. Geologic Map of the central India-Asia suture zone. Based on mapping in this study and mapping by Cai et al., 2011; 2012. GCT: Great Counter Thrust.

Figure 3. Geologic map of the Lazi locality.

Figure 4. Geologic map of the Xigaze locality based on this study and Wang et al. (2013) (Wang et al., 2013).

Figure 5. Oblique view of satellite imagery (Google Earth) showing intense deformation of the Kailas Formation. Measured section start and end marked by a, b, c, and a', b', and c', respectively. GCT: Great Counter Thrust.

Figure 6. Measured section from Lazi locality. Stratigraphic height is in meters. See Figs. 2 and 3 for location. See Table 1 for lithofacies codes.

Figure 7. Stratigraphic correlation for measured sections at the Lazi locality with paleocurrent indicators shown.

Figure 8. Measured section from Xigaze locality. Stratigraphic height is in meters. See Figs. 2 and 4 for location. See Table 1. for lithofacies codes.

Figure 9. Measured section from Dazhuka locality. Stratigraphic height is in meters. See Fig. 2 for location. See Table 1 for lithofacies codes.

Figure 10. Photographs of Kailas Formation outcrops. A) Middle member at section 2KS, Lazi locality showing lateral accretion elements. B) Weakly imbricated clast-supported cobble conglomerate from the lower member of section 1KS, Lazi locality. C) Upper member at 3KS, Lazi locality. D) Ductilely deformed granitic clasts within the mylonitic shear zone cutting the

Kailas Formation; Lazi locality. E) Imbricated clast-supported cobble conglomerate, Deri Member, Xigaze locality. Jake staff is 1.5 m. F) Lower member, section 1DK, Dazhuka locality. G) Trachy-andesite within a welded conglomerate, Dazhuka locality.

Figure. 11. Probability density plots, histograms, and maximum depositional ages of Kailas Formation detrital zircons (see Figs. 2-4 for locations). Histogram bin width is 5 Ma for 0-200 Ma plots and 20 Ma for 200-2000 Ma plots. Number at top left of each plot indicates the maximum vertical extent of the histogram y-axis. Maximum depositional ages calculated Unmix Ages (Ludwig, 2012) and by weighted average. Uncertainty reported is total 2 sigma uncertainty. Analyses in blue were excluded in the weighted average. Sources for Lhasa terrane compilation: Quidelleur et al., 1997; Chung et al., 2003; Mo et al., 2003; Kapp et al., 2005; Guynn et al., 2006; He et al., 2007; Kapp et al., 2007; Ji et al., 2009; Volkmer et al., 2007; Wen et al., 2008; Xu et al., 2010; Zhu et al., 2009; 2010; 2011; DeCelles et al., 2011.

Figure 12. A) 1- red chert, 2- green chert, 3- black chert, 4- quartzite, 5- green lithic sandstone, 6- brown sandstone, 7- white sandstone, 8- limestone, 9- volcanic, 10- basalt, 11- granite B) results of sandstone points. Fields after Dickinson (1985).

Figure. 13. Photographs from Wang et al., 2015, SII-8a, showing extensional growth strata within the Kailas Conglomerate taken (A) 15 km and (B) 5 km west of Mt. Kailas in western Tibet (81° E). C) Schematic depiction of our interpretation of the structure of the Kailas Basin, matching growth structures shown in (A) and (B). D-F) Schematic post-depositional evolution of the Kailas Basin. D) Schematic cross section of the Kailas Basin near the end of sedimentation. E) Schematic cross section showing future locations of GCT in this study area (1) and western Tibet (~81° E) (2). Blue box shows currently exposed portion of the basin in this study area; red box shows currently exposed basin in western Tibet. F) Schematic cross section of modern Kailas Basin structure. GCT: Great Counter Thrust.

Figure 14. A) Figure. 14. A) Spatio-temporal distribution of Kailas Formation sedimentation within the India-Asia suture zone from this study, DeCelles et al (2011), and Carrapa et al. (2014). Age control shown with arrows. Basin initiation calculated using average sedimentation

rates from DeCelles et al. (2011). B) Spatio-temporal distribution of adakitic and ultrapotassic rocks near the India-Asia suture zone compared to Gangrinboche sedimentation (red boxes). Sedimentary data sources: 1: Kailas Formation, DeCelles et al. (2011); 2: Gangdese Conglomerate, Li et al. (2015); 3: Luobusa Conglomerate, Kong et al. (2015); 4: Kailas Formation, Carrapa et al., 2014; Magmatic data sources: Zhang et al. (2014)'s compilation and references therein, Rex et al. (1988), Parrish and Turrill (1989), Scharer et al. (1990), Maheo et al. (2002), and Ravikant (2006). Trends are indicated with blue arrows.

Figure 15. Schematic diagrams showing the tectonic evolution of the India-Asia suture zone. Boxes show 2D north-south cross sections of the central suture zone. A: Following India-Asia collision, the Indian continental slab is underthrust beneath the Lhasa Terrane driving magmatism northward. B: Beginning around 35 Ma, Indian slab rollback causes the southward migration of magmatism as well as formation of the Kailas Basin in the India-Asia suture zone. C: Beginning around 25 Ma, a tear initiates along the edge(s) of the Indian slab producing rapid subsidence followed by uplift. This also initiates a pulse of ultrapotassic and adakitic magmatism in the southern Lhasa terrane. Both of these processes follow the slab tear and migrate toward the center of the suture zone. D: Around 20 Ma, the Indian slab breaks off completely and the contractional deformation resumes in the suture zone. The Liuqu Conglomerate is deposited in the central suture zone in a wedge-top position within the GCT system.

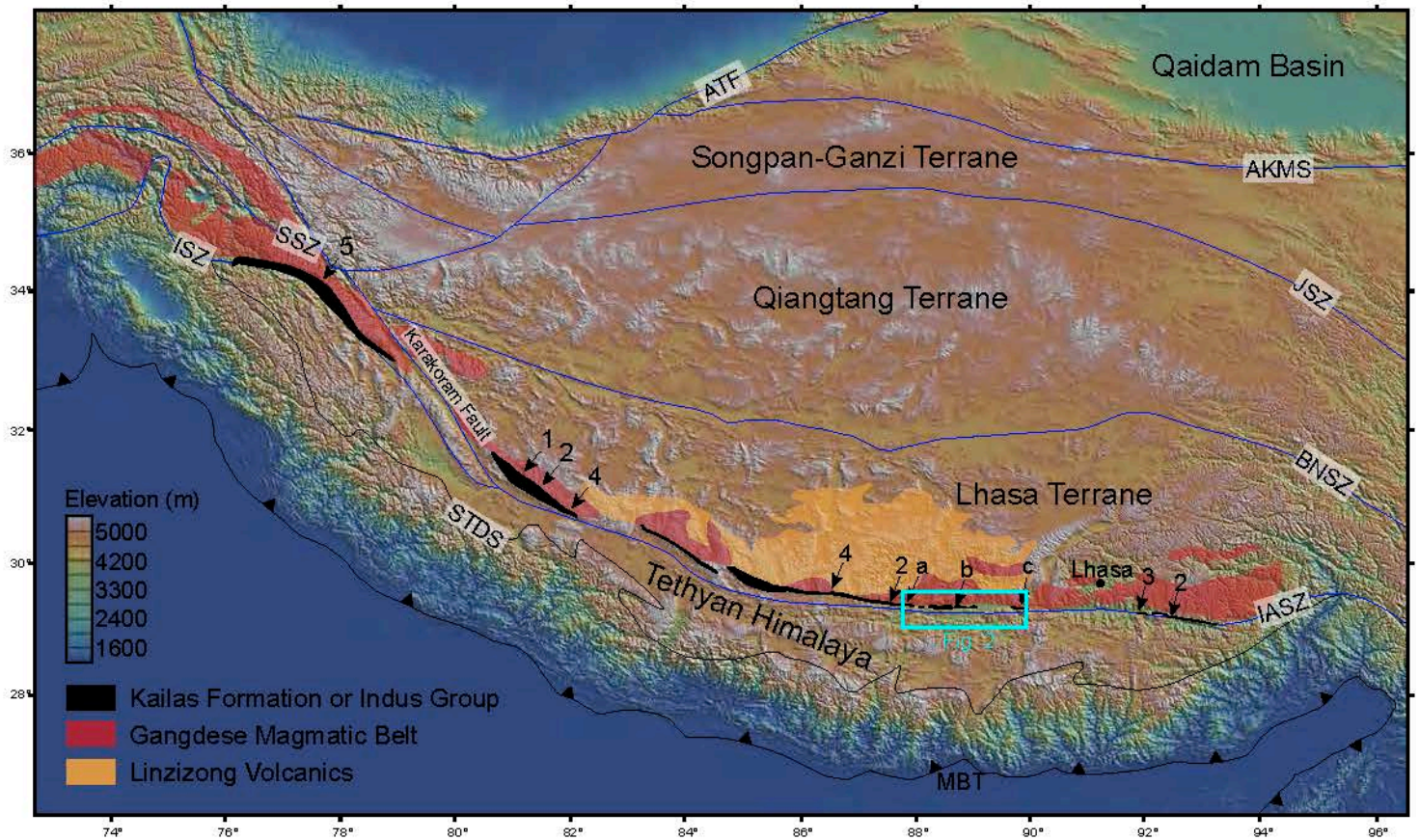
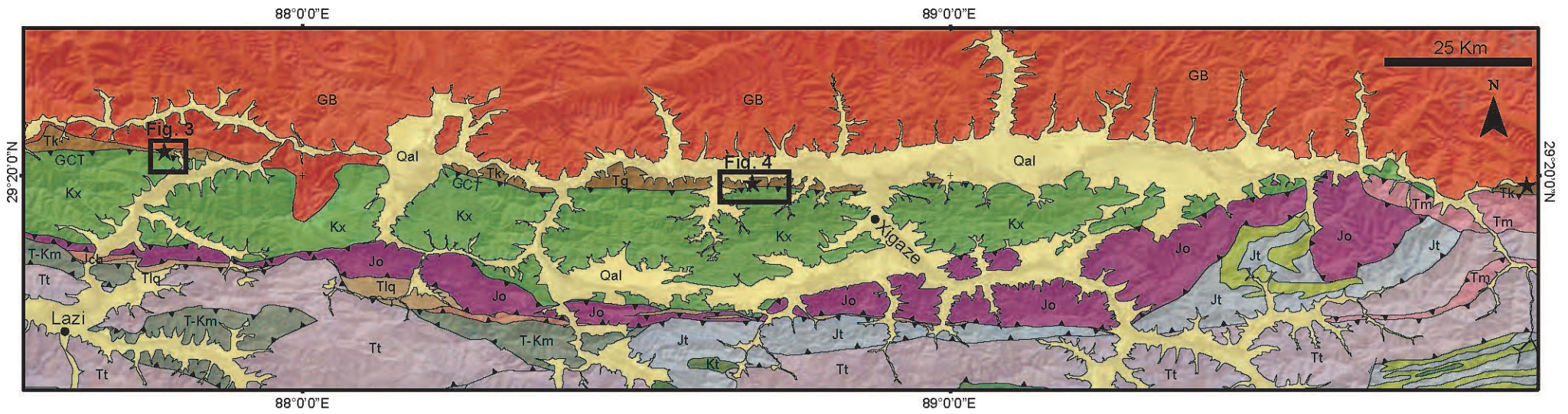


Fig. 1. Digital elevation model and simplified geologic map (after Yin and Harrison, 2000) of the Tibetan Plateau showing The Kailas Formation and Indus Group in black. Literature study locations numbered; locations from for this study are lettered. Kailas Basin: 1-4, a, b, c; Indus Basin, 5. Specific study locations: 1. Kailas Formation, DeCelles et al. (2011); 2. Gangdese Conglomerate, Li et al. (2015); 3. Luobusa Conglomerate, Kong et al. (2015); 4. Kailas Formation, Carrapa et al., 2014; 5. Indus Group, Henderson et al. (2010; 2011). IASZ: India-Asia suture zone; ISZ: Indus suture zone; SSZ: Shyok suture zone; BNSZ: Bangong-Nujian suture zone; STDS: South Tibetan Detachment System; AKMS: Ayimaqin-Kunlun-Mutztagh suture zone; JSZ: Jinsha suture zone; ATF: Altyn Tagh Fault; MBT: Main Boundary Thrust.



- |  |   |   |                    |
|--|---|---|--------------------|
| <span style="background-color: yellow; border: 1px solid black; padding: 2px;">Qal</span> Quaternary Alluvium                        | <span style="background-color: #808080; border: 1px solid black; padding: 2px;">T-Km</span> Sedimentary Melange | <span style="background-color: #ADD8E6; border: 1px solid black; padding: 2px;">Jt</span> Jurassic Tethyan          | ★ Measured Section |
| <span style="background-color: #FFD700; border: 1px solid black; padding: 2px;">Tlq</span> Liuqu Conglomerate                        | <span style="background-color: #90EE90; border: 1px solid black; padding: 2px;">Kj</span> Cretaceous Jiabula Fm | <span style="background-color: #F08080; border: 1px solid black; padding: 2px;">Tm</span> Melange (Triassic Blocks) | — Contact          |
| <span style="background-color: #8B4513; border: 1px solid black; padding: 2px;">Tk</span> Kailas Formation                           | <span style="background-color: #FFA07A; border: 1px solid black; padding: 2px;">Jch</span> Radiolarian Chert    | <span style="background-color: #D8BFD8; border: 1px solid black; padding: 2px;">Tt</span> Triassic Tethyan          | ↗ Thrust Fault     |
| <span style="background-color: #3CB371; border: 1px solid black; padding: 2px;">Kx</span> Xigaze Formation                           | <span style="background-color: #800080; border: 1px solid black; padding: 2px;">Jo</span> Ophiolitic Rocks      | <span style="background-color: #FF0000; border: 1px solid black; padding: 2px;">GB</span> Gangdese Batholith        | ● City             |
| <span style="background-color: #654321; border: 1px solid black; padding: 2px;">Kt</span> Upper Cretaceous to Lower Paleocene strata |   |   |                    |

Fig. 2. Geologic Map of the central Yarlung-Tsangpo suture zone. Based on mapping in this study and mapping by Cai et al., 2011; 2012. GCT: Great Counter Thrust.

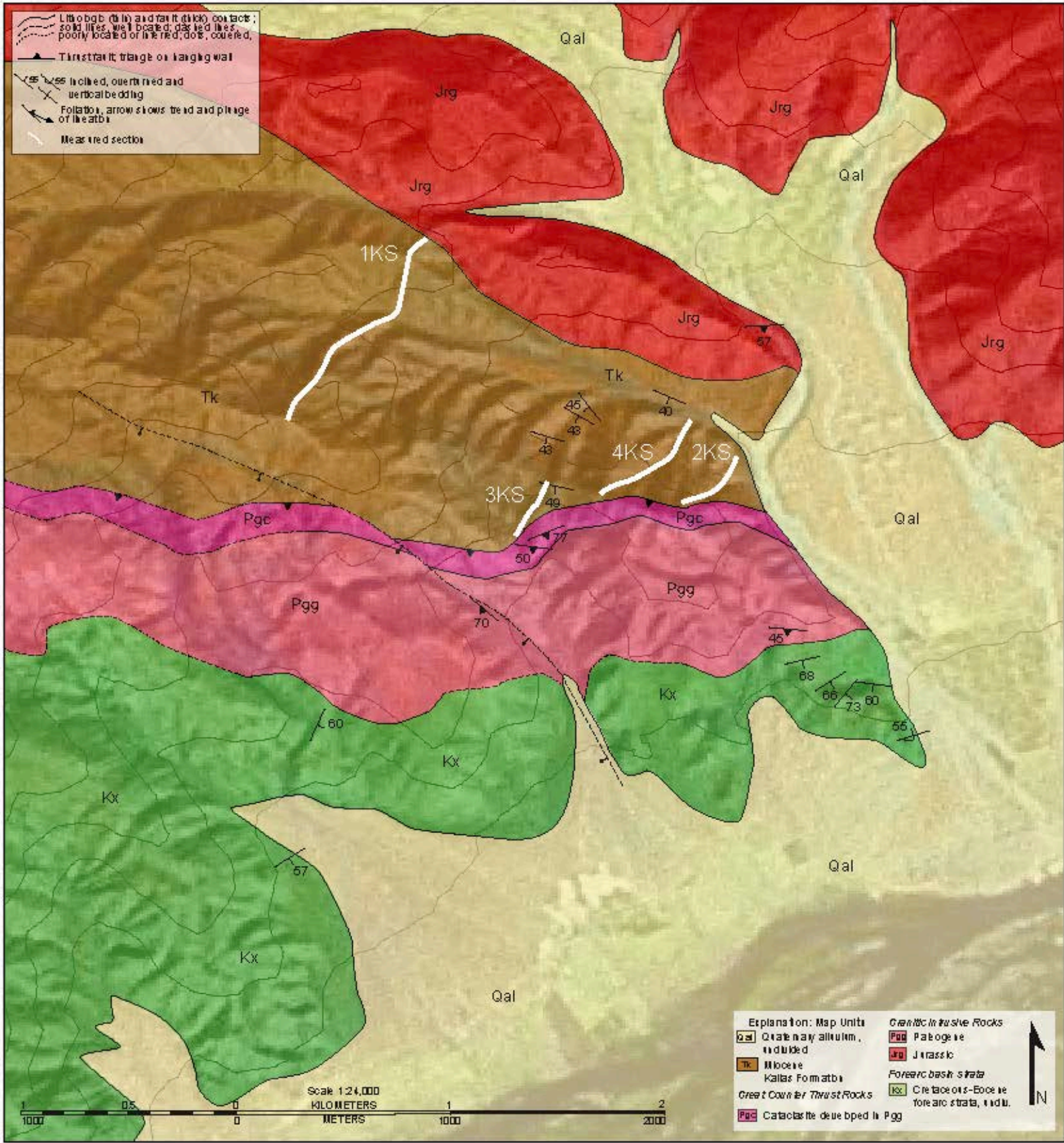


Figure 3. Geologic map of the Lhatse locality.

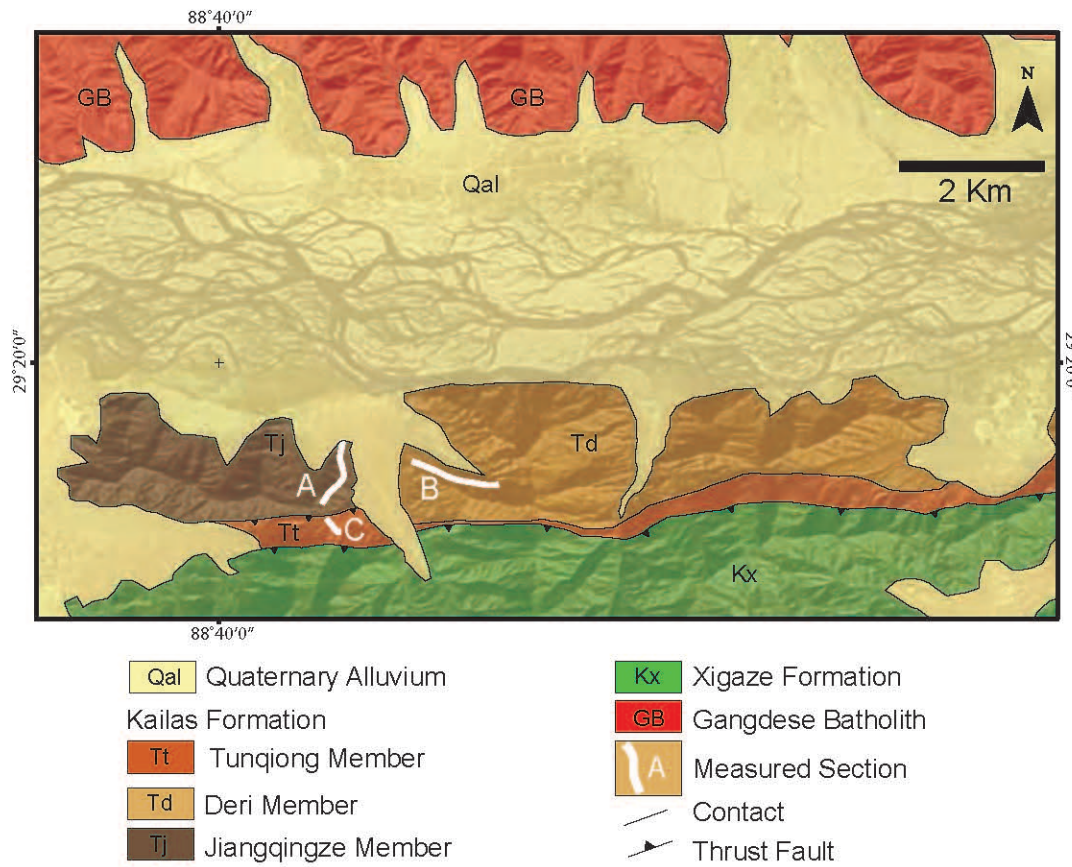


Figure 4. Geologic map of the Xigaze locality based on this study and Wang et al. (2013).



Fig. 5. Oblique view of satellite imagery (Google Earth) showing intense deformation of the Kailas Formation. Measured section start and end marked by a, b, c, and a', b', and c', respectively. GCT: Great Counter Thrust.



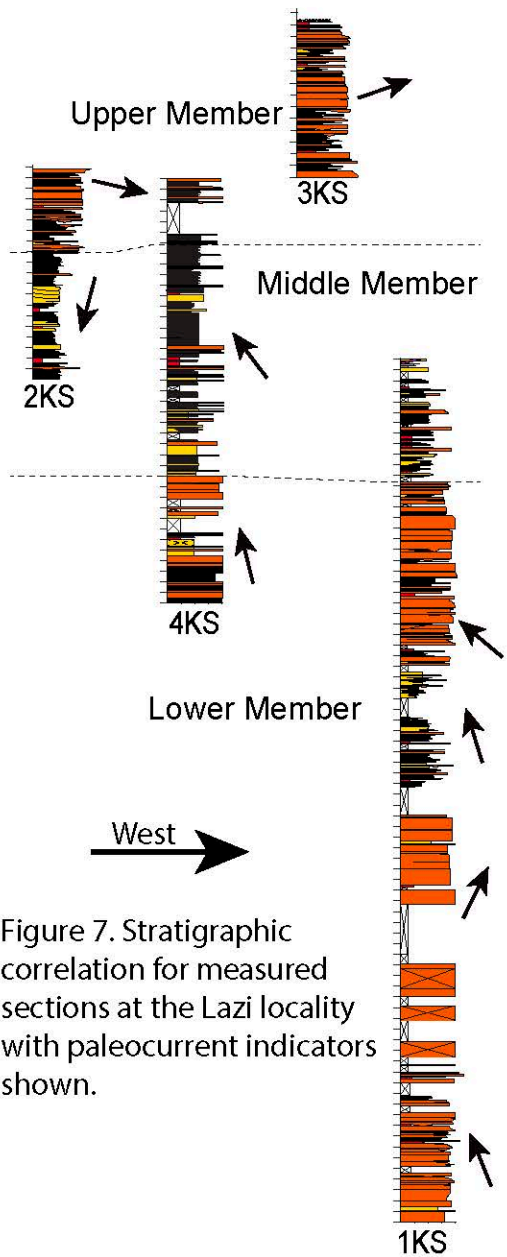
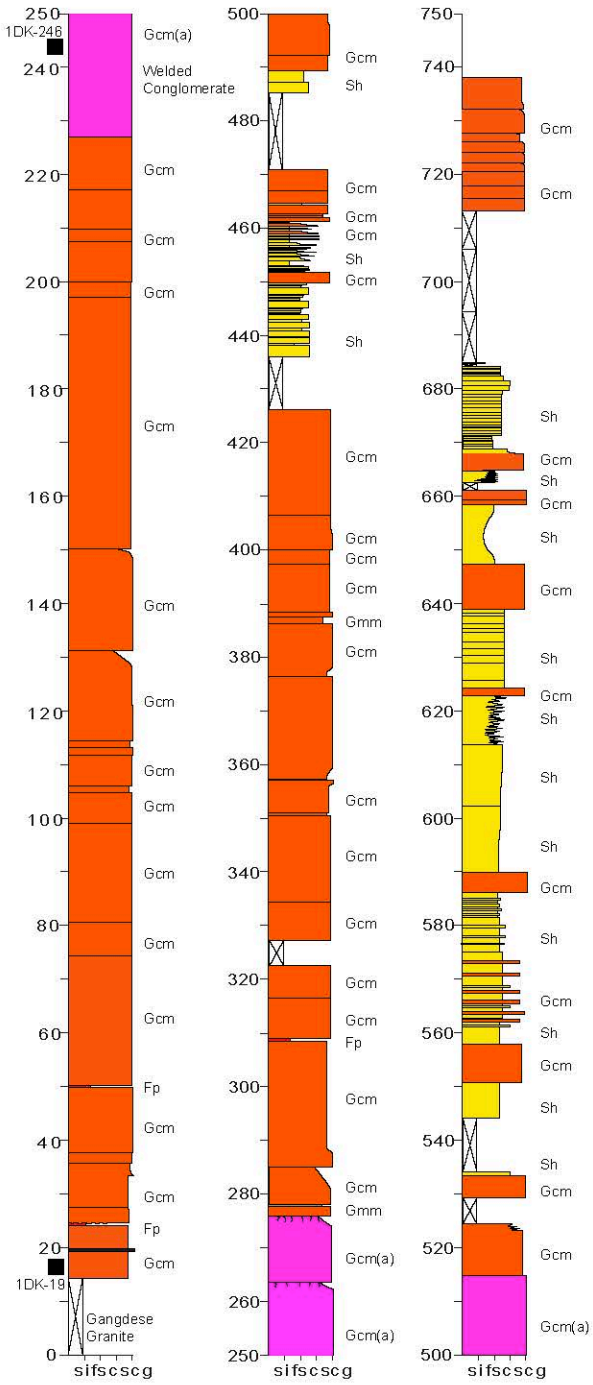


Figure 7. Stratigraphic correlation for measured sections at the Lazi locality with paleocurrent indicators shown.





**1DK** N29.30775  
E89.82238

Figure 9. Measured section from Dazhuka locality. Stratigraphic height is in meters. See Fig. 2 for location. See Table 1 for lithofacies codes.

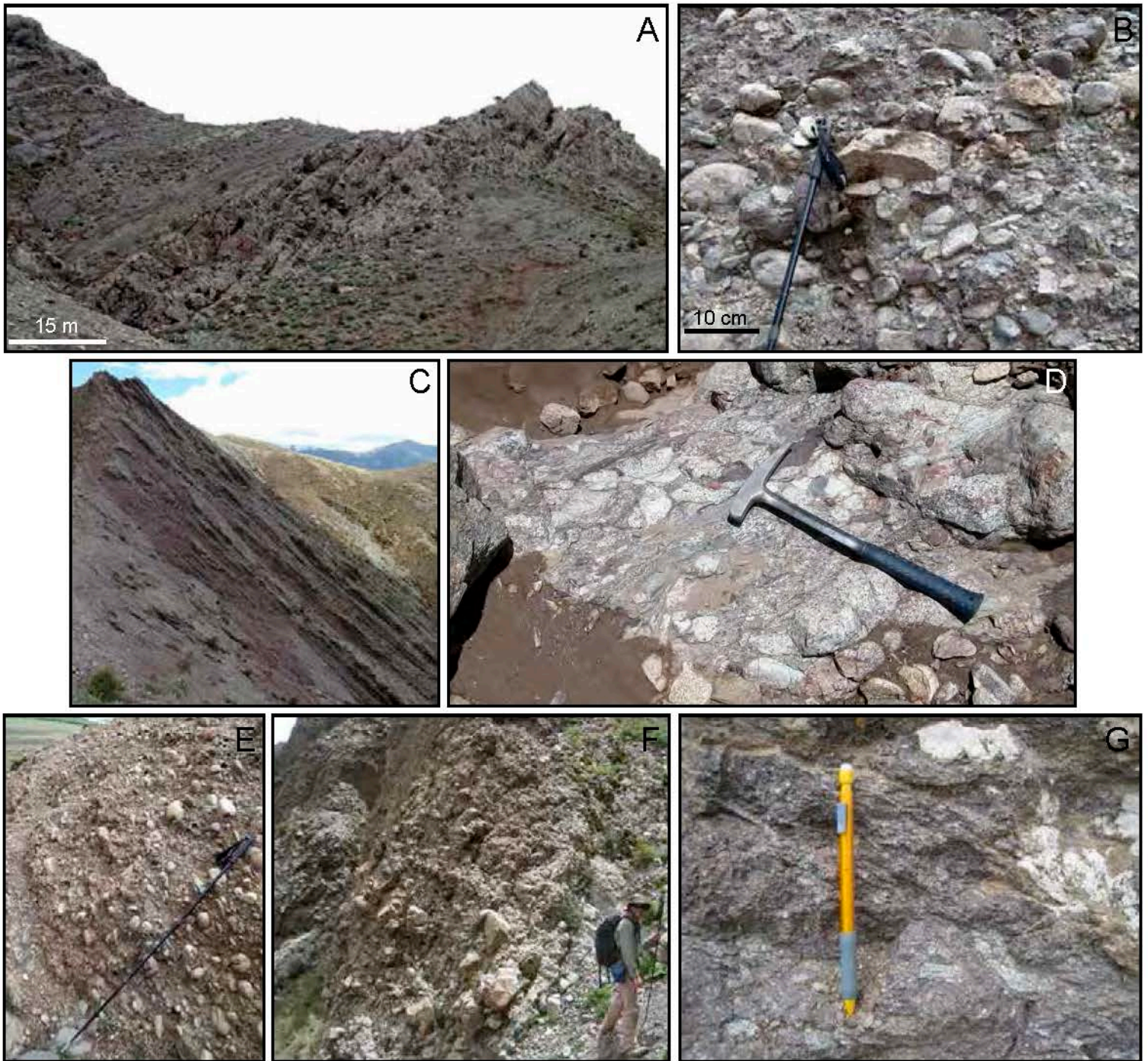


Figure 10. Photographs of Kailas Formation outcrops. A) Middle member at section 2KS, Lhatse locality showing lateral accretion elements. B) Weakly imbricated clast-supported cobble conglomerate from the lower member of section 1KS, Lhatse locality. C) Upper member at 3KS, Lhatse locality. D) Ductilely deformed granitic clasts within the mylonitic shear zone cutting the Kailas Formation; Lhatse locality. E) Imbricated clast-supported cobble conglomerate, Deri Member, Xigaze locality. Jake staff is 1.5 m. F) Lower member, section 1DK, Dazhuka locality. G) Trachy-andesite within a welded conglomerate, Dazhuka locality.

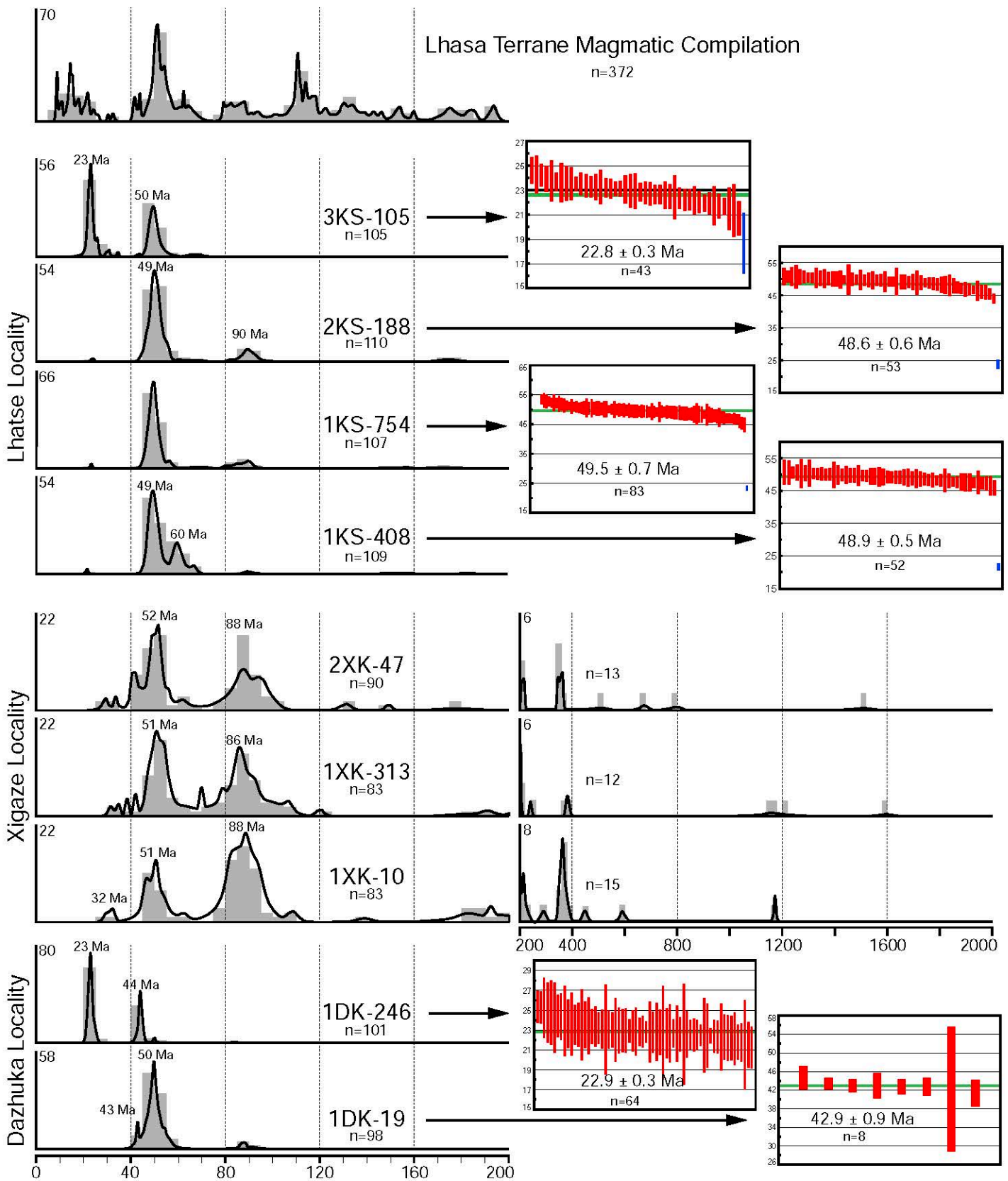


Fig. 11. Probability density plots, histograms, and maximum depositional ages of Kailas Formation detrital zircons (see Figs. 2-4 for locations). Histogram bin width is 5 Ma for 0-200 Ma plots and 20 Ma for 200-2000 Ma plots. Number at top left of each plot indicates the maximum vertical extent of the histogram y-axis. Maximum depositional ages calculated Unmix Ages (Ludwig, 2012) and by weighted average. Uncertainty reported is total 2 sigma uncertainty. Analyses in blue were excluded in the weighted average. Sources for Lhasa terrane compilation: Quidelleur et al., 1997; Chung et al., 2003; Mo et al., 2005; Kapp et al., 2005; Guynn et al., 2006; He et al., 2007; Kapp et al., 2007; Ji et al., 2009; Volkmer et al., 2007; Wen et al., 2008; Xu et al., 2010; Zhu et al., 2009; 2010; 2011; DeCelles et al., 2011.

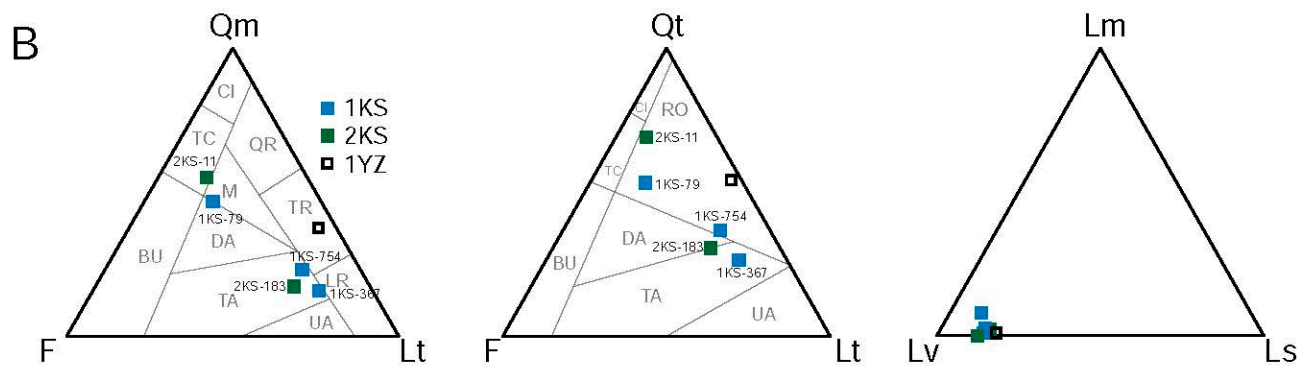
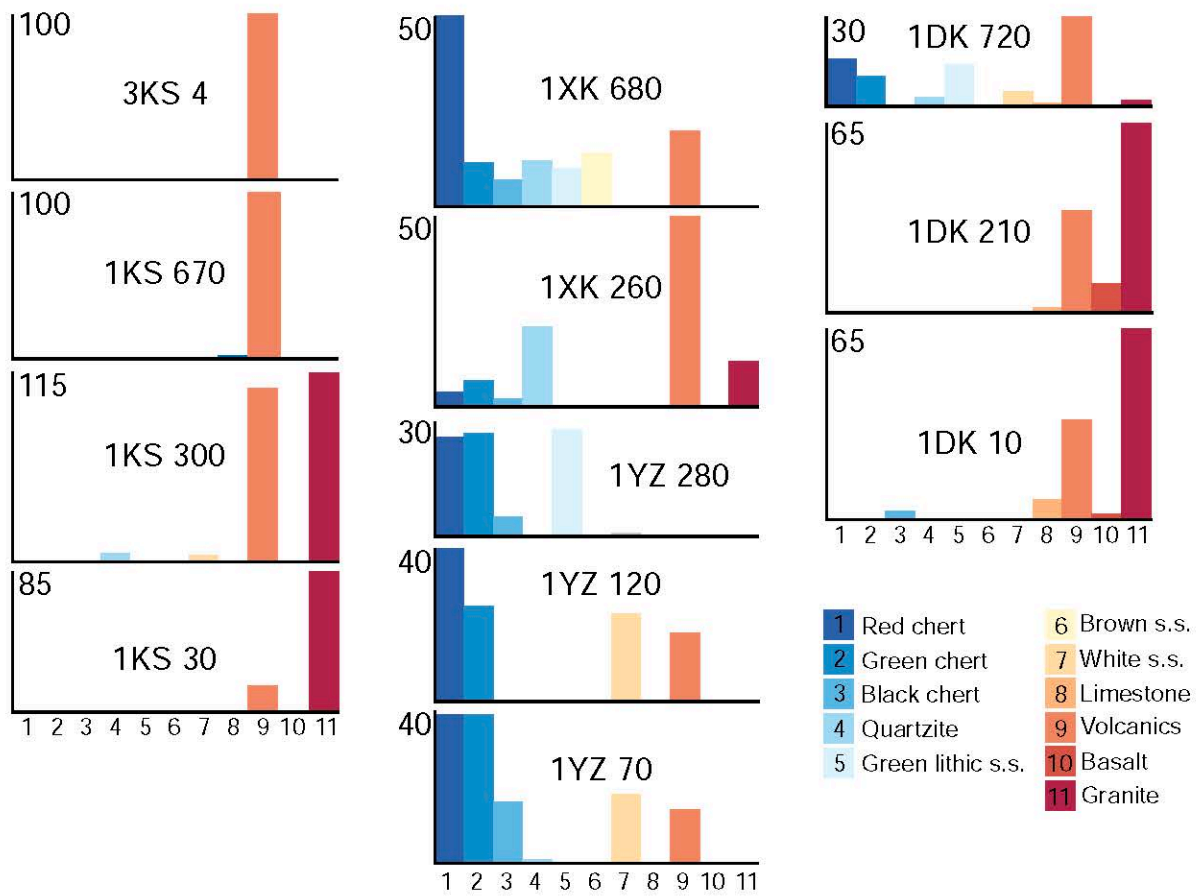


Figure 12. A) 1- red chert, 2- green chert, 3- black chert, 4- quartzite, 5- green lithic sandstone, 6- brown sandstone, 7- white sandstone, 8- limestone, 9- volcanic, 10- basalt, 11- granite B) results of sandstone points. Fields after Dickinson (1985).

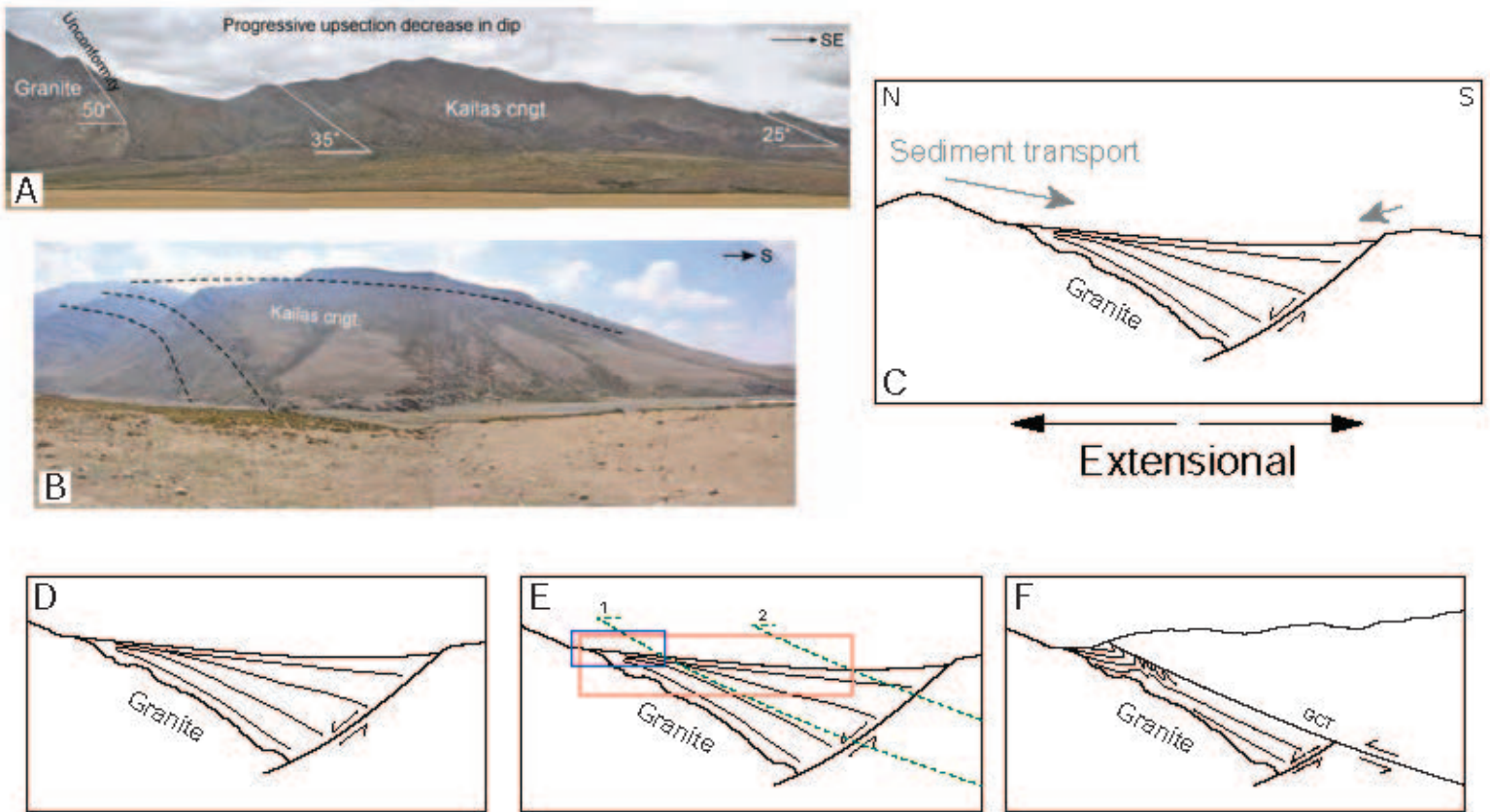


Fig. 13. Photographs from Wang et al., 2015, S11-8a, showing extensional growth strata within the Kailas Conglomerate taken (A) 15 km and (B) 5 km west of Mt. Kailas in western Tibet (81° E). C) Schematic depiction of our interpretation of the structure of the Kailas Basin, matching growth structures shown in (A) and (B). D-F) Schematic post-depositional evolution of the Kailas Basin. D) Schematic cross section of the Kailas Basin near the end of sedimentation. E) Schematic cross section showing future locations of GCT in this study area (1) and western Tibet (~81° E) (2). Blue box shows currently exposed portion of the basin in this study area; red box shows currently exposed basin in western Tibet. F) Schematic cross section of modern Kailas Basin structure. GCT: Great Counter Thrust.

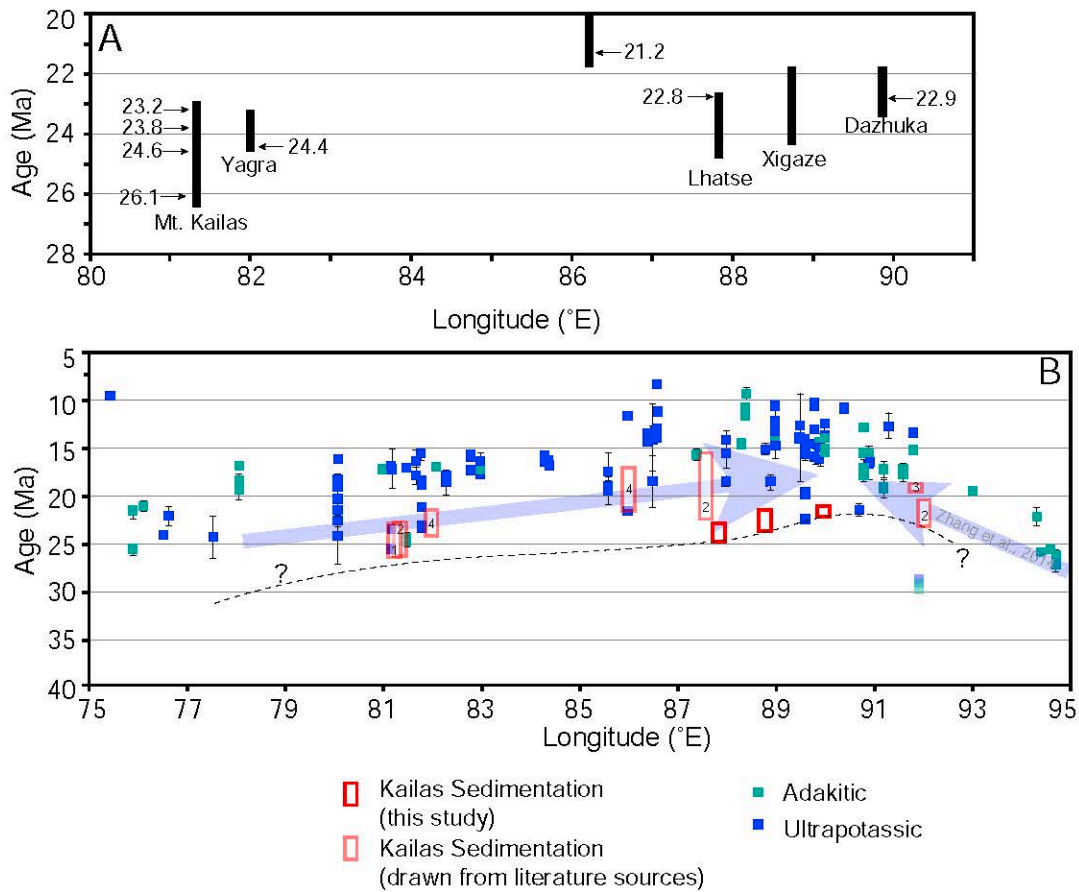


Figure 14. A) Spatio-temporal distribution of Kailas Formation sedimentation within the India-Asia suture zone from this study, DeCelles et al. (2011), and Carrapa et al. (2014). Age control shown with arrows. Basin initiation calculated using average sedimentation rates from DeCelles et al. (2011). B) Spatio-temporal distribution of adakitic and ultrapotassic rocks near the India-Asia suture zone compared to Gangrinboche sedimentation (red boxes). Sedimentary data sources: 1: Kailas Formation, DeCelles et al. (2011); 2: Gangdese Conglomerate, Li et al. (2015); 3: Luobusa Conglomerate, Kong et al. (2015); 4: Kailas Formation, Carrapa et al., 2014; Magmatic data sources: Zhang et al. (2014)'s compilation and references therein, Rex et al. (1988), Parrish and Tirrul (1989), Schärer et al. (1990), Maheo et al. (2002), and Ravikant (2006). Trends are indicated with blue arrows.

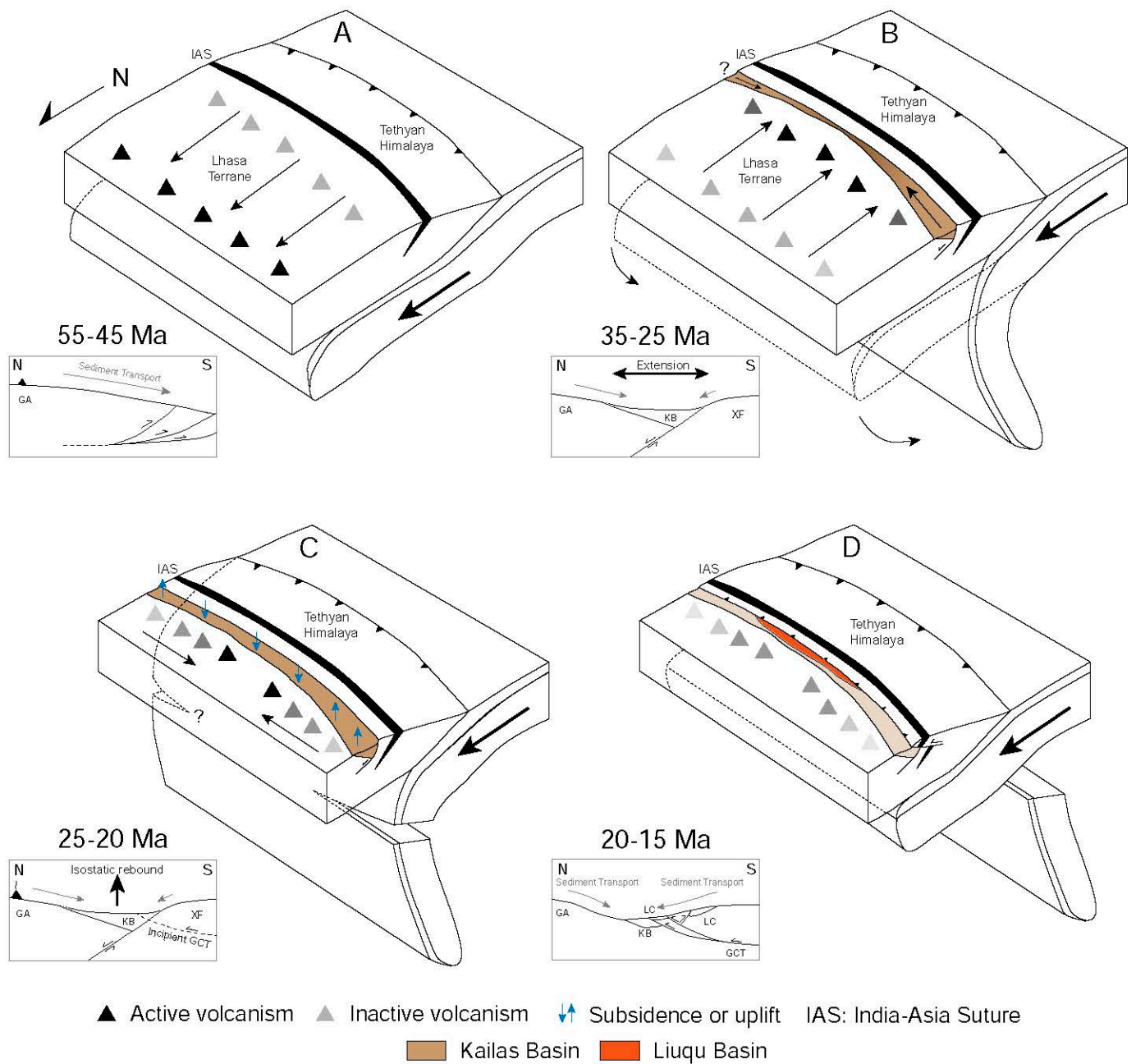


Figure 15. Schematic diagrams showing the tectonic evolution of the India-Asia suture zone. Boxes show 2D north-south cross sections of the central suture zone. A: Following India-Asia collision, the Indian continental slab is underthrust beneath the Lhasa Terrane driving magmatism northward. B: Beginning around 35 Ma, Indian slab rollback causes the southward migration of magmatism as well as formation of the Kailas Basin in the India-Asia suture zone. C: Beginning around 25 Ma, a tear initiates along the edge(s) of the Indian slab producing rapid subsidence followed by uplift. This also initiates a pulse of ultrapotassic and adakitic magmatism in the southern Lhasa terrane. Both of these processes follow the slab tear and migrate toward the center of the suture zone. D: Around 20 Ma, the Indian slab breaks off completely and the contractional deformation resumes in the suture zone. The Liuqu Conglomerate is deposited in the central suture zone in a wedge-top position within the GCT system.

U-Pb geochronologic analyses.							
						Isotope ratios	
Analysis	U	206Pb	U/Th	206Pb*	±	207Pb*	±
	(ppm)	204Pb		207Pb*	(%)	235U*	(%)
Sample:	1KS-408	N29.36290		E87.79128			
1KS-408-Spot 8	496	10745	0.8	19.7296	4.5	0.0234	5.1
1KS-408-Spot 49	313	4275	1.0	23.7780	6.8	0.0414	7.2
1KS-408-Spot 16	1034	39474	1.2	21.5697	4.0	0.0462	5.1
1KS-408-Spot 37	504	3384	1.3	23.0351	5.6	0.0439	6.1
1KS-408-Spot 57	1158	14405	0.6	20.3855	3.0	0.0498	3.6
1KS-408-Spot 31	1167	36723	1.3	20.9884	3.3	0.0485	5.0
1KS-408-Spot 36	642	27153	1.6	21.5089	3.6	0.0474	4.0
1KS-408-Spot 27	942	14491	1.6	20.5301	3.4	0.0497	4.5
1KS-408-Spot 104	864	9801	1.3	22.0026	3.4	0.0463	4.5
1KS-408-Spot 81	1070	39381	0.9	20.9102	4.5	0.0489	5.2
1KS-408-Spot 32	301	5322	2.8	20.8710	8.7	0.0490	8.9
1KS-408-Spot 29	1279	43781	1.0	19.8262	3.3	0.0517	3.6
1KS-408-Spot 61	766	14563	1.2	21.1781	5.3	0.0486	5.8
1KS-408-Spot 92	1020	12116	1.1	21.7516	4.2	0.0474	5.6
1KS-408-Spot 100	1071	61094	1.0	20.9887	4.0	0.0492	4.4
1KS-408-Spot 58	310	8185	1.8	20.7493	5.6	0.0498	5.8
1KS-408-Spot 102	1209	19853	1.1	21.1754	3.0	0.0488	3.8
1KS-408-Spot 74	896	11169	1.0	21.6779	3.3	0.0478	3.9
1KS-408-Spot 88	1020	24212	1.1	20.1926	3.4	0.0516	3.9
1KS-408-Spot 71	1755	49725	0.6	19.7549	3.3	0.0528	4.0
1KS-408-Spot 76	717	125622	1.8	19.0780	3.0	0.0548	4.1
1KS-408-Spot 5	751	12267	1.5	21.8270	3.9	0.0479	4.5
1KS-408-Spot 30	552	11303	1.2	22.2324	4.9	0.0473	5.6
1KS-408-Spot 35	487	6919	1.5	21.4853	4.5	0.0490	5.2
1KS-408-Spot 95	821	6614	4.9	21.5562	3.4	0.0489	4.0
1KS-408-Spot 60	742	40515	1.2	21.3021	3.3	0.0495	3.9
1KS-408-Spot 33	545	16281	1.2	21.4630	4.1	0.0491	4.5
1KS-408-Spot 10	1342	43334	0.8	20.2194	4.2	0.0522	4.6
1KS-408-Spot 105	285	136976	2.2	14.9082	9.4	0.0709	9.7
1KS-408-Spot 23	1294	20052	1.1	19.5981	4.1	0.0539	5.1
1KS-408-Spot 91	604	60102	1.2	20.2562	5.0	0.0523	5.6
1KS-408-Spot 62	312	98564	2.1	20.5694	6.5	0.0516	7.0
1KS-408-Spot 68	1782	25954	1.0	21.6727	4.0	0.0490	4.4
1KS-408-Spot 4	1505	18917	13.3	16.7374	2.8	0.0635	3.2
1KS-408-Spot 41	316	3720	2.7	21.9352	7.6	0.0485	8.2
1KS-408-Spot 64	564	18652	1.3	20.9749	4.7	0.0509	5.2
1KS-408-Spot 47	530	12460	3.2	21.9862	5.5	0.0486	6.0
1KS-408-Spot 98	631	49388	0.9	20.2407	2.8	0.0529	3.9
1KS-408-Spot 12	564	22858	1.5	18.2460	4.2	0.0586	4.7
1KS-408-Spot 51	876	28989	1.2	21.2535	3.6	0.0504	4.6

1KS-408-Spot 96	614	16089	3.4	22.4339	5.9	0.0477	7.1
1KS-408-Spot 107	468	40634	1.8	14.3225	10.2	0.0750	10.4
1KS-408-Spot 101	831	32313	2.0	20.5061	4.0	0.0524	4.4
1KS-408-Spot 66	549	14945	0.7	21.2975	3.2	0.0505	3.7
1KS-408-Spot 84	605	4435	0.7	22.1231	4.3	0.0487	4.7
1KS-408-Spot 55	678	6744	1.5	22.2495	3.6	0.0484	4.0
1KS-408-Spot 65	842	25600	1.8	20.5971	3.6	0.0525	5.3
1KS-408-Spot 72	657	6323	1.3	21.4193	4.3	0.0505	5.0
1KS-408-Spot 80	552	8001	1.4	21.0760	4.4	0.0514	6.4
1KS-408-Spot 56	1681	41461	0.6	14.6105	11.1	0.0743	11.3
1KS-408-Spot 85	604	39544	1.0	21.4644	4.2	0.0506	4.6
1KS-408-Spot 50	303	6823	1.0	20.8667	5.3	0.0520	6.4
1KS-408-Spot 75	916	25474	1.1	20.8423	4.4	0.0522	5.8
1KS-408-Spot 83	327	9511	1.8	19.9464	7.0	0.0548	7.4
1KS-408-Spot 46	567	6865	1.3	22.3822	4.1	0.0489	4.6
1KS-408-Spot 69	970	16985	1.4	21.4876	4.5	0.0510	4.8
1KS-408-Spot 1	686	6969	0.7	13.9208	9.6	0.0795	9.7
1KS-408-Spot 77	426	44133	1.2	18.6358	4.7	0.0594	5.3
1KS-408-Spot 18	466	12655	3.3	21.4470	5.0	0.0518	6.1
1KS-408-Spot 67	869	7440	0.5	11.6735	16.3	0.0952	16.5
1KS-408-Spot 42	1141	39630	0.7	20.4515	3.3	0.0543	3.9
1KS-408-Spot 14	3412	26084	0.7	21.1678	1.6	0.0526	2.3
1KS-408-Spot 93	252	14124	1.5	20.2905	6.0	0.0549	6.9
1KS-408-Spot 2	898	99211	1.2	20.4689	4.0	0.0546	4.7
1KS-408-Spot 9	877	35337	1.7	22.7640	4.7	0.0491	5.0
1KS-408-Spot 63	388	8390	1.7	19.4450	4.0	0.0578	4.5
1KS-408-Spot 86	4265	67128	0.6	20.9704	2.4	0.0536	3.2
1KS-408-Spot 99	712	9777	1.5	10.5146	18.7	0.1072	18.9
1KS-408-Spot 48	544	15193	1.5	8.2272	33.0	0.1371	33.2
1KS-408-Spot 108	533	5942	0.8	21.3145	6.0	0.0538	6.3
1KS-408-Spot 26	1788	13838	1.2	21.7656	2.2	0.0534	3.1
1KS-408-Spot 106	2297	38520	1.8	20.5454	2.6	0.0575	2.9
1KS-408-Spot 17	1107	11768	5.5	7.8534	35.8	0.1517	36.0
1KS-408-Spot 24	531	10721	1.8	22.4390	4.2	0.0542	5.7
1KS-408-Spot 39	883	35730	2.4	20.8833	4.0	0.0584	4.4
1KS-408-Spot 34	263	4408	2.3	22.0975	6.0	0.0559	6.5
1KS-408-Spot 28	627	7997	1.5	21.0699	3.8	0.0593	4.2
1KS-408-Spot 53	1016	38627	1.4	20.8279	3.0	0.0601	3.6
1KS-408-Spot 59	401	14695	2.3	20.5816	6.6	0.0609	7.5
1KS-408-Spot 15	592	20266	2.9	22.1946	4.0	0.0572	4.3
1KS-408-Spot 89	1129	104000	2.4	20.6676	3.5	0.0615	4.2
1KS-408-Spot 44	1185	95169	1.9	21.0059	3.3	0.0606	3.8
1KS-408-Spot 97	127	4055	2.3	22.2683	9.6	0.0572	10.0
1KS-408-Spot 11	243	8818	3.2	19.1450	7.1	0.0667	7.4
1KS-408-Spot 110	806	27338	1.6	20.9791	2.8	0.0611	3.9
1KS-408-Spot 82	1272	21588	1.1	21.4586	2.8	0.0598	4.1
1KS-408-Spot 21	1685	33138	1.3	20.2061	3.1	0.0636	3.8

1KS-408-Spot 22	451	6049	2.1	22.3836	5.0	0.0575	5.3
1KS-408-Spot 13	405	16727	2.2	22.7556	5.0	0.0566	5.6
1KS-408-Spot 43	1063	29612	1.6	19.9379	4.3	0.0647	4.9
1KS-408-Spot 94	2086	54314	0.9	21.0466	1.7	0.0616	2.3
1KS-408-Spot 7	2047	41483	0.8	20.9360	3.5	0.0622	3.9
1KS-408-Spot 3	2661	54941	1.2	20.7122	2.5	0.0636	3.5
1KS-408-Spot 87	382	3636	3.0	14.8314	6.8	0.0891	7.2
1KS-408-Spot 109	3870	30197	5.1	20.6971	1.9	0.0640	2.3
1KS-408-Spot 20	836	19435	2.2	21.8476	3.8	0.0608	4.5
1KS-408-Spot 19	751	19316	1.5	20.6531	4.2	0.0651	4.8
1KS-408-Spot 70	250	11602	2.0	20.9098	6.5	0.0647	7.0
1KS-408-Spot 103	840	28750	1.7	21.1587	3.0	0.0647	3.5
1KS-408-Spot 73	770	106054	1.6	16.6719	6.7	0.0834	7.6
1KS-408-Spot 25	9013	30779	13.3	13.8592	10.4	0.1023	10.6
1KS-408-Spot 40	224	7276	1.2	21.7224	5.6	0.0657	5.9
1KS-408-Spot 6	4381	49247	0.7	21.4385	2.7	0.0671	3.0
1KS-408-Spot 45	3880	109793	1.0	21.2796	1.5	0.0689	2.4
1KS-408-Spot 79	883	32786	1.4	20.7181	1.7	0.0930	2.3
1KS-408-Spot 54	136	2187	1.1	2.4326	12.0	0.8123	12.3
1KS-408-Spot 90	448	36861	1.0	20.6359	3.5	0.1584	4.6
1KS-408-Spot 38	338	45797	1.2	19.4299	3.0	0.1750	4.2
1KS-408-Spot 78	409	90670	1.1	19.7987	2.5	0.2006	3.2

Sample:	1KS-754	N29.36008	E87.78842				
1KS-754-Spot 83	595	6442	2.5	21.1547	3.6	0.0235	4.1
1KS-754-Spot 98	229	95237	0.7	20.0878	5.2	0.0479	5.9
1KS-754-Spot 49	214	4992	0.9	20.6378	5.0	0.0472	5.5
1KS-754-Spot 15	320	11770	0.7	20.8730	4.7	0.0473	5.2
1KS-754-Spot 8	638	27982	4.0	21.4194	3.0	0.0469	3.4
1KS-754-Spot 82	201	21239	1.2	21.0599	5.4	0.0477	5.8
1KS-754-Spot 51	688	31074	1.0	21.5555	2.4	0.0467	2.8
1KS-754-Spot 81	349	16545	0.6	19.0063	4.4	0.0530	4.7
1KS-754-Spot 77	822	48549	0.8	21.5493	2.8	0.0469	3.2
1KS-754-Spot 75	167	43509	1.3	20.4605	6.2	0.0495	6.5
1KS-754-Spot 78	297	8931	1.6	20.3720	3.3	0.0498	3.9
1KS-754-Spot 36	84	2722	1.4	19.9277	9.2	0.0511	9.8
1KS-754-Spot 110	197	7590	1.4	20.4365	5.1	0.0501	5.7
1KS-754-Spot 10	194	13830	1.4	20.0944	5.9	0.0512	6.2
1KS-754-Spot 33	107	3476	1.2	20.6279	7.9	0.0499	8.2
1KS-754-Spot 45	135	21899	1.4	20.5469	5.2	0.0504	5.9
1KS-754-Spot 64	89	18561	0.9	20.1539	6.5	0.0514	7.5
1KS-754-Spot 70	202	4962	1.5	21.0925	6.4	0.0491	6.6
1KS-754-Spot 105	173	7249	1.2	19.1344	5.5	0.0542	6.2
1KS-754-Spot 100	115	42840	1.0	20.5209	4.8	0.0506	5.6
1KS-754-Spot 31	69	20086	1.2	19.0505	7.7	0.0546	8.6
1KS-754-Spot 89	83	7380	1.5	21.9090	8.4	0.0475	8.9
1KS-754-Spot 109	269	12444	1.8	21.3345	4.7	0.0488	5.2

1KS-754-Spot 56	235	6853	1.2	21.4268	5.1	0.0486	5.5
1KS-754-Spot 95	203	19742	1.6	21.4401	3.4	0.0486	4.1
1KS-754-Spot 4	145	6773	1.6	20.5489	6.7	0.0508	7.1
1KS-754-Spot 92	132	8687	1.5	23.2234	4.6	0.0450	5.2
1KS-754-Spot 20	121	5209	0.9	22.7928	6.2	0.0460	6.7
1KS-754-Spot 39	133	12597	1.9	18.1641	7.9	0.0578	8.1
1KS-754-Spot 87	217	15191	0.9	20.8802	5.9	0.0504	6.3
1KS-754-Spot 40	413	81391	1.6	20.7935	3.9	0.0507	4.4
1KS-754-Spot 26	229	45407	2.0	20.5714	5.9	0.0513	6.2
1KS-754-Spot 2	262	31733	1.9	20.9091	4.5	0.0505	5.1
1KS-754-Spot 28	228	6040	1.1	20.7034	5.9	0.0510	6.2
1KS-754-Spot 61	387	11052	1.1	21.3322	4.6	0.0495	5.1
1KS-754-Spot 17	51	7352	0.9	27.1374	6.6	0.0389	7.5
1KS-754-Spot 59	162	6155	1.4	21.1499	5.6	0.0500	5.8
1KS-754-Spot 23	137	6192	1.0	23.3996	4.8	0.0452	5.2
1KS-754-Spot 7	127	13252	1.1	19.5262	7.5	0.0542	8.0
1KS-754-Spot 43	141	18071	2.1	21.2175	6.0	0.0499	6.3
1KS-754-Spot 47	403	23256	1.4	21.4741	3.1	0.0493	3.7
1KS-754-Spot 3	241	8553	2.3	21.6352	4.1	0.0490	4.5
1KS-754-Spot 38	108	11259	1.1	22.2862	7.2	0.0475	7.5
1KS-754-Spot 16	190	11559	1.6	18.8559	6.9	0.0562	7.1
1KS-754-Spot 107	272	14088	1.4	22.0763	5.9	0.0480	6.2
1KS-754-Spot 67	140	11053	1.4	21.5164	6.9	0.0493	7.3
1KS-754-Spot 80	410	17669	1.5	21.2934	3.3	0.0499	3.9
1KS-754-Spot 58	152	11013	1.2	20.2966	5.9	0.0524	6.4
1KS-754-Spot 108	175	17693	1.1	20.7320	4.9	0.0515	5.2
1KS-754-Spot 66	111	3692	1.1	20.8962	7.0	0.0511	7.4
1KS-754-Spot 1	254	11307	0.7	21.7123	4.2	0.0493	4.6
1KS-754-Spot 96	106	2432	1.5	22.9679	9.9	0.0466	10.2
1KS-754-Spot 50	220	6590	1.1	22.3873	4.6	0.0480	5.0
1KS-754-Spot 91	128	5232	1.1	20.2787	7.5	0.0530	8.0
1KS-754-Spot 22	140	6166	1.8	21.9269	6.0	0.0490	6.3
1KS-754-Spot 97	522	33526	0.6	21.2486	3.0	0.0506	3.3
1KS-754-Spot 21	126	9674	1.7	20.7024	6.3	0.0520	6.8
1KS-754-Spot 99	102	4487	0.9	22.6072	5.3	0.0476	5.9
1KS-754-Spot 79	211	17265	1.6	20.6564	4.6	0.0522	5.1
1KS-754-Spot 52	86	5197	1.4	22.5216	5.7	0.0479	6.2
1KS-754-Spot 68	148	20419	1.5	20.4506	7.0	0.0529	7.4
1KS-754-Spot 55	193	5039	1.5	22.1107	6.2	0.0490	6.6
1KS-754-Spot 53	215	10605	1.2	21.2113	4.7	0.0511	5.5
1KS-754-Spot 86	219	60762	0.9	20.8927	5.5	0.0519	5.9
1KS-754-Spot 57	98	25512	1.4	19.1671	4.0	0.0566	5.0
1KS-754-Spot 65	317	9700	0.7	20.0300	3.5	0.0542	4.1
1KS-754-Spot 104	94	3556	0.8	23.8176	7.3	0.0456	7.5
1KS-754-Spot 29	139	33047	1.4	20.8598	7.1	0.0521	7.3
1KS-754-Spot 60	569	42013	0.5	21.3803	3.5	0.0511	4.0
1KS-754-Spot 14	253	9131	1.3	22.3304	3.9	0.0490	4.2

1KS-754-Spot 101	229	7780	0.9	21.7523	4.7	0.0504	5.3
1KS-754-Spot 90	455	16792	0.7	20.3595	2.5	0.0540	2.9
1KS-754-Spot 76	501	28465	1.2	20.9727	3.4	0.0526	3.7
1KS-754-Spot 74	278	32795	1.7	21.7300	4.1	0.0508	4.6
1KS-754-Spot 63	168	33656	1.0	19.6710	5.3	0.0566	5.7
1KS-754-Spot 106	119	3336	1.3	18.8704	9.3	0.0591	9.6
1KS-754-Spot 103	279	9695	1.0	22.0553	3.8	0.0508	4.2
1KS-754-Spot 84	111	19275	1.5	17.0042	7.1	0.0660	7.6
1KS-754-Spot 27	970	65498	0.6	21.1038	2.8	0.0533	3.2
1KS-754-Spot 32	225	117427	1.8	20.9854	3.9	0.0540	4.2
1KS-754-Spot 73	369	13603	1.1	21.4851	3.0	0.0528	3.7
1KS-754-Spot 5	226	12633	2.0	22.6701	5.6	0.0503	6.0
1KS-754-Spot 25	206	32914	1.6	19.4842	4.6	0.0589	4.9
1KS-754-Spot 12	118	45234	1.3	5.9402	38.9	0.1943	39.1
1KS-754-Spot 24	350	140080	1.3	20.9483	3.5	0.0573	3.8
1KS-754-Spot 42	212	39204	1.9	20.7310	5.9	0.0585	6.1
1KS-754-Spot 13	59	11900	1.9	20.3397	8.0	0.0599	8.4
1KS-754-Spot 94	101	3528	0.8	6.5710	3.8	0.1854	4.9
1KS-754-Spot 62	166	17842	1.8	5.9043	49.8	0.2277	50.1
1KS-754-Spot 9	102	1978	1.9	3.6937	8.6	0.3944	9.2
1KS-754-Spot 19	102	4906	3.0	18.1074	6.9	0.0846	7.3
1KS-754-Spot 18	466	25723	1.5	20.6080	2.6	0.0838	2.9
1KS-754-Spot 72	69	39100	2.5	20.6042	5.5	0.0871	6.3
1KS-754-Spot 30	52	6588	1.9	20.7046	7.5	0.0874	8.2
1KS-754-Spot 93	121	21190	2.4	20.4814	4.9	0.0887	5.4
1KS-754-Spot 35	197	43317	1.7	19.8801	3.5	0.0930	3.9
1KS-754-Spot 11	87	14235	2.4	20.0521	5.9	0.0925	6.3
1KS-754-Spot 37	236	32299	1.5	21.0005	3.7	0.0915	4.0
1KS-754-Spot 34	133	220086	1.5	19.9995	4.8	0.0962	5.2
1KS-754-Spot 44	914	46144	0.8	20.8227	1.7	0.0928	2.4
1KS-754-Spot 88	167	128262	1.5	20.0481	4.0	0.0964	4.5
1KS-754-Spot 46	194	57972	1.9	19.6035	3.9	0.0995	4.2
1KS-754-Spot 71	185	39493	1.5	18.9405	5.8	0.1044	6.2
1KS-754-Spot 102	222	20785	1.8	20.9509	2.2	0.1538	2.8
1KS-754-Spot 85	1483	160902	3.3	20.1428	1.3	0.1684	1.7
1KS-754-Spot 69	155	48758	2.5	20.0944	3.0	0.1854	4.2
1KS-754-Spot 6	214	150994	2.1	19.9195	2.5	0.1900	3.4

Sample:	2KS-188	N29.35435	E87.80480				
2KS-188-Spot 57	998	27552	3.3	20.3761	3.8	0.0250	4.8
2KS-188-Spot 1	755	35600	1.1	21.3239	4.3	0.0442	4.6
2KS-188-Spot 40	756	51878	0.6	20.1458	3.1	0.0484	3.6
2KS-188-Spot 92	186	13098	1.0	19.1419	7.5	0.0516	7.9
2KS-188-Spot 22	436	12097	0.9	20.5750	4.7	0.0480	5.2
2KS-188-Spot 98	44	778	1.0	58.8188	9.2	0.0169	9.8
2KS-188-Spot 42	391	32165	1.7	21.0267	4.4	0.0477	4.6
2KS-188-Spot 6	1298	49737	0.8	21.1286	2.3	0.0475	3.0

2KS-188-Spot 24	237	11453	1.2	20.9958	5.8	0.0478	6.3
2KS-188-Spot 91	1245	34813	3.5	20.8928	2.7	0.0484	3.2
2KS-188-Spot 10	683	30438	1.6	21.7328	3.5	0.0468	4.0
2KS-188-Spot 43	94	14153	1.0	20.2408	9.4	0.0507	9.8
2KS-188-Spot 68	188	50541	1.6	20.0233	9.3	0.0515	9.9
2KS-188-Spot 72	84	4494	1.1	19.9804	10.5	0.0517	10.9
2KS-188-Spot 51	112	3816	1.4	22.2400	7.4	0.0466	7.8
2KS-188-Spot 16	581	7934	1.5	19.3589	5.2	0.0536	5.5
2KS-188-Spot 20	851	40153	1.5	21.0866	3.2	0.0494	3.7
2KS-188-Spot 2	450	27506	0.7	20.1820	3.3	0.0519	3.7
2KS-188-Spot 54	187	22129	1.7	19.0811	6.7	0.0549	6.9
2KS-188-Spot 39	276	29221	1.5	21.4859	5.5	0.0488	5.9
2KS-188-Spot 19	55	1500	1.9	25.6621	9.8	0.0409	10.5
2KS-188-Spot 55	204	46305	1.2	22.1256	6.5	0.0475	7.0
2KS-188-Spot 74	780	25024	1.7	21.4045	2.8	0.0492	3.3
2KS-188-Spot 47	181	35671	0.9	20.1592	6.2	0.0523	6.6
2KS-188-Spot 96	173	5296	1.6	22.0070	7.0	0.0480	7.3
2KS-188-Spot 52	63	3514	1.5	19.9864	10.2	0.0529	11.1
2KS-188-Spot 7	696	30786	1.0	21.3818	4.2	0.0494	4.4
2KS-188-Spot 53	532	25796	1.3	21.3928	3.3	0.0494	3.6
2KS-188-Spot 78	461	26250	1.6	21.4266	3.7	0.0493	4.8
2KS-188-Spot 109	186	5396	1.5	22.7172	6.2	0.0468	6.5
2KS-188-Spot 31	612	26791	1.1	20.1051	4.4	0.0529	4.7
2KS-188-Spot 45	176	6072	1.2	21.6166	8.2	0.0492	8.6
2KS-188-Spot 95	182	35859	1.1	20.8962	6.3	0.0510	6.7
2KS-188-Spot 69	367	37207	2.0	22.2173	4.4	0.0480	4.7
2KS-188-Spot 50	132	15516	1.2	17.8947	5.4	0.0597	6.2
2KS-188-Spot 11	198	6994	1.6	22.0729	6.1	0.0484	6.2
2KS-188-Spot 41	469	8987	1.8	21.6582	3.9	0.0494	4.4
2KS-188-Spot 71	294	5228	1.9	22.3897	4.0	0.0478	6.2
2KS-188-Spot 63	169	6517	1.9	21.3036	5.8	0.0503	5.9
2KS-188-Spot 99	406	25616	1.7	19.9350	4.9	0.0537	5.6
2KS-188-Spot 93	333	11113	1.6	21.1877	5.0	0.0506	5.5
2KS-188-Spot 34	135	5742	1.0	23.2097	7.7	0.0463	8.0
2KS-188-Spot 106	1038	60380	0.9	20.4177	2.5	0.0526	3.2
2KS-188-Spot 27	110	17307	1.8	22.1864	8.2	0.0485	8.7
2KS-188-Spot 107	433	9829	1.4	21.6371	3.1	0.0498	3.8
2KS-188-Spot 62	257	20365	1.4	20.9820	6.4	0.0515	7.1
2KS-188-Spot 81	482	35231	2.1	21.4934	4.5	0.0503	4.8
2KS-188-Spot 73	500	12683	1.6	16.6413	9.1	0.0651	9.2
2KS-188-Spot 102	657	46660	0.7	21.6932	4.4	0.0501	4.8
2KS-188-Spot 58	133	33374	1.3	24.3371	6.0	0.0446	6.5
2KS-188-Spot 5	102	28259	1.5	19.2759	9.4	0.0565	10.1
2KS-188-Spot 29	380	44672	1.7	21.4154	5.3	0.0508	6.0
2KS-188-Spot 49	422	17157	1.7	20.9885	4.6	0.0519	4.9
2KS-188-Spot 77	81	2793	1.5	21.2227	8.4	0.0514	8.8
2KS-188-Spot 33	266	6896	1.2	20.9176	6.7	0.0524	7.2

2KS-188-Spot 17	244	33302	1.7	22.0583	5.1	0.0497	5.6
2KS-188-Spot 94	287	43811	0.7	20.9323	4.5	0.0524	4.7
2KS-188-Spot 86	209	10097	1.6	21.4160	5.5	0.0514	6.3
2KS-188-Spot 66	185	32978	1.1	22.8031	7.3	0.0483	7.9
2KS-188-Spot 97	179	20401	1.1	22.0120	5.2	0.0500	5.6
2KS-188-Spot 4	430	35328	0.9	20.7771	2.6	0.0530	3.3
2KS-188-Spot 15	341	18714	0.6	22.2017	5.0	0.0496	5.3
2KS-188-Spot 65	588	14107	1.6	21.9322	4.1	0.0504	4.4
2KS-188-Spot 21	323	7808	1.1	21.1969	5.1	0.0523	5.4
2KS-188-Spot 79	535	57164	1.8	18.2192	6.4	0.0610	6.7
2KS-188-Spot 36	282	29741	1.8	20.1038	5.9	0.0553	6.2
2KS-188-Spot 32	311	22870	1.3	19.2410	5.5	0.0578	5.8
2KS-188-Spot 104	244	9948	1.2	20.0676	6.1	0.0555	6.4
2KS-188-Spot 30	1452	67588	2.5	21.3214	2.5	0.0526	3.2
2KS-188-Spot 44	73	51327	0.9	20.1140	9.7	0.0558	10.2
2KS-188-Spot 108	467	20523	1.7	20.9819	4.6	0.0535	5.0
2KS-188-Spot 46	188	2089	1.2	24.3861	6.2	0.0462	6.4
2KS-188-Spot 37	640	32808	1.2	21.1032	3.9	0.0534	5.4
2KS-188-Spot 56	176	6697	0.4	21.2557	5.6	0.0531	6.7
2KS-188-Spot 18	351	13111	1.6	20.5647	4.6	0.0550	5.4
2KS-188-Spot 35	408	9620	1.7	21.6354	5.1	0.0523	5.6
2KS-188-Spot 60	594	24323	3.2	20.8998	3.3	0.0547	3.8
2KS-188-Spot 82	576	29157	1.7	21.3146	4.2	0.0538	4.5
2KS-188-Spot 38	423	8708	1.7	21.2062	4.8	0.0541	5.6
2KS-188-Spot 26	148	3629	2.6	23.3446	5.4	0.0494	6.3
2KS-188-Spot 48	697	16998	2.1	21.6696	4.1	0.0537	4.6
2KS-188-Spot 23	475	28730	2.1	20.2839	2.8	0.0582	3.3
2KS-188-Spot 89	213	12231	2.1	21.8348	4.3	0.0543	4.6
2KS-188-Spot 85	254	9274	1.8	20.1903	4.6	0.0588	5.1
2KS-188-Spot 64	161	11952	2.5	20.6872	5.2	0.0575	5.7
2KS-188-Spot 3	125	3063	2.3	21.7633	7.5	0.0552	7.8
2KS-188-Spot 13	2792	108044	1.8	21.4685	2.2	0.0560	2.6
2KS-188-Spot 25	84	2609	1.5	5.3338	7.3	0.2408	7.8
2KS-188-Spot 84	43	7410	2.8	18.3592	10.4	0.0750	11.2
2KS-188-Spot 14	3891	22390	0.6	12.1209	9.4	0.1152	11.5
2KS-188-Spot 83	117	5673	2.4	20.6505	8.6	0.0722	9.2
2KS-188-Spot 76	810	33539	39.8	20.5046	2.7	0.0863	3.2
2KS-188-Spot 61	832	41242	3.7	21.1634	3.0	0.0879	3.4
2KS-188-Spot 88	106	3004	2.7	20.7392	6.0	0.0907	6.6
2KS-188-Spot 12	163	18861	2.1	20.8049	6.1	0.0905	7.4
2KS-188-Spot 103	434	30968	1.3	21.5858	3.4	0.0884	3.8
2KS-188-Spot 59	463	127111	2.2	20.6473	3.4	0.0930	3.6
2KS-188-Spot 105	903	25865	2.5	20.6333	2.5	0.0932	2.8
2KS-188-Spot 70	383	226436	3.9	20.5117	4.2	0.0941	4.8
2KS-188-Spot 75	215	12888	2.5	21.8093	5.0	0.0897	5.4
2KS-188-Spot 90	182	6439	2.0	20.7913	4.8	0.0941	5.4
2KS-188-Spot 100	397	66962	1.6	20.2401	2.9	0.0974	3.5

2KS-188-Spot 8	152	2444	1.7	2.6335	0.2	0.7500	4.8
2KS-188-Spot 101	358	17289	1.2	20.3867	4.3	0.0970	4.6
2KS-188-Spot 28	177	10951	1.9	21.4548	4.8	0.0935	5.3
2KS-188-Spot 9	272	619775	1.0	20.3898	3.7	0.1021	5.6
2KS-188-Spot 87	185	44719	2.4	20.4834	3.5	0.1825	4.0
2KS-188-Spot 80	109	9285	2.2	20.0836	4.6	0.1872	5.2
2KS-188-Spot 110	178	17419	2.5	19.5897	3.5	0.1953	3.9
2KS-188-Spot 67	86	6804	2.2	20.5921	5.0	0.1867	5.8

Sample:	3KS-105	N29.35467	E87.79879				
3KS-105-Spot 3	63	524	1.0	44.5786	12.6	0.0090	14.3
3KS-105-Spot 102	446	28495	0.8	19.8530	4.7	0.0223	5.8
3KS-105-Spot 93	1096	25209	2.2	21.0462	4.4	0.0217	6.7
3KS-105-Spot 69	896	10085	1.9	20.8628	4.3	0.0221	5.9
3KS-105-Spot 95	2078	42091	1.8	20.8907	2.4	0.0222	2.9
3KS-105-Spot 110	824	11226	1.3	20.6244	5.4	0.0225	5.9
3KS-105-Spot 36	1409	80614	2.4	21.1406	2.9	0.0220	4.7
3KS-105-Spot 20	844	28187	0.7	17.8420	6.2	0.0263	6.5
3KS-105-Spot 52	1753	49700	0.7	20.6830	2.9	0.0227	3.3
3KS-105-Spot 18	1412	68494	1.6	20.2622	3.4	0.0233	3.9
3KS-105-Spot 49	781	25829	0.9	19.2592	6.2	0.0247	6.7
3KS-105-Spot 63	1251	19987	2.7	21.1771	5.2	0.0225	5.6
3KS-105-Spot 40	1682	52927	2.0	21.2956	2.4	0.0224	3.1
3KS-105-Spot 17	841	25257	2.9	20.5694	3.2	0.0233	3.7
3KS-105-Spot 80	1991	42003	0.7	19.0343	2.9	0.0252	4.9
3KS-105-Spot 6	361	31509	0.4	20.3381	6.8	0.0237	7.2
3KS-105-Spot 92	264	2678	10.8	22.5300	4.1	0.0215	4.8
3KS-105-Spot 2	1709	40481	1.4	21.2799	2.7	0.0228	3.2
3KS-105-Spot 61	1924	60227	2.0	21.3820	2.0	0.0227	2.7
3KS-105-Spot 94	2348	34581	2.1	21.6142	3.0	0.0225	3.7
3KS-105-Spot 25	911	28939	2.0	21.3390	3.9	0.0229	4.4
3KS-105-Spot 96	2394	25012	1.1	20.7872	2.9	0.0235	3.3
3KS-105-Spot 50	1221	20545	0.7	11.6464	16.9	0.0422	17.2
3KS-105-Spot 51	1912	59897	2.2	21.0730	2.8	0.0233	4.1
3KS-105-Spot 55	1105	37330	4.0	20.8578	4.7	0.0237	5.4
3KS-105-Spot 82	2791	35644	1.8	21.1244	2.2	0.0234	2.6
3KS-105-Spot 84	2964	35087	0.9	21.4378	2.5	0.0231	2.8
3KS-105-Spot 12	2009	29151	1.6	21.0126	2.9	0.0236	3.4
3KS-105-Spot 76	1969	32570	1.5	21.5298	2.3	0.0231	2.9
3KS-105-Spot 86	166	14108	3.8	22.5014	7.9	0.0221	8.4
3KS-105-Spot 15	1686	85743	1.3	19.9894	2.7	0.0249	3.5
3KS-105-Spot 23	1755	230449	2.2	21.0098	3.1	0.0238	3.6
3KS-105-Spot 108	2100	34069	2.1	21.0432	2.6	0.0238	3.3
3KS-105-Spot 87	1922	25351	2.5	21.3444	2.7	0.0236	3.3
3KS-105-Spot 39	2604	53573	1.3	21.7635	2.3	0.0232	2.6
3KS-105-Spot 11	2151	30687	1.9	21.1010	2.7	0.0239	3.9
3KS-105-Spot 54	2263	18040	2.0	21.3533	1.5	0.0237	3.4

3KS-105-Spot 45	2419	55580	2.4	21.2492	2.8	0.0238	4.4
3KS-105-Spot 81	2479	28525	1.3	20.8894	2.5	0.0243	2.9
3KS-105-Spot 13	1399	14050	2.0	9.9225	15.3	0.0513	15.7
3KS-105-Spot 19	360	17478	3.3	22.1609	5.9	0.0231	6.4
3KS-105-Spot 44	2731	30309	1.4	21.4205	2.7	0.0242	3.3
3KS-105-Spot 32	497	4104	0.7	23.3350	4.9	0.0223	5.8
3KS-105-Spot 42	930	22298	0.9	19.8620	4.5	0.0266	5.0
3KS-105-Spot 104	3429	32680	0.8	20.4941	3.2	0.0265	4.5
3KS-105-Spot 103	1766	76668	1.8	19.8373	4.1	0.0276	5.4
3KS-105-Spot 105	3167	35949	1.8	21.1937	2.1	0.0260	2.9
3KS-105-Spot 83	3826	78177	1.5	21.3141	2.1	0.0261	2.6
3KS-105-Spot 38	3840	62166	1.6	20.6126	2.3	0.0270	2.8
3KS-105-Spot 66	2821	7956	1.0	5.4758	18.0	0.1143	20.5
3KS-105-Spot 56	4589	30019	1.2	18.3602	2.6	0.0348	3.0
3KS-105-Spot 64	3971	123581	2.4	20.6407	2.1	0.0321	2.4
3KS-105-Spot 22	2750	79008	1.7	21.1046	2.0	0.0351	2.4
3KS-105-Spot 24	3071	37059	2.1	21.1289	1.4	0.0442	2.5
3KS-105-Spot 59	159	7560	0.9	20.2227	6.2	0.0508	7.4
3KS-105-Spot 109	162	9234	1.3	21.3879	4.7	0.0481	5.3
3KS-105-Spot 97	641	43395	1.3	21.1504	3.0	0.0488	3.4
3KS-105-Spot 88	111	2355	1.5	24.1481	7.8	0.0428	8.5
3KS-105-Spot 78	188	14218	1.3	21.1326	6.2	0.0489	7.2
3KS-105-Spot 62	375	12059	0.7	20.3676	3.9	0.0510	4.4
3KS-105-Spot 91	164	5417	1.3	21.3630	5.4	0.0487	5.9
3KS-105-Spot 99	96	3511	0.9	20.9429	9.0	0.0497	9.4
3KS-105-Spot 67	196	30558	1.4	19.5914	6.0	0.0531	6.8
3KS-105-Spot 89	139	2928	0.8	21.9437	6.0	0.0475	6.4
3KS-105-Spot 21	80	3581	1.1	24.3349	8.2	0.0430	9.1
3KS-105-Spot 57	188	58658	1.3	20.2226	5.5	0.0518	6.1
3KS-105-Spot 75	142	37615	1.4	22.3785	5.0	0.0469	5.7
3KS-105-Spot 4	147	3773	1.2	21.0216	6.2	0.0499	7.1
3KS-105-Spot 27	72	3568	1.9	23.6649	6.1	0.0444	6.9
3KS-105-Spot 100	143	4160	1.0	22.5792	5.4	0.0466	6.1
3KS-105-Spot 35	104	49422	1.4	18.7773	7.5	0.0562	8.0
3KS-105-Spot 30	96	4967	0.7	20.7109	5.4	0.0510	6.3
3KS-105-Spot 72	96	2013	1.1	23.2163	8.5	0.0455	9.5
3KS-105-Spot 9	163	8381	1.3	21.1498	6.3	0.0501	7.0
3KS-105-Spot 5	183	8068	1.4	19.7026	6.9	0.0538	7.1
3KS-105-Spot 77	146	6108	1.4	19.7060	5.4	0.0539	6.0
3KS-105-Spot 98	216	13138	1.3	19.2801	5.9	0.0552	6.9
3KS-105-Spot 28	56	3535	1.1	27.6394	7.3	0.0385	7.8
3KS-105-Spot 74	229	64210	1.2	21.3684	5.0	0.0499	5.6
3KS-105-Spot 46	164	22151	1.4	21.1485	4.7	0.0505	5.1
3KS-105-Spot 16	184	4056	1.3	23.0194	5.9	0.0464	6.4
3KS-105-Spot 26	305	31804	0.7	22.4098	5.6	0.0477	6.0
3KS-105-Spot 60	215	31633	1.0	20.8197	4.6	0.0515	6.9
3KS-105-Spot 70	224	8809	1.2	21.6496	4.2	0.0495	4.8

3KS-105-Spot 34	113	3144	1.4	25.1199	5.4	0.0428	6.6
3KS-105-Spot 58	177	7469	1.0	21.3217	6.6	0.0504	6.8
3KS-105-Spot 85	219	15919	1.3	21.5138	4.6	0.0500	5.0
3KS-105-Spot 65	199	38592	1.2	21.9003	5.4	0.0494	5.8
3KS-105-Spot 41	155	3652	1.5	23.2723	5.9	0.0464	7.5
3KS-105-Spot 79	128	2139	1.7	22.7446	5.7	0.0476	6.4
3KS-105-Spot 8	212	8142	1.3	21.6890	6.1	0.0502	6.5
3KS-105-Spot 90	311	12473	1.2	21.1384	3.9	0.0516	4.3
3KS-105-Spot 71	386	130954	1.4	19.6309	4.9	0.0557	5.4
3KS-105-Spot 48	217	49591	1.2	19.8685	5.8	0.0562	6.2
3KS-105-Spot 29	214	3657	1.0	23.1453	4.8	0.0483	5.8
3KS-105-Spot 10	143	5133	1.6	8.7419	15.0	0.1279	15.3
3KS-105-Spot 53	140	5529	1.0	21.0660	5.1	0.0532	5.8
3KS-105-Spot 68	86	6403	1.3	14.7730	14.5	0.0766	14.8
3KS-105-Spot 43	216	5576	1.0	10.9993	18.6	0.1038	18.8
3KS-105-Spot 14	570	11381	2.2	22.3751	2.3	0.0528	4.6
3KS-105-Spot 106	147	17704	1.6	16.8018	6.0	0.0706	6.4
3KS-105-Spot 73	33	1798	1.3	23.4990	9.6	0.0529	10.1
3KS-105-Spot 107	683	47026	0.7	21.1243	2.7	0.0657	3.5
3KS-105-Spot 33	164	43423	1.7	20.0709	3.5	0.0730	4.4
3KS-105-Spot 7	115	10319	1.8	19.2352	7.0	0.0775	7.6
3KS-105-Spot 101	2095	64027	13.6	17.4249	1.2	0.6319	2.9

Sample:	1XK-10	N29.32592	E88.67300				
1XK-10-89 <>	370	4810	1.3	18.9008	21.9	0.0339	22.4
1XK-10-37 <>	1192	10997	0.8	20.6665	8.8	0.0336	9.3
1XK-10-73 <>	981	10507	1.8	20.9222	9.8	0.0470	10.1
1XK-10-15 <>	104	4558	0.8	19.9402	45.5	0.0496	46.5
1XK-10-9 <>	65	971	1.0	15.1148	45.3	0.0655	47.3
1XK-10-68 <>	551	19784	0.6	21.2088	10.3	0.0473	10.5
1XK-10-17 <>	145	2930	1.1	21.1338	37.9	0.0485	39.0
1XK-10-104 <>	426	3195	1.2	17.4246	26.8	0.0590	27.2
1XK-10-31 <>	549	6682	1.6	22.5409	18.1	0.0463	19.2
1XK-10-96 <>	162	8445	1.4	27.3224	53.8	0.0383	54.4
1XK-10-100 <>	543	6353	0.7	21.5724	10.5	0.0487	11.0
1XK-10-13 <>	350	4918	3.7	22.3521	21.9	0.0475	22.2
1XK-10-6 <>	98	514	1.0	17.0315	49.7	0.0629	52.8
1XK-10-85 <>	475	7991	0.6	20.8184	12.3	0.0522	12.5
1XK-10-8 <>	218	7920	1.1	25.1742	38.5	0.0433	38.7
1XK-10-47 <>	1460	17694	3.5	20.6893	4.0	0.0528	4.3
1XK-10-32 <>	224	9555	1.4	20.6435	21.1	0.0541	21.7
1XK-10-14 <>	122	6337	1.4	17.5903	23.9	0.0652	27.9
1XK-10-16 <>	241	8042	1.0	20.0910	31.1	0.0575	31.2
1XK-10-57 <>	146	2312	1.2	18.2838	31.1	0.0645	31.6
1XK-10-12 <>	245	2956	1.6	15.7025	24.9	0.0765	25.8
1XK-10-27 <>	240	984	1.1	21.6145	15.9	0.0622	16.1
1XK-10-103 <>	73	8230	0.9	21.6434	61.3	0.0776	61.7

1XK-10-76 <>	66	3083	1.0	14.6857	28.8	0.1145	29.9
1XK-10-1 <>	87	1754	1.1	18.2607	37.0	0.0930	38.2
1XK-10-2 <>	113	5710	1.7	23.8670	43.7	0.0733	43.8
1XK-10-74 <>	52	2263	1.1	25.0500	40.8	0.0700	42.2
1XK-10-19 <>	208	7416	1.0	21.8811	31.7	0.0803	31.9
1XK-10-2 <>	198	35124	1.0	21.7222	10.6	0.0812	10.8
1XK-10-84 <>	643	32939	0.4	21.4755	5.2	0.0822	5.4
1XK-10-21 <>	97	765	1.0	14.0354	22.8	0.1260	24.7
1XK-10-77 <>	88	4124	1.2	29.6242	48.3	0.0599	48.9
1XK-10-78 <>	243	17300	0.8	20.5643	14.6	0.0864	15.0
1XK-10-102 <>	68	4840	1.2	19.7456	35.8	0.0909	36.5
1XK-10-58 <>	99	3700	1.0	22.1076	32.1	0.0817	32.6
1XK-10-44 <>	102	4618	1.1	23.0878	29.2	0.0787	29.7
1XK-10-60 <>	225	11349	1.3	21.2765	16.1	0.0854	17.8
1XK-10-45 <>	379	6052	3.5	20.7902	9.0	0.0876	9.2
1XK-10-4 <>	207	8088	1.5	23.0008	28.3	0.0794	28.4
1XK-10-40 <>	144	9277	1.0	33.3347	39.3	0.0550	39.6
1XK-10-24 <>	45	2989	1.2	18.7420	51.7	0.0985	52.4
1XK-10-23 <>	93	7211	1.0	23.0684	40.5	0.0805	40.7
1XK-10-72 <>	181	7748	0.7	18.2524	20.9	0.1020	21.1
1XK-10-41 <>	130	12309	1.0	18.0919	25.7	0.1036	26.2
1XK-10-87 <>	324	11907	1.2	22.3497	18.1	0.0839	18.9
1XK-10-75 <>	213	27682	0.8	24.9477	17.2	0.0751	17.6
1XK-10-92 <>	219	13370	0.8	20.7200	12.6	0.0913	13.3
1XK-10-90 <>	97	9289	1.0	18.8871	22.1	0.1007	23.2
1XK-10-70 <>	1820	64739	1.8	20.5626	1.3	0.0927	1.7
1XK-10-55 <>	77	3245	0.9	34.4063	60.2	0.0554	60.3
1XK-10-83 <>	364	41181	1.4	21.9758	11.5	0.0868	11.7
1XK-10-3 <>	229	3811	1.8	20.8895	9.4	0.0918	10.1
1XK-10-26 <>	842	12527	1.1	20.4379	4.8	0.0940	6.5
1XK-10-91 <>	114	7819	1.4	20.5579	20.1	0.0935	21.6
1XK-10-88 <>	113	519	1.4	23.5482	64.5	0.0816	64.9
1XK-10-98 <>	112	4963	1.0	33.0775	88.9	0.0584	89.0
1XK-10-62 <>	514	7951	0.6	19.8830	6.7	0.0975	6.9
1XK-10-67 <>	196	11334	1.0	24.6938	25.5	0.0789	25.8
1XK-10-105 <>	70	4058	0.9	19.5733	32.1	0.0996	34.6
1XK-10-18 <>	188	8173	0.9	19.6193	17.3	0.0997	17.5
1XK-10-53 <>	107	6558	1.2	30.0994	49.3	0.0661	49.5
1XK-10-38 <>	109	3121	0.8	27.4487	36.3	0.0724	36.7
1XK-10-101 <>	102	5770	3.0	21.5628	26.4	0.0923	26.8
1XK-10-52 <>	76	5135	1.0	21.6617	47.8	0.0928	48.0
1XK-10-65 <>	1114	13000	1.7	20.4213	2.0	0.0987	3.0
1XK-10-11 <>	528	17275	2.4	20.8356	4.5	0.0968	5.3
1XK-10-33 <>	123	5463	0.9	22.0213	20.8	0.0917	21.2
1XK-10-80 <>	527	18013	1.4	21.6366	7.1	0.0937	7.3
1XK-10-71 <>	136	5550	1.3	27.4669	34.3	0.0746	34.5
1XK-10-48 <>	192	2451	1.1	18.3472	13.9	0.1123	14.4

1XK-10-94 <>	218	8650	0.9	19.4431	11.6	0.1113	12.1
1XK-10-36 <>	359	23793	1.5	20.9879	7.8	0.1110	8.1
1XK-10-50 <>	776	41011	0.8	20.7768	3.0	0.1133	3.7
1XK-10-39 <>	796	190268	0.7	20.1295	2.3	0.1490	3.2
1XK-10-99 <>	47	12694	1.4	18.4648	27.8	0.2121	29.0
1XK-10-61 <>	76	10175	0.9	20.7113	31.8	0.1897	32.4
1XK-10-10 <>	173	14284	1.6	20.1184	9.3	0.1964	9.5
1XK-10-51 <>	97	10452	1.7	22.3501	16.9	0.1804	17.3
1XK-10-25 <>	66	5170	1.3	18.4543	12.8	0.2185	13.6
1XK-10-64 <>	95	5181	0.7	19.1388	18.3	0.2127	19.7
1XK-10-66 <>	212	17969	0.9	19.6351	7.0	0.2125	7.0
1XK-10-42 <>	214	26807	1.2	20.2895	6.9	0.2100	7.4
1XK-10-69 <>	183	20227	1.1	20.6572	10.9	0.2095	11.1
1XK-10-82 <>	273	37291	0.7	19.3204	5.7	0.2392	6.0
1XK-10-30 <>	144	17767	0.5	18.7520	11.6	0.2509	11.8
1XK-10-86 <>	101	7251	1.3	19.9292	9.2	0.2486	10.2
1XK-10-59 <>	1501	9369	3.4	18.7389	0.9	0.3394	3.8
1XK-10-49 <>	278	126652	2.9	18.3123	1.3	0.4225	1.8
1XK-10-43 <>	250	11183	2.6	18.7207	2.9	0.4138	3.7
1XK-10-63 <>	592	30050	6.1	18.4850	1.5	0.4288	1.9
1XK-10-93 <>	425	79128	3.9	18.5250	1.8	0.4307	2.1
1XK-10-95 <>	535	156228	3.2	18.5688	1.7	0.4361	2.1
1XK-10-22 <>	191	48468	1.6	18.1524	2.4	0.4473	3.5
1XK-10-81 <>	232	29370	3.8	18.2840	1.9	0.4490	3.4
1XK-10-20 <>	414	97436	2.8	18.6051	1.4	0.4512	2.9
1XK-10-79 <>	238	43409	1.3	13.6424	8.8	0.7279	9.1
1XK-10-29 <>	234	74116	0.9	16.8508	1.6	0.7875	2.5
1XK-10-56 <>	726	271646	1.9	12.6584	0.2	2.1817	1.5

Sample:	1XK-313	N29.32057	E88.67187				
LEARY-1XK-313-101 <	683	12414	1.3	22.2147	13.0	0.0305	13.4
LEARY-1XK-313-14 <>	706	22230	1.8	23.1801	12.2	0.0320	12.5
LEARY-1XK-313-75 <>	1343	79556	2.3	21.3084	5.6	0.0384	5.7
LEARY-1XK-313-102 <	2669	23566	2.8	21.2645	2.8	0.0422	3.0
LEARY-1XK-313-2 <>	139	3831	0.8	24.1142	61.4	0.0403	62.8
LEARY-1XK-313-56 <>	338	14239	1.0	21.4397	16.2	0.0476	16.4
LEARY-1XK-313-58 <>	202	10394	1.0	22.5765	21.6	0.0452	22.4
LEARY-1XK-313-32 <>	293	6435	0.6	18.8773	23.0	0.0546	23.1
LEARY-1XK-313-24 <>	192	6089	0.9	22.8659	30.7	0.0460	31.0
LEARY-1XK-313-47 <>	257	8560	1.1	21.3175	25.3	0.0495	25.7
LEARY-1XK-313-36 <>	145	3883	0.9	34.8393	49.1	0.0304	49.3
LEARY-1XK-313-28 <>	296	9061	1.4	29.0774	24.5	0.0364	24.8
LEARY-1XK-313-38 <>	186	7893	1.2	19.4550	23.9	0.0544	24.1
LEARY-1XK-313-105 <	665	21582	1.5	21.7536	8.5	0.0494	8.9
LEARY-1XK-313-42 <>	145	5041	1.0	25.5637	25.8	0.0423	26.2
LEARY-1XK-313-29 <>	177	16131	1.3	21.8943	34.0	0.0497	34.5
LEARY-1XK-313-19 <>	1434	2204	2.3	20.5377	4.4	0.0534	4.6

LEARY-1XK-313-77 <>	91	2515	1.3	12.0976	133.8	0.0908	134.1
LEARY-1XK-313-23 <>	363	14155	1.1	20.2516	23.9	0.0545	24.0
LEARY-1XK-313-60 <>	180	1046	0.6	21.9450	25.0	0.0505	25.2
LEARY-1XK-313-95 <>	1071	11214	0.8	20.1043	3.9	0.0554	4.4
LEARY-1XK-313-50 <>	500	22869	1.2	23.6067	13.4	0.0476	13.5
LEARY-1XK-313-39 <>	160	389	1.2	13.3919	30.4	0.0844	31.0
LEARY-1XK-313-73 <>	166	5484	0.9	25.1857	30.4	0.0450	31.3
LEARY-1XK-313-72 <>	99	4523	1.7	18.7982	92.1	0.0611	92.4
LEARY-1XK-313-8 <>	507	9950	0.8	19.7868	8.7	0.0581	9.0
LEARY-1XK-313-20 <>	248	7240	1.2	21.7856	14.6	0.0532	15.1
LEARY-1XK-313-40 <>	701	16427	0.6	21.6739	8.9	0.0538	9.0
LEARY-1XK-313-90 <>	288	7403	1.3	21.3046	24.7	0.0548	24.8
LEARY-1XK-313-37 <>	181	7657	1.2	22.8603	24.8	0.0515	25.5
LEARY-1XK-313-104 <	306	3949	1.1	21.9027	20.2	0.0540	20.5
LEARY-1XK-313-87 <>	913	24995	1.4	21.5309	5.8	0.0556	6.3
LEARY-1XK-313-43 <>	295	2948	0.6	20.0336	27.7	0.0603	27.9
LEARY-1XK-313-59 <>	284	199	1.5	19.7376	37.5	0.0645	38.6
LEARY-1XK-313-3 <>	138	8364	1.5	19.3047	24.1	0.0679	24.7
LEARY-1XK-313-54 <>	154	10727	2.3	20.5938	26.2	0.0660	26.8
LEARY-1XK-313-80 <>	136	3312	1.1	22.2459	44.9	0.0628	45.4
LEARY-1XK-313-96 <>	1606	2163	1.5	19.5268	9.1	0.0772	9.2
LEARY-1XK-313-100 <	98	3006	1.0	22.1143	37.1	0.0709	37.4
LEARY-1XK-313-4 <>	99	1996	1.1	15.8555	27.4	0.1045	29.2
LEARY-1XK-313-89 <>	703	13134	0.9	20.0090	5.0	0.0847	5.2
LEARY-1XK-313-53 <>	151	5230	1.2	23.4715	48.1	0.0723	49.1
LEARY-1XK-313-22 <>	61	4755	1.2	23.7373	41.1	0.0726	41.9
LEARY-1XK-313-51 <>	1145	60282	1.0	20.5064	3.2	0.0842	4.2
LEARY-1XK-313-5 <>	71	5395	2.9	21.4299	53.1	0.0824	54.0
LEARY-1XK-313-71 <>	139	3953	1.1	21.2296	31.2	0.0841	33.0
LEARY-1XK-313-67 <>	64	3181	1.3	37.7089	91.0	0.0474	91.6
LEARY-1XK-313-82 <>	147	10062	0.9	22.3663	23.6	0.0804	24.5
LEARY-1XK-313-78 <>	421	34699	1.2	20.6189	6.5	0.0886	6.7
LEARY-1XK-313-68 <>	274	11693	0.9	21.3522	11.2	0.0858	11.4
LEARY-1XK-313-46 <>	181	11799	1.5	20.3991	9.3	0.0900	9.7
LEARY-1XK-313-62 <>	76	5389	1.3	22.7801	70.3	0.0806	70.9
LEARY-1XK-313-93 <>	165	4681	1.1	17.3722	15.8	0.1059	16.6
LEARY-1XK-313-41 <>	281	22816	0.9	23.9148	8.6	0.0770	8.8
LEARY-1XK-313-84 <>	155	6081	1.4	19.7924	19.5	0.0932	19.7
LEARY-1XK-313-27 <>	229	17272	0.8	20.6160	11.0	0.0897	11.2
LEARY-1XK-313-99 <>	60	2724	1.1	10.1763	232.9	0.1819	233.1
LEARY-1XK-313-13 <>	143	19854	0.9	22.5209	31.0	0.0822	31.3
LEARY-1XK-313-97 <>	151	10869	1.2	19.9900	20.4	0.0928	20.7
LEARY-1XK-313-33 <>	155	7577	1.4	24.1502	27.7	0.0774	27.8
LEARY-1XK-313-63 <>	338	28087	1.0	20.6884	6.4	0.0906	6.6
LEARY-1XK-313-70 <>	56	3087	1.4	15.9013	23.5	0.1194	27.0
LEARY-1XK-313-30 <>	377	9548	1.7	20.7144	8.2	0.0917	8.4
LEARY-1XK-313-69 <>	146	3070	1.9	26.9704	29.4	0.0719	29.8

LEARY-1XK-313-31 <>	134	9253	1.0	18.5672	13.0	0.1049	13.8
LEARY-1XK-313-103 <	564	5575	2.2	20.2621	8.7	0.0963	8.8
LEARY-1XK-313-81 <>	133	7309	1.2	20.9669	20.9	0.0936	21.1
LEARY-1XK-313-49 <>	68	2601	0.8	18.5059	58.1	0.1064	59.2
LEARY-1XK-313-16 <>	131	8238	1.3	21.5503	24.3	0.0923	25.3
LEARY-1XK-313-94 <>	456	24436	0.9	21.5776	4.9	0.0924	5.1
LEARY-1XK-313-61 <>	354	41659	1.5	21.8121	9.8	0.0919	10.0
LEARY-1XK-313-66 <>	147	10154	1.1	24.2582	23.0	0.0849	23.4
LEARY-1XK-313-17 <>	98	3431	0.8	21.4611	35.2	0.0980	35.6
LEARY-1XK-313-57 <>	83	7229	0.9	20.6701	32.3	0.1032	32.9
LEARY-1XK-313-15 <>	118	1061	1.1	16.9287	16.7	0.1276	17.0
LEARY-1XK-313-26 <>	55	487	0.6	15.8937	25.0	0.1370	28.6
LEARY-1XK-313-21 <>	179	4724	1.0	25.6199	19.3	0.0866	19.6
LEARY-1XK-313-85 <>	722	40493	0.5	19.9015	5.8	0.1158	5.9
LEARY-1XK-313-48 <>	355	4967	0.8	19.2861	11.8	0.1203	12.1
LEARY-1XK-313-65 <>	626	65816	1.5	20.5679	3.7	0.1262	3.9
LEARY-1XK-313-98 <>	73	10719	1.2	21.6144	21.4	0.1818	21.7
LEARY-1XK-313-45 <>	61	7369	1.1	23.9158	36.3	0.1721	36.7
LEARY-1XK-313-83 <>	321	18594	1.2	20.4020	4.0	0.2034	4.2
LEARY-1XK-313-91 <>	1401	4778	0.4	20.1587	2.4	0.2194	2.5
LEARY-1XK-313-44 <>	239	24954	1.6	20.7582	7.2	0.2132	7.4
LEARY-1XK-313-9 <>	154	14844	1.1	18.9089	9.4	0.2780	9.6
LEARY-1XK-313-86 <>	745	28085	3.4	18.5348	1.3	0.4517	1.9
LEARY-1XK-313-76 <>	211	90556	2.2	18.6995	1.8	0.4546	2.5
LEARY-1XK-313-10 <>	99	103209	0.9	12.7638	1.4	2.2199	3.4
LEARY-1XK-313-35 <>	21	31691	0.7	12.7179	6.8	2.1090	7.1
LEARY-1XK-313-11 <>	67	64486	0.4	12.4054	2.7	2.2026	3.0
LEARY-1XK-313-17 <>	65	68286	1.6	10.1644	1.5	3.1914	3.1
LEARY-1XK-313-12 <>	79	114367	2.1	8.0766	0.5	6.0293	1.6
LEARY-1XK-313-16 <>	559	121717	4.0	7.4944	0.5	7.0402	1.5
LEARY-1XK-313-1 <>	112	265414	2.4	4.0030	0.2	19.2895	3.2

Sample:	2XK-47	N29.31403	E88.67413				
LEARY-2XK-47-13 <>	476	8617	1.1	20.5309	14.4	0.0305	14.7
LEARY-2XK-47-90 <>	149	2390	1.0	20.0644	46.4	0.0313	47.4
LEARY-2XK-47-34 <>	557	9558	1.8	21.6931	20.5	0.0334	20.6
LEARY-2XK-47-86 <>	232	3590	0.9	20.2001	15.1	0.0367	19.6
LEARY-2XK-47-4 <>	948	28282	1.3	21.2895	5.5	0.0404	5.8
LEARY-2XK-47-108 <>	807	16471	0.7	19.9285	9.9	0.0435	10.0
LEARY-2XK-47-83 <>	1158	7869	1.2	20.5361	9.3	0.0433	9.5
LEARY-2XK-47-70 <>	913	28493	0.8	21.2487	7.2	0.0422	7.3
LEARY-2XK-47-47 <>	620	6625	1.2	18.9613	16.7	0.0477	17.5
LEARY-2XK-47-80 <>	1147	26185	1.4	22.1196	4.6	0.0414	4.9
LEARY-2XK-47-32 <>	304	714	2.4	16.8748	52.5	0.0551	53.5
LEARY-2XK-47-107 <>	747	21931	1.2	22.0449	7.3	0.0430	7.5
LEARY-2XK-47-62 <>	448	20685	1.4	19.9916	13.8	0.0505	14.7
LEARY-2XK-47-103 <>	193	2603	1.4	16.5542	36.9	0.0615	38.8

LEARY-2XK-47-36 <>	88	931	0.8	15.2675	65.7	0.0672	67.4
LEARY-2XK-47-15 <>	423	2237	0.6	21.6062	18.0	0.0478	18.1
LEARY-2XK-47-5 <>	238	3430	1.5	25.2977	39.0	0.0412	39.3
LEARY-2XK-47-16 <>	223	6857	0.9	26.5601	42.2	0.0396	42.5
LEARY-2XK-47-98 <>	3074	63149	2.1	21.0981	2.5	0.0501	2.6
LEARY-2XK-47-102 <>	96	2129	1.0	13.5290	96.6	0.0782	97.3
LEARY-2XK-47-79 <>	199	7477	1.0	23.9905	27.3	0.0442	27.6
LEARY-2XK-47-101 <>	442	12865	2.1	20.0364	7.3	0.0529	8.3
LEARY-2XK-47-55 <>	106	1879	1.4	36.6904	97.7	0.0290	98.1
LEARY-2XK-47-92 <>	277	2269	0.9	19.7173	15.7	0.0540	17.1
LEARY-2XK-47-33 <>	283	7459	1.4	18.1476	7.1	0.0588	8.1
LEARY-2XK-47-51 <>	288	8406	1.5	22.1240	28.7	0.0483	28.9
LEARY-2XK-47-17 <>	74	2091	0.9	1.0659	3557.3	1.0076	3557.4
LEARY-2XK-47-20 <>	143	10472	0.6	16.1377	18.8	0.0672	20.0
LEARY-2XK-47-100 <>	255	7222	0.9	17.6317	16.5	0.0616	16.8
LEARY-2XK-47-49 <>	398	1309	1.0	17.9001	16.5	0.0607	16.8
LEARY-2XK-47-99 <>	400	11433	1.3	23.7037	14.9	0.0460	15.2
LEARY-2XK-47-56 <>	309	9950	1.5	20.1018	12.9	0.0546	13.3
LEARY-2XK-47-1 <>	944	18467	1.2	20.9793	6.2	0.0525	6.4
LEARY-2XK-47-48 <>	369	23776	1.3	22.8085	10.0	0.0484	10.3
LEARY-2XK-47-88 <>	293	6380	1.7	25.5068	28.6	0.0433	28.8
LEARY-2XK-47-29 <>	132	6242	1.1	23.7230	58.9	0.0465	59.2
LEARY-2XK-47-89 <>	578	14777	1.6	20.4177	8.7	0.0545	8.8
LEARY-2XK-47-7 <>	390	11116	0.7	19.6645	22.4	0.0566	22.6
LEARY-2XK-47-2 <>	485	18752	1.1	22.4936	11.3	0.0497	12.2
LEARY-2XK-47-78 <>	445	11489	1.1	21.8187	8.8	0.0518	8.9
LEARY-2XK-47-94 <>	455	14545	1.0	21.7684	14.8	0.0524	15.8
LEARY-2XK-47-87 <>	152	2047	1.5	23.7925	39.5	0.0494	39.8
LEARY-2XK-47-109 <>	222	8294	0.8	26.2224	23.3	0.0450	24.1
LEARY-2XK-47-61 <>	755	28990	1.4	21.9372	8.1	0.0548	8.3
LEARY-2XK-47-45 <>	228	349	1.5	16.8310	35.3	0.0775	38.1
LEARY-2XK-47-71 <>	341	12206	0.8	23.1457	17.3	0.0569	17.6
LEARY-2XK-47-60 <>	1199	39941	1.2	21.6209	3.8	0.0619	4.9
LEARY-2XK-47-96 <>	123	3865	1.2	25.8326	47.8	0.0550	48.1
LEARY-2XK-47-85 <>	119	163	0.8	15.8923	44.3	0.1029	44.7
LEARY-2XK-47-82 <>	37	2387	1.4	-0.5973	2965.4	-2.8514	2965.4
LEARY-2XK-47-12 <>	42	4047	2.0	18.4855	82.8	0.0934	83.6
LEARY-2XK-47-63 <>	96	4079	1.0	16.9880	28.8	0.1036	29.9
LEARY-2XK-47-35 <>	100	6704	2.2	26.2829	29.8	0.0675	30.4
LEARY-2XK-47-39 <>	133	7563	0.9	22.9039	30.6	0.0777	30.9
LEARY-2XK-47-26 <>	128	14349	1.0	21.1551	23.5	0.0861	24.1
LEARY-2XK-47-58 <>	112	9302	0.8	28.7583	40.9	0.0638	42.5
LEARY-2XK-47-38 <>	148	7864	1.5	19.2171	19.3	0.0960	20.0
LEARY-2XK-47-9 <>	100	6541	0.9	25.1397	57.0	0.0736	57.3
LEARY-2XK-47-30 <>	262	19156	1.0	19.6646	7.7	0.0943	8.3
LEARY-2XK-47-76 <>	387	10587	1.0	21.1678	5.6	0.0879	5.8
LEARY-2XK-47-28 <>	304	22812	0.7	20.9849	12.2	0.0891	12.5

LEARY-2XK-47-42 <>	157	4829	0.9	21.8465	36.2	0.0859	37.4
LEARY-2XK-47-68 <>	89	8135	0.9	22.7775	32.6	0.0827	33.2
LEARY-2XK-47-59 <>	824	43601	0.9	20.0838	5.3	0.0938	5.6
LEARY-2XK-47-65 <>	114	7111	1.3	19.3929	27.6	0.0985	28.1
LEARY-2XK-47-67 <>	183	8619	2.7	19.5219	15.8	0.0981	16.4
LEARY-2XK-47-93 <>	60	3330	1.7	24.3454	84.6	0.0787	85.1
LEARY-2XK-47-46 <>	163	6012	1.3	22.4530	34.1	0.0854	34.3
LEARY-2XK-47-8 <>	570	42364	0.9	20.0513	7.2	0.0957	7.3
LEARY-2XK-47-95 <>	72	1529	1.7	16.2833	32.5	0.1180	33.2
LEARY-2XK-47-75 <>	140	3254	1.6	20.4687	22.0	0.0944	22.6
LEARY-2XK-47-23 <>	122	6109	1.3	19.7087	31.0	0.0983	31.4
LEARY-2XK-47-105 <>	85	3899	1.3	22.4561	40.0	0.0874	40.6
LEARY-2XK-47-19 <>	756	46259	0.6	21.4538	3.0	0.0935	3.5
LEARY-2XK-47-14 <>	351	41075	1.5	21.6738	9.9	0.0928	10.5
LEARY-2XK-47-69 <>	209	3711	1.1	20.3042	17.6	0.0998	18.0
LEARY-2XK-47-104 <>	128	4804	0.7	20.0261	22.5	0.1014	22.9
LEARY-2XK-47-52 <>	254	10127	3.1	25.3642	12.4	0.0801	12.9
LEARY-2XK-47-110 <>	257	10582	1.4	22.1852	18.2	0.0916	18.2
LEARY-2XK-47-66 <>	180	6965	0.9	22.0947	19.7	0.0922	20.1
LEARY-2XK-47-31 <>	911	44694	1.3	20.9489	3.7	0.0990	4.0
LEARY-2XK-47-6 <>	239	16572	0.8	20.1436	5.1	0.1040	5.9
LEARY-2XK-47-27 <>	1006	41971	1.3	20.8932	3.2	0.1007	3.6
LEARY-2XK-47-25 <>	394	32127	0.9	20.1558	4.8	0.1072	5.2
LEARY-2XK-47-22 <>	193	9421	1.0	17.3425	10.5	0.1270	10.9
LEARY-2XK-47-97 <>	651	43419	2.3	20.8089	1.8	0.1350	3.0
LEARY-2XK-47-3 <>	1146	7603	1.8	20.1830	2.4	0.1409	2.8
LEARY-2XK-47-73 <>	313	9575	0.8	19.7086	8.2	0.1638	8.3
LEARY-2XK-47-91 <>	320	48801	1.2	20.6132	5.5	0.1873	7.9
LEARY-2XK-47-41 <>	70	4645	1.6	21.6623	19.2	0.1790	19.5
LEARY-2XK-47-43 <>	264	49767	2.8	20.3336	3.9	0.2235	4.2
LEARY-2XK-47-84 <>	1233	219325	4.2	19.7607	1.2	0.2340	3.0
LEARY-2XK-47-24 <>	1094	106144	15.4	19.3483	1.8	0.2450	2.2
LEARY-2XK-47-44 <>	655	4632	3.6	18.2858	2.6	0.4149	2.7
LEARY-2XK-47-77 <>	312	55309	2.5	18.7252	2.1	0.4156	2.4
LEARY-2XK-47-18 <>	157	40287	7.9	18.7372	5.1	0.4186	5.3
LEARY-2XK-47-57 <>	241	9985	1.2	18.5591	2.3	0.4235	3.0
LEARY-2XK-47-53 <>	698	111257	3.1	18.6928	1.1	0.4297	1.3
LEARY-2XK-47-40 <>	431	20221	2.0	17.5233	2.2	0.6468	5.6
LEARY-2XK-47-64 <>	758	269700	1.2	16.2175	0.6	0.9394	2.3
LEARY-2XK-47-74 <>	38	11589	1.2	14.6908	5.2	1.2317	5.8
LEARY-2XK-47-106 <>	126	112983	2.7	10.6412	1.6	2.9673	2.7
LEARY-2XK-47-37 <>	34	53651	1.1	5.6256	1.0	12.2680	1.7

Sample:	1DK-19	N29.30775	E89.82238				
LEARY-1DK-19-1	779	20282	1.2	18.3770	15.8	0.0482	16.2
LEARY-1DK-19-106 <>	149	862	0.9	9.2587	75.7	0.0967	77.3
LEARY-1DK-19-89 <>	815	20208	0.9	21.9153	10.0	0.0418	10.3

LEARY-1DK-19-92 <>	683	16134	1.1	22.4312	9.6	0.0409	9.7
LEARY-1DK-19-8 <>	556	19406	1.2	20.0199	14.7	0.0460	15.1
LEARY-1DK-19-5 <>	1060	16809	0.6	20.8764	6.2	0.0441	6.4
LEARY-1DK-19-28 <>	826	23154	1.5	19.8351	7.0	0.0468	7.2
LEARY-1DK-19-68 <>	1240	52220	0.4	21.3346	3.5	0.0449	4.5
LEARY-1DK-19-50 <>	113	5046	1.1	16.3626	47.7	0.0598	50.4
LEARY-1DK-19-38 <>	123	1802	1.0	9.4218	259.0	0.1053	259.3
LEARY-1DK-19-64 <>	580	8188	1.4	22.9849	10.4	0.0432	10.7
LEARY-1DK-19-99 <>	143	5013	1.1	22.1624	35.3	0.0449	36.2
LEARY-1DK-19-107 <>	111	3213	1.0	29.2706	68.5	0.0341	68.8
LEARY-1DK-19-34 <>	87	2013	1.2	15.0246	123.7	0.0666	124.3
LEARY-1DK-19-3 <>	152	3698	0.6	43.9401	89.9	0.0229	90.2
LEARY-1DK-19-20 <>	136	4642	1.1	19.9793	57.1	0.0507	57.6
LEARY-1DK-19-83 <>	187	3281	0.3	17.5064	21.7	0.0581	22.7
LEARY-1DK-19-2	86	3311	1.0	15.2948	176.6	0.0667	176.9
LEARY-1DK-19-41 <>	75	1749	1.2	16.8784	189.1	0.0606	189.9
LEARY-1DK-19-35 <>	151	3901	1.0	22.7770	35.4	0.0450	35.9
LEARY-1DK-19-95 <>	99	2656	1.1	21.4038	63.7	0.0479	64.5
LEARY-1DK-19-69 <>	103	2420	1.0	34.2657	67.6	0.0300	68.9
LEARY-1DK-19-73 <>	102	4513	1.5	10.9020	134.7	0.0945	134.8
LEARY-1DK-19-9 <>	222	8629	1.1	28.6252	24.8	0.0360	25.0
LEARY-1DK-19-101 <>	185	2616	1.3	18.1874	42.5	0.0569	42.7
LEARY-1DK-19-75 <>	181	11851	1.3	26.8671	38.3	0.0385	39.0
LEARY-1DK-19-47 <>	76	2532	1.0	10.0078	132.9	0.1036	133.6
LEARY-1DK-19-10 <>	89	6093	1.3	23.9000	66.3	0.0434	67.2
LEARY-1DK-19-58 <>	137	5795	0.8	19.3474	37.8	0.0538	38.2
LEARY-1DK-19-94 <>	125	2017	1.5	16.8495	34.1	0.0622	34.8
LEARY-1DK-19-71 <>	140	3992	1.5	21.4303	43.0	0.0490	43.7
LEARY-1DK-19-16 <>	77	1930	1.3	-24.5538	193.4	-0.0428	193.9
LEARY-1DK-19-18 <>	157	5283	1.2	21.4805	39.6	0.0490	40.0
LEARY-1DK-19-100 <>	307	2418	1.2	19.3846	23.8	0.0544	25.4
LEARY-1DK-19-45 <>	336	12889	1.1	20.9405	17.0	0.0504	17.3
LEARY-1DK-19-13 <>	241	7929	0.8	27.2869	41.0	0.0388	41.3
LEARY-1DK-19-36 <>	62	2329	1.8	20.8736	122.2	0.0507	122.5
LEARY-1DK-19-31 <>	255	8555	1.0	23.2803	14.7	0.0456	15.2
LEARY-1DK-19-96 <>	286	17306	0.8	26.7591	19.2	0.0397	19.7
LEARY-1DK-19-15 <>	454	9333	1.1	19.5762	11.1	0.0543	11.4
LEARY-1DK-19-52 <>	139	6932	0.6	18.5941	27.1	0.0572	27.6
LEARY-1DK-19-108 <>	325	17952	1.0	22.9719	18.0	0.0464	18.3
LEARY-1DK-19-81 <>	395	10162	0.8	20.5564	11.5	0.0518	11.9
LEARY-1DK-19-57 <>	198	9301	0.8	19.2648	44.5	0.0553	44.7
LEARY-1DK-19-97 <>	158	4560	1.9	27.8381	40.1	0.0383	40.6
LEARY-1DK-19-84 <>	187	5712	1.4	25.0388	46.3	0.0426	47.3
LEARY-1DK-19-98 <>	106	4228	1.6	15.6522	25.2	0.0682	27.5
LEARY-1DK-19-51	243	10155	0.9	22.5336	28.3	0.0474	29.4
LEARY-1DK-19-90 <>	280	14793	0.7	22.7912	17.2	0.0469	17.5
LEARY-1DK-19-6 <>	1032	43023	1.3	20.4400	3.5	0.0524	4.2

LEARY-1DK-19-12 <>	662	20129	0.6	22.2007	11.2	0.0482	11.3
LEARY-1DK-19-40 <>	271	7740	0.8	22.9741	21.3	0.0467	21.8
LEARY-1DK-19-85 <>	570	18765	0.7	20.4842	11.4	0.0524	11.5
LEARY-1DK-19-23 <>	89	2541	1.5	20.5165	120.1	0.0524	120.9
LEARY-1DK-19-105 <>	1389	53370	0.9	20.7466	2.6	0.0518	3.1
LEARY-1DK-19-88 <>	385	10313	0.8	22.1714	14.7	0.0485	15.0
LEARY-1DK-19-7 <>	124	4288	1.1	24.9499	45.1	0.0432	45.5
LEARY-1DK-19-74 <>	213	4964	1.3	24.8332	33.4	0.0434	33.8
LEARY-1DK-19-14 <>	170	6170	1.3	24.3075	46.9	0.0444	47.2
LEARY-1DK-19-63 <>	193	8067	4.4	21.8917	32.3	0.0494	33.1
LEARY-1DK-19-82 <>	1630	26054	2.1	20.9371	6.4	0.0517	7.0
LEARY-1DK-19-29 <>	276	7640	1.1	21.2486	25.3	0.0510	25.7
LEARY-1DK-19-49 <>	105	4249	1.5	7.0429	327.1	0.1539	327.3
LEARY-1DK-19-70 <>	244	11611	1.4	21.9123	18.6	0.0495	20.2
LEARY-1DK-19-61 <>	81	2168	2.0	26.4679	72.1	0.0410	73.0
LEARY-1DK-19-39 <>	146	5167	1.4	23.6803	33.8	0.0458	34.8
LEARY-1DK-19-17 <>	151	217	1.0	11.8717	34.8	0.0919	37.5
LEARY-1DK-19-26 <>	123	535	0.8	18.5129	37.4	0.0589	38.6
LEARY-1DK-19-33 <>	196	5108	1.3	20.9887	18.1	0.0521	18.7
LEARY-1DK-19-102 <>	98	1841	1.2	19.8103	48.3	0.0555	50.5
LEARY-1DK-19-54 <>	250	10932	1.6	23.7392	21.8	0.0464	22.2
LEARY-1DK-19-66 <>	583	15927	0.9	21.5171	4.9	0.0514	5.4
LEARY-1DK-19-87 <>	121	6704	0.7	19.2003	41.9	0.0577	42.9
LEARY-1DK-19-65 <>	205	5910	1.2	36.0702	36.7	0.0308	36.8
LEARY-1DK-19-104 <>	144	4447	1.3	18.0841	28.9	0.0616	29.8
LEARY-1DK-19-67 <>	179	4266	1.0	21.5648	45.7	0.0518	46.3
LEARY-1DK-19-25 <>	106	8847	0.8	18.3420	47.5	0.0615	48.7
LEARY-1DK-19-42 <>	494	4965	1.1	19.0673	11.2	0.0592	11.8
LEARY-1DK-19-60 <>	428	4258	0.7	19.6682	9.6	0.0574	10.0
LEARY-1DK-19-80 <>	80	2239	1.0	15.8008	129.2	0.0723	129.9
LEARY-1DK-19-77 <>	124	23411	1.0	18.9429	59.6	0.0606	60.7
LEARY-1DK-19-48 <>	123	405	1.5	13.1223	33.9	0.0877	36.9
LEARY-1DK-19-32 <>	389	1727	0.7	18.1511	13.0	0.0636	13.8
LEARY-1DK-19-109 <>	219	2761	0.9	21.0712	44.1	0.0551	44.5
LEARY-1DK-19-53 <>	430	7136	0.7	19.7965	11.1	0.0591	11.3
LEARY-1DK-19-4 <>	53	1196	1.0	-13.3127	225.3	-0.0883	226.0
LEARY-1DK-19-62 <>	167	3408	1.2	19.8381	26.2	0.0597	27.0
LEARY-1DK-19-103 <>	116	4959	1.4	20.9357	23.8	0.0567	24.5
LEARY-1DK-19-59 <>	116	2995	0.9	27.6333	65.0	0.0437	65.1
LEARY-1DK-19-86 <>	116	3573	0.9	21.0714	53.7	0.0573	55.4
LEARY-1DK-19-43 <>	258	2531	0.5	17.3801	22.7	0.0699	23.5
LEARY-1DK-19-22 <>	136	4695	1.7	26.4840	103.8	0.0481	104.6
LEARY-1DK-19-93 <>	82	6285	0.9	18.2272	30.1	0.1004	30.8
LEARY-1DK-19-24 <>	430	36310	0.9	20.7955	6.2	0.0901	6.4
LEARY-1DK-19-27 <>	411	21663	1.8	20.8229	4.9	0.0904	5.4
LEARY-1DK-19-30 <>	1581	64327	2.0	20.5881	2.0	0.0927	2.3
LEARY-1DK-19-21 <>	113	6309	1.6	19.9294	16.3	0.0989	16.8

LEARY-1DK-19-79 <>	726	6952	1.6	19.7791	6.0	0.1006	12.2
--------------------	-----	------	-----	---------	-----	--------	------

Sample:	1DK-246	N29.30596	E89.82294				
LEARY-1DK-246-106 <	396	1561	0.9	19.5835	30.3	0.0232	30.7
LEARY-1DK-246-61 <>	430	297	1.2	14.4315	24.5	0.0319	25.1
LEARY-1DK-246-16 <>	324	2629	1.1	24.9781	53.2	0.0184	54.3
LEARY-1DK-246-60 <>	415	3416	1.0	25.2298	35.7	0.0184	36.0
LEARY-1DK-246-105 <	508	5306	1.1	17.4678	18.1	0.0267	18.6
LEARY-1DK-246-31 <>	461	9910	0.7	21.4834	26.9	0.0220	27.5
LEARY-1DK-246-27 <>	509	4415	0.9	20.5079	25.5	0.0232	26.0
LEARY-1DK-246-2 <>	444	4349	1.0	21.6004	16.7	0.0220	17.5
LEARY-1DK-246-17 <>	586	1282	0.7	20.2524	16.0	0.0235	16.8
LEARY-1DK-246-100 <	322	675	1.2	19.9173	22.1	0.0240	23.4
LEARY-1DK-246-14 <>	477	4260	1.0	20.8928	30.8	0.0229	31.0
LEARY-1DK-246-63 <>	620	6817	1.2	26.7936	32.7	0.0179	33.0
LEARY-1DK-246-57 <>	742	5535	0.6	22.1119	15.3	0.0217	15.4
LEARY-1DK-246-38 <>	407	5046	1.1	21.1900	40.9	0.0227	41.6
LEARY-1DK-246-96 <>	513	188	0.8	15.0000	31.0	0.0321	32.1
LEARY-1DK-246-34 <>	462	5344	0.9	24.4720	25.9	0.0197	26.1
LEARY-1DK-246-82 <>	529	11703	0.8	25.4396	39.3	0.0189	39.5
LEARY-1DK-246-43 <>	646	4980	0.9	20.8630	22.9	0.0231	23.2
LEARY-1DK-246-18 <>	622	5297	1.0	19.9851	30.0	0.0241	30.2
LEARY-1DK-246-68 <>	441	2702	0.9	22.1024	28.2	0.0218	28.7
LEARY-1DK-246-24 <>	320	1726	1.2	24.8278	63.8	0.0195	64.8
LEARY-1DK-246-53 <>	430	5476	0.9	18.6649	21.1	0.0259	21.5
LEARY-1DK-246-83 <>	349	3859	1.0	21.2266	43.0	0.0228	43.5
LEARY-1DK-246-10 <>	480	10815	1.1	33.7500	47.5	0.0144	47.6
LEARY-1DK-246-45 <>	513	2822	1.3	20.3922	23.4	0.0238	24.3
LEARY-1DK-246-36 <>	571	4149	0.8	23.9818	18.0	0.0202	18.9
LEARY-1DK-246-42 <>	420	1136	1.0	22.7193	40.3	0.0214	41.6
LEARY-1DK-246-86 <>	473	7347	0.8	22.0527	16.0	0.0221	16.8
LEARY-1DK-246-6 <>	428	4168	0.9	22.2330	36.4	0.0219	36.9
LEARY-1DK-246-28 <>	559	1285	0.8	21.4797	16.8	0.0227	17.4
LEARY-1DK-246-9 <>	490	4343	1.0	25.1006	17.1	0.0195	18.4
LEARY-1DK-246-20 <>	508	4854	1.0	20.1418	14.1	0.0243	14.3
LEARY-1DK-246-66 <>	576	4250	0.8	18.0043	14.9	0.0271	15.3
LEARY-1DK-246-71 <>	483	3075	0.9	24.2116	44.2	0.0202	44.3
LEARY-1DK-246-55 <>	425	3495	1.1	24.0986	21.4	0.0203	22.0
LEARY-1DK-246-70 <>	472	3606	1.0	18.0169	12.0	0.0272	12.8
LEARY-1DK-246-64 <>	537	2080	0.9	20.6634	22.2	0.0237	22.3
LEARY-1DK-246-21 <>	449	2323	1.0	17.8725	31.6	0.0275	31.9
LEARY-1DK-246-97 <>	424	7154	0.9	19.9906	43.3	0.0246	43.5
LEARY-1DK-246-48 <>	471	4599	1.2	32.4419	43.1	0.0152	43.4
LEARY-1DK-246-47 <>	341	24586	0.9	19.4162	30.4	0.0254	31.2
LEARY-1DK-246-40 <>	407	5037	1.1	21.3544	30.0	0.0231	30.3
LEARY-1DK-246-56 <>	633	5772	0.7	20.5404	17.4	0.0240	17.9
LEARY-1DK-246-44 <>	496	1943	1.2	23.7660	24.7	0.0208	26.6

LEARY-1DK-246-52 <>	425	1310	0.9	20.2354	21.8	0.0244	22.2
LEARY-1DK-246-30 <>	575	3553	1.0	21.3722	25.5	0.0232	25.8
LEARY-1DK-246-51 <>	646	1799	0.6	26.0401	34.2	0.0192	34.5
LEARY-1DK-246-22 <>	479	2974	0.8	23.3948	29.6	0.0214	29.9
LEARY-1DK-246-81 <>	466	1025	0.9	19.5253	17.3	0.0257	18.4
LEARY-1DK-246-25 <>	375	3081	0.7	25.2883	30.8	0.0199	31.2
LEARY-1DK-246-79 <>	499	2432	0.9	20.1385	15.6	0.0250	17.3
LEARY-1DK-246-91 <>	446	8765	1.3	19.5240	35.8	0.0258	36.1
LEARY-1DK-246-103 <	399	4228	0.9	22.3406	36.6	0.0226	36.8
LEARY-1DK-246-46 <>	350	898	1.0	15.9460	18.6	0.0317	19.8
LEARY-1DK-246-58 <>	477	3362	1.4	23.5852	20.2	0.0214	20.9
LEARY-1DK-246-7 <>	420	762	0.9	16.4983	32.3	0.0307	33.0
LEARY-1DK-246-73 <>	439	1541	1.1	17.5777	36.9	0.0297	37.3
LEARY-1DK-246-101 <	483	1589	1.2	24.8679	23.2	0.0210	23.6
LEARY-1DK-246-12 <>	446	533	0.9	16.1294	40.6	0.0328	41.4
LEARY-1DK-246-108 <	319	666	1.0	13.6685	40.0	0.0388	40.5
LEARY-1DK-246-78 <>	248	1138	1.3	6.9587	125.2	0.0762	125.4
LEARY-1DK-246-109 <	380	1243	1.3	13.7599	28.4	0.0393	29.0
LEARY-1DK-246-23 <>	577	5257	0.8	20.0480	16.4	0.0270	16.7
LEARY-1DK-246-67 <>	660	6436	1.4	20.3454	16.0	0.0267	16.3
LEARY-1DK-246-33 <>	454	3738	0.5	18.7136	22.8	0.0482	22.9
LEARY-1DK-246-39 <>	355	8601	0.5	23.5571	21.6	0.0384	22.5
LEARY-1DK-246-59 <>	479	5910	0.9	19.0498	21.4	0.0478	22.4
LEARY-1DK-246-75 <>	375	4962	0.6	19.1209	11.1	0.0485	11.4
LEARY-1DK-246-87 <>	385	809	0.7	19.1754	19.6	0.0485	19.8
LEARY-1DK-246-85 <>	435	4745	0.6	22.5636	18.8	0.0413	19.1
LEARY-1DK-246-80 <>	630	7136	0.6	22.3971	8.7	0.0418	8.9
LEARY-1DK-246-65 <>	753	1099	1.8	21.8203	12.0	0.0429	12.0
LEARY-1DK-246-104 <	217	9626	0.5	24.9304	52.4	0.0375	52.5
LEARY-1DK-246-99 <>	934	35304	0.7	22.7842	5.5	0.0411	5.6
LEARY-1DK-246-13 <>	568	10882	0.6	21.4526	9.8	0.0438	10.4
LEARY-1DK-246-107 <	851	3037	0.3	19.5283	11.8	0.0482	11.9
LEARY-1DK-246-72 <>	476	12022	0.6	22.7027	17.2	0.0415	17.3
LEARY-1DK-246-49 <>	533	12923	0.6	22.9042	15.4	0.0412	15.7
LEARY-1DK-246-77 <>	1040	12997	0.9	21.4268	8.2	0.0440	8.3
LEARY-1DK-246-19 <>	776	12428	0.4	21.7884	8.3	0.0433	8.4
LEARY-1DK-246-94 <>	983	3435	0.5	21.2448	10.7	0.0445	10.9
LEARY-1DK-246-3 <>	449	6888	1.3	22.1860	21.6	0.0427	21.9
LEARY-1DK-246-62 <>	277	5364	0.7	25.4425	39.4	0.0372	39.8
LEARY-1DK-246-5 <>	594	52575	0.5	20.5025	10.2	0.0463	10.3
LEARY-1DK-246-95 <>	642	17485	0.6	20.9183	8.1	0.0453	8.3
LEARY-1DK-246-54 <>	319	1976	0.5	19.2404	13.8	0.0493	14.1
LEARY-1DK-246-26 <>	338	1584	0.5	16.0748	13.4	0.0591	14.1
LEARY-1DK-246-90 <>	464	15175	0.7	22.5745	18.6	0.0421	19.0
LEARY-1DK-246-15 <>	726	13172	0.7	20.8690	7.7	0.0456	8.0
LEARY-1DK-246-35 <>	642	23817	0.3	21.3577	12.3	0.0446	12.7
LEARY-1DK-246-93 <>	1056	19454	8.9	18.7658	11.8	0.0510	14.0

LEARY-1DK-246-76 <>	1738	13636	0.3	21.4843	5.5	0.0446	5.6
LEARY-1DK-246-102 <	398	6488	1.3	21.9326	14.6	0.0437	14.9
LEARY-1DK-246-29 <>	657	7133	0.5	20.0678	15.5	0.0481	15.6
LEARY-1DK-246-11 <>	756	4221	0.5	18.4405	11.3	0.0526	11.4
LEARY-1DK-246-4 <>	484	593	0.4	19.7957	23.9	0.0490	24.2
LEARY-1DK-246-74 <>	277	9920	0.5	19.9576	25.5	0.0488	25.6
LEARY-1DK-246-69 <>	223	13546	3.2	21.6624	23.7	0.0492	24.0
LEARY-1DK-246-110 <	1010	42237	0.9	21.2948	6.2	0.0506	6.3
LEARY-1DK-246-37 <>	85	4128	1.0	9.3995	210.4	0.1171	210.6
LEARY-1DK-246-88 <>	145	7273	0.8	26.3379	29.3	0.0687	29.5
LEARY-1DK-246-92 <>	140	64673	1.6	8.6263	0.5	5.7246	5.3

					Apparent ages (Ma)			
206Pb*	±	error	206Pb*	±	207Pb*	±	206Pb*	±
238U	(%)	corr.	238U*	(Ma)	235U	(Ma)	207Pb*	(Ma)

0.0034	2.4	0.47	21.6	0.5	23.5	1.2	226.5	104.9
0.0071	2.6	0.35	45.8	1.2	41.2	2.9	223.2	170.9
0.0072	3.2	0.63	46.4	1.5	45.9	2.3	16.4	95.3
0.0073	2.3	0.39	47.2	1.1	43.7	2.6	143.9	139.4
0.0074	1.9	0.54	47.3	0.9	49.4	1.7	150.4	70.0
0.0074	3.8	0.75	47.4	1.8	48.1	2.4	81.7	78.9
0.0074	1.7	0.42	47.5	0.8	47.0	1.8	23.3	86.5
0.0074	3.0	0.66	47.5	1.4	49.2	2.2	133.8	79.6
0.0074	2.9	0.66	47.5	1.4	46.0	2.0	31.5	81.9
0.0074	2.7	0.51	47.6	1.3	48.5	2.5	90.5	106.3
0.0074	1.8	0.21	47.7	0.9	48.6	4.2	95.0	207.5
0.0074	1.5	0.42	47.8	0.7	51.2	1.8	215.3	76.3
0.0075	2.3	0.40	48.0	1.1	48.2	2.7	60.3	127.2
0.0075	3.8	0.67	48.1	1.8	47.1	2.6	3.7	101.4
0.0075	2.0	0.45	48.1	0.9	48.7	2.1	81.6	93.9
0.0075	1.6	0.27	48.1	0.8	49.3	2.8	108.8	132.7
0.0075	2.3	0.61	48.2	1.1	48.4	1.8	60.6	71.4
0.0075	1.9	0.50	48.2	0.9	47.4	1.8	4.4	80.6
0.0076	2.0	0.51	48.5	1.0	51.1	2.0	172.7	79.0
0.0076	2.3	0.57	48.6	1.1	52.2	2.0	223.6	76.1
0.0076	2.9	0.69	48.7	1.4	54.2	2.2	303.6	67.5
0.0076	2.2	0.48	48.7	1.0	47.5	2.1	12.1	95.3
0.0076	2.8	0.50	49.0	1.4	47.0	2.6	56.7	118.8
0.0076	2.4	0.47	49.1	1.2	48.6	2.4	25.9	109.1
0.0076	2.0	0.51	49.1	1.0	48.5	1.9	17.9	82.2
0.0076	2.1	0.53	49.1	1.0	49.0	1.9	46.4	78.9
0.0076	1.8	0.41	49.1	0.9	48.7	2.1	28.4	97.9
0.0077	1.9	0.40	49.2	0.9	51.7	2.3	169.6	98.2
0.0077	2.5	0.26	49.2	1.2	69.5	6.5	840.2	195.5
0.0077	3.0	0.59	49.2	1.5	53.3	2.6	242.0	94.2
0.0077	2.6	0.47	49.4	1.3	51.8	2.9	165.3	116.8
0.0077	2.5	0.36	49.4	1.2	51.1	3.5	129.4	154.2
0.0077	1.8	0.41	49.5	0.9	48.6	2.1	5.0	95.4
0.0077	1.7	0.51	49.5	0.8	62.5	2.0	594.4	60.2
0.0077	3.1	0.38	49.6	1.5	48.1	3.9	24.1	184.4
0.0077	2.2	0.42	49.7	1.1	50.4	2.5	83.2	111.7
0.0077	2.2	0.37	49.7	1.1	48.2	2.8	29.7	134.5
0.0078	2.7	0.69	49.8	1.3	52.3	2.0	167.1	65.9
0.0078	1.9	0.41	49.8	1.0	57.9	2.6	404.3	95.1
0.0078	2.9	0.63	49.9	1.4	49.9	2.3	51.8	85.7

0.0078	4.0	0.56	49.9	2.0	47.3	3.3	78.8	144.2
0.0078	1.9	0.18	50.0	0.9	73.4	7.3	923.1	209.8
0.0078	1.8	0.40	50.0	0.9	51.8	2.2	136.6	93.5
0.0078	2.0	0.53	50.1	1.0	50.0	1.8	46.9	75.3
0.0078	1.9	0.40	50.1	0.9	48.2	2.2	44.8	103.7
0.0078	1.7	0.42	50.2	0.8	48.0	1.9	58.6	88.1
0.0078	4.0	0.75	50.3	2.0	51.9	2.7	126.2	83.6
0.0078	2.4	0.49	50.4	1.2	50.0	2.4	33.2	103.8
0.0079	4.7	0.73	50.4	2.3	50.9	3.2	71.8	103.9
0.0079	2.4	0.21	50.5	1.2	72.7	8.0	882.0	229.8
0.0079	1.8	0.39	50.5	0.9	50.1	2.2	28.2	101.3
0.0079	3.6	0.57	50.6	1.8	51.5	3.2	95.5	124.6
0.0079	3.8	0.65	50.6	1.9	51.6	2.9	98.2	105.2
0.0079	2.4	0.32	50.9	1.2	54.2	3.9	201.2	161.9
0.0079	2.1	0.45	51.0	1.1	48.5	2.2	73.1	101.5
0.0080	1.6	0.34	51.1	0.8	50.5	2.4	25.6	107.8
0.0080	1.6	0.17	51.5	0.8	77.7	7.3	981.3	195.9
0.0080	2.4	0.45	51.6	1.2	58.6	3.0	356.8	107.2
0.0080	3.4	0.56	51.7	1.8	51.2	3.0	30.2	119.9
0.0081	2.2	0.13	51.8	1.1	92.3	14.6	1330.6	318.5
0.0081	2.1	0.53	51.8	1.1	53.7	2.0	142.9	77.4
0.0081	1.7	0.72	51.8	0.9	52.0	1.2	61.4	38.5
0.0081	3.5	0.51	51.8	1.8	54.2	3.7	161.3	139.8
0.0081	2.4	0.52	52.0	1.3	53.9	2.5	140.9	94.2
0.0081	1.5	0.29	52.1	0.8	48.7	2.4	114.6	116.9
0.0082	2.1	0.46	52.3	1.1	57.1	2.5	260.0	92.4
0.0082	2.1	0.67	52.4	1.1	53.0	1.6	83.7	56.3
0.0082	2.5	0.13	52.5	1.3	103.4	18.6	1530.2	355.9
0.0082	4.1	0.12	52.5	2.1	130.4	40.7	1979.1	605.1
0.0083	1.9	0.30	53.4	1.0	53.2	3.3	45.0	143.5
0.0084	2.1	0.70	54.1	1.2	52.9	1.6	5.3	53.5
0.0086	1.3	0.43	55.0	0.7	56.8	1.6	132.1	61.9
0.0086	4.2	0.12	55.5	2.3	143.5	48.2	2061.5	654.4
0.0088	3.8	0.68	56.6	2.2	53.6	3.0	79.3	101.8
0.0088	1.9	0.43	56.8	1.1	57.6	2.5	93.6	93.7
0.0090	2.5	0.39	57.4	1.4	55.2	3.5	41.9	145.3
0.0091	1.8	0.43	58.2	1.1	58.5	2.4	72.5	90.7
0.0091	2.1	0.58	58.3	1.2	59.3	2.1	99.9	69.8
0.0091	3.6	0.48	58.3	2.1	60.0	4.4	128.0	156.3
0.0092	1.4	0.33	59.1	0.8	56.5	2.3	52.6	97.9
0.0092	2.2	0.53	59.1	1.3	60.6	2.4	118.1	82.9
0.0092	1.8	0.49	59.3	1.1	59.8	2.2	79.7	78.8
0.0092	2.8	0.28	59.3	1.6	56.5	5.5	60.7	234.2
0.0093	2.2	0.29	59.5	1.3	65.6	4.7	295.6	161.8
0.0093	2.8	0.71	59.6	1.6	60.2	2.3	82.7	65.6
0.0093	3.1	0.74	59.7	1.8	59.0	2.4	28.9	66.5
0.0093	2.1	0.56	59.8	1.3	62.6	2.3	171.1	72.5

0.0093	1.9	0.35	59.9	1.1	56.8	2.9	73.3	121.3
0.0093	2.4	0.44	59.9	1.5	55.9	3.0	113.7	123.0
0.0094	2.4	0.49	60.0	1.4	63.7	3.0	202.2	98.8
0.0094	1.5	0.66	60.4	0.9	60.7	1.4	75.1	41.5
0.0094	1.9	0.48	60.6	1.1	61.3	2.3	87.7	82.2
0.0096	2.5	0.71	61.3	1.5	62.6	2.1	113.1	58.3
0.0096	2.4	0.33	61.5	1.5	86.6	6.0	850.9	142.0
0.0096	1.4	0.59	61.6	0.9	63.0	1.4	114.7	44.4
0.0096	2.4	0.53	61.8	1.5	59.9	2.6	14.4	93.0
0.0097	2.4	0.50	62.5	1.5	64.0	3.0	119.8	98.5
0.0098	2.5	0.36	62.9	1.6	63.6	4.3	90.6	154.5
0.0099	1.8	0.52	63.7	1.2	63.6	2.2	62.5	72.0
0.0101	3.7	0.48	64.7	2.4	81.3	6.0	602.9	145.4
0.0103	2.0	0.19	65.9	1.3	98.9	10.0	990.3	211.6
0.0104	1.9	0.33	66.4	1.3	64.6	3.7	0.5	134.4
0.0104	1.4	0.46	66.9	0.9	65.9	1.9	31.1	63.9
0.0106	1.8	0.77	68.1	1.2	67.6	1.5	48.9	36.1
0.0140	1.5	0.68	89.4	1.4	90.3	2.0	112.4	39.3
0.0143	2.9	0.23	91.7	2.6	603.8	56.1	3950.1	180.4
0.0237	2.9	0.63	151.1	4.3	149.3	6.3	121.8	83.5
0.0247	2.9	0.69	157.0	4.5	163.7	6.3	261.8	69.5
0.0288	1.9	0.60	183.1	3.4	185.6	5.4	218.5	58.7

0.0036	1.8	0.45	23.2	0.4	23.6	1.0	62.9	86.9
0.0070	2.7	0.45	44.9	1.2	47.5	2.7	184.8	122.2
0.0071	2.3	0.42	45.4	1.0	46.8	2.5	121.5	118.0
0.0072	2.4	0.46	46.0	1.1	47.0	2.4	94.8	110.3
0.0073	1.8	0.51	46.8	0.8	46.5	1.6	33.2	70.7
0.0073	2.1	0.37	46.8	1.0	47.4	2.7	73.6	127.7
0.0073	1.5	0.53	46.9	0.7	46.3	1.3	18.0	57.4
0.0073	1.6	0.35	47.0	0.8	52.5	2.4	312.2	99.8
0.0073	1.7	0.53	47.0	0.8	46.5	1.5	18.7	66.2
0.0073	2.2	0.33	47.2	1.0	49.0	3.1	141.8	144.5
0.0074	2.2	0.55	47.3	1.0	49.4	1.9	152.0	76.8
0.0074	3.3	0.34	47.4	1.6	50.6	4.8	203.4	213.8
0.0074	2.5	0.43	47.7	1.2	49.6	2.8	144.6	120.8
0.0075	2.1	0.33	47.9	1.0	50.7	3.1	184.0	137.3
0.0075	2.5	0.30	48.0	1.2	49.5	4.0	122.6	185.4
0.0075	2.8	0.47	48.2	1.3	49.9	2.9	131.9	121.9
0.0075	3.7	0.49	48.2	1.8	50.9	3.7	177.1	152.6
0.0075	1.4	0.21	48.3	0.7	48.7	3.1	70.0	153.1
0.0075	2.7	0.45	48.3	1.3	53.6	3.2	296.9	126.1
0.0075	2.9	0.51	48.4	1.4	50.1	2.7	134.9	113.7
0.0075	3.7	0.43	48.4	1.8	54.0	4.5	306.9	176.6
0.0075	2.9	0.32	48.5	1.4	47.1	4.1	21.2	204.2
0.0075	2.3	0.44	48.5	1.1	48.3	2.5	42.7	112.4

0.0076	2.0	0.36	48.5	1.0	48.2	2.6	32.4	123.4
0.0076	2.4	0.57	48.6	1.1	48.2	1.9	30.9	80.9
0.0076	2.4	0.33	48.6	1.1	50.3	3.5	131.7	158.5
0.0076	2.4	0.46	48.7	1.2	44.7	2.3	164.1	114.8
0.0076	2.6	0.38	48.9	1.2	45.7	3.0	117.8	152.5
0.0076	2.2	0.27	48.9	1.1	57.0	4.5	414.4	175.8
0.0076	2.3	0.36	49.0	1.1	49.9	3.1	93.9	139.8
0.0076	2.2	0.49	49.1	1.1	50.2	2.2	103.8	91.3
0.0077	2.0	0.32	49.1	1.0	50.8	3.1	129.1	137.9
0.0077	2.3	0.46	49.1	1.1	50.0	2.5	90.6	106.6
0.0077	1.8	0.29	49.1	0.9	50.5	3.0	114.0	139.7
0.0077	2.2	0.42	49.2	1.1	49.1	2.5	43.0	110.8
0.0077	3.5	0.46	49.2	1.7	38.8	2.9	567.5	179.5
0.0077	1.6	0.27	49.2	0.8	49.5	2.8	63.5	133.6
0.0077	2.0	0.38	49.3	1.0	44.9	2.3	183.0	120.8
0.0077	2.8	0.35	49.3	1.4	53.6	4.2	250.4	171.7
0.0077	1.8	0.28	49.3	0.9	49.4	3.0	55.9	143.9
0.0077	2.0	0.54	49.3	1.0	48.9	1.8	27.1	75.5
0.0077	2.0	0.44	49.3	1.0	48.5	2.1	9.1	97.6
0.0077	2.2	0.29	49.3	1.1	47.2	3.5	62.6	175.6
0.0077	1.8	0.25	49.4	0.9	55.6	3.8	330.2	156.0
0.0077	2.1	0.34	49.4	1.0	47.6	2.9	39.6	142.7
0.0077	2.3	0.32	49.4	1.1	48.9	3.5	22.4	165.8
0.0077	2.1	0.53	49.5	1.0	49.4	1.9	47.4	79.7
0.0077	2.5	0.39	49.5	1.2	51.9	3.2	160.7	137.9
0.0077	1.9	0.36	49.7	0.9	50.9	2.6	110.8	114.6
0.0077	2.3	0.31	49.8	1.1	50.6	3.6	92.1	166.0
0.0078	1.9	0.42	49.8	1.0	48.8	2.2	0.6	101.6
0.0078	2.2	0.22	49.9	1.1	46.3	4.6	136.7	246.5
0.0078	1.8	0.36	50.0	0.9	47.6	2.3	73.7	113.1
0.0078	2.8	0.35	50.0	1.4	52.4	4.1	162.7	174.7
0.0078	1.8	0.29	50.1	0.9	48.6	3.0	23.1	145.4
0.0078	1.3	0.40	50.1	0.7	50.1	1.6	52.4	72.8
0.0078	2.8	0.41	50.1	1.4	51.4	3.4	114.2	147.6
0.0078	2.6	0.45	50.1	1.3	47.2	2.7	97.6	129.1
0.0078	2.1	0.41	50.2	1.1	51.6	2.6	119.4	109.0
0.0078	2.4	0.39	50.3	1.2	47.5	2.9	88.3	140.1
0.0078	2.5	0.33	50.4	1.2	52.3	3.8	143.0	164.6
0.0079	2.2	0.33	50.5	1.1	48.6	3.1	43.4	151.0
0.0079	2.9	0.53	50.5	1.5	50.6	2.7	56.6	111.4
0.0079	2.0	0.35	50.5	1.0	51.4	2.9	92.5	130.1
0.0079	3.0	0.61	50.6	1.5	55.9	2.7	293.0	90.8
0.0079	2.1	0.52	50.6	1.1	53.6	2.2	191.5	82.1
0.0079	1.9	0.26	50.6	1.0	45.3	3.3	227.4	182.9
0.0079	1.8	0.24	50.6	0.9	51.5	3.7	96.2	168.8
0.0079	1.9	0.48	50.9	1.0	50.6	2.0	37.6	84.0
0.0079	1.5	0.35	51.0	0.7	48.6	2.0	67.5	95.1

0.0080	2.4	0.46	51.1	1.2	50.0	2.6	3.8	113.0
0.0080	1.3	0.45	51.2	0.7	53.4	1.5	153.4	59.7
0.0080	1.6	0.43	51.3	0.8	52.0	1.9	83.4	79.6
0.0080	2.2	0.47	51.4	1.1	50.3	2.3	1.3	98.2
0.0081	2.1	0.37	51.8	1.1	55.9	3.1	233.4	122.4
0.0081	2.5	0.26	51.9	1.3	58.3	5.4	328.5	211.2
0.0081	1.7	0.42	52.2	0.9	50.3	2.0	37.3	92.1
0.0081	2.6	0.34	52.3	1.4	64.9	4.8	560.0	154.9
0.0082	1.5	0.46	52.3	0.8	52.7	1.6	68.7	67.3
0.0082	1.5	0.36	52.8	0.8	53.4	2.2	82.0	92.3
0.0082	2.2	0.59	52.8	1.1	52.2	1.9	25.9	71.6
0.0083	2.3	0.38	53.1	1.2	49.9	2.9	104.5	137.5
0.0083	1.5	0.31	53.4	0.8	58.1	2.7	255.4	106.4
0.0084	3.6	0.09	53.8	1.9	180.3	64.7	2541.2	682.5
0.0087	1.5	0.40	55.9	0.9	56.6	2.1	86.3	82.8
0.0088	1.7	0.28	56.5	1.0	57.7	3.5	110.9	139.4
0.0088	2.5	0.30	56.7	1.4	59.1	4.8	155.7	188.0
0.0088	3.1	0.63	56.7	1.7	172.7	7.7	2370.6	64.3
0.0098	6.0	0.12	62.6	3.7	208.3	94.7	2551.4	900.2
0.0106	3.4	0.37	67.8	2.3	337.6	26.5	3310.2	134.8
0.0111	2.3	0.32	71.3	1.7	82.5	5.8	421.4	154.4
0.0125	1.3	0.44	80.2	1.0	81.7	2.3	124.9	61.8
0.0130	3.1	0.50	83.4	2.6	84.8	5.1	125.3	128.7
0.0131	3.4	0.41	84.0	2.8	85.0	6.7	113.9	176.9
0.0132	2.1	0.39	84.4	1.8	86.3	4.4	139.4	115.6
0.0134	1.7	0.42	85.9	1.4	90.3	3.4	208.9	82.1
0.0135	2.2	0.35	86.1	1.9	89.8	5.4	188.9	137.7
0.0139	1.5	0.38	89.2	1.3	88.9	3.4	80.3	88.3
0.0140	2.0	0.38	89.3	1.8	93.3	4.6	195.1	111.1
0.0140	1.8	0.72	89.7	1.6	90.1	2.1	100.5	40.1
0.0140	2.1	0.46	89.7	1.8	93.4	4.0	189.4	92.2
0.0141	1.4	0.33	90.5	1.2	96.3	3.8	241.3	90.6
0.0143	2.3	0.37	91.8	2.1	100.9	6.0	320.1	132.2
0.0234	1.7	0.60	148.9	2.5	145.3	3.8	86.0	52.8
0.0246	1.1	0.65	156.7	1.7	158.1	2.5	178.4	30.6
0.0270	2.9	0.69	171.9	4.9	172.7	6.7	184.0	70.5
0.0274	2.4	0.69	174.6	4.1	176.6	5.6	204.3	58.2

0.0037	2.9	0.61	23.8	0.7	25.1	1.2	151.5	88.7
0.0068	1.7	0.37	44.0	0.8	44.0	2.0	43.9	102.1
0.0071	1.8	0.51	45.4	0.8	48.0	1.7	178.1	71.6
0.0072	2.4	0.30	46.0	1.1	51.1	3.9	296.0	172.1
0.0072	2.2	0.43	46.0	1.0	47.6	2.4	128.7	111.3
0.0072	3.3	0.33	46.4	1.5	17.0	1.7	0.0	1467.2
0.0073	1.3	0.29	46.7	0.6	47.3	2.1	77.3	104.4
0.0073	1.9	0.62	46.7	0.9	47.1	1.4	65.9	55.9

0.0073	2.5	0.39	46.8	1.1	47.4	2.9	80.8	138.7
0.0073	1.8	0.57	47.1	0.9	48.0	1.5	92.5	62.9
0.0074	1.9	0.48	47.4	0.9	46.4	1.8	1.7	84.1
0.0074	2.4	0.25	47.8	1.2	50.3	4.8	167.1	221.0
0.0075	3.4	0.34	48.0	1.6	51.0	4.9	192.3	215.7
0.0075	2.9	0.27	48.1	1.4	51.2	5.4	197.3	244.8
0.0075	2.4	0.31	48.3	1.2	46.3	3.5	57.6	180.1
0.0075	1.9	0.34	48.3	0.9	53.0	2.9	270.2	119.0
0.0075	2.0	0.53	48.5	1.0	48.9	1.8	70.6	75.0
0.0076	1.7	0.47	48.8	0.8	51.4	1.9	173.9	76.9
0.0076	1.4	0.21	48.8	0.7	54.3	3.6	303.2	153.2
0.0076	2.3	0.38	48.9	1.1	48.4	2.8	25.8	131.3
0.0076	3.7	0.35	48.9	1.8	40.7	4.2	418.9	257.4
0.0076	2.5	0.36	49.0	1.2	47.2	3.2	45.0	158.2
0.0076	1.7	0.53	49.0	0.8	48.8	1.6	34.9	67.3
0.0076	2.2	0.33	49.1	1.1	51.8	3.3	176.5	144.9
0.0077	2.3	0.31	49.2	1.1	47.6	3.4	32.0	169.7
0.0077	4.2	0.38	49.2	2.1	52.3	5.6	196.6	237.9
0.0077	1.5	0.33	49.2	0.7	49.0	2.1	37.4	100.4
0.0077	1.5	0.43	49.2	0.8	49.0	1.7	36.2	78.1
0.0077	3.1	0.65	49.2	1.5	48.9	2.3	32.4	87.8
0.0077	1.9	0.30	49.5	1.0	46.4	3.0	109.6	153.5
0.0077	1.7	0.36	49.5	0.8	52.4	2.4	182.8	101.5
0.0077	2.8	0.32	49.6	1.4	48.8	4.1	11.2	196.8
0.0077	2.1	0.32	49.7	1.1	50.5	3.3	92.1	150.0
0.0077	1.7	0.36	49.7	0.8	47.6	2.2	55.1	106.2
0.0077	3.1	0.50	49.7	1.5	58.9	3.5	447.7	119.3
0.0077	1.5	0.24	49.7	0.7	48.0	2.9	39.2	147.4
0.0078	2.0	0.45	49.8	1.0	49.0	2.1	6.6	94.4
0.0078	4.7	0.76	49.9	2.3	47.4	2.9	74.0	98.9
0.0078	1.3	0.22	49.9	0.7	49.8	2.9	46.2	138.6
0.0078	2.7	0.48	49.9	1.3	53.1	2.9	202.6	113.7
0.0078	2.3	0.42	50.0	1.2	50.2	2.7	59.2	119.3
0.0078	2.2	0.28	50.0	1.1	45.9	3.6	162.7	191.6
0.0078	2.0	0.62	50.1	1.0	52.1	1.6	146.8	59.4
0.0078	2.8	0.32	50.1	1.4	48.1	4.1	51.7	200.3
0.0078	2.3	0.59	50.2	1.1	49.3	1.8	9.0	74.2
0.0078	3.0	0.42	50.3	1.5	51.0	3.5	82.4	152.7
0.0078	1.6	0.34	50.4	0.8	49.8	2.3	25.0	107.5
0.0079	1.5	0.16	50.5	0.8	64.1	5.7	606.8	197.3
0.0079	1.9	0.39	50.6	0.9	49.6	2.3	2.7	106.8
0.0079	2.3	0.35	50.6	1.1	44.3	2.8	282.0	154.1
0.0079	3.6	0.35	50.7	1.8	55.8	5.5	280.1	216.6
0.0079	2.8	0.47	50.7	1.4	50.4	2.9	33.7	125.9
0.0079	1.7	0.34	50.7	0.9	51.4	2.5	81.7	109.7
0.0079	2.6	0.30	50.8	1.3	50.9	4.4	55.3	200.1
0.0079	2.5	0.35	51.0	1.3	51.8	3.6	89.7	160.1

0.0080	2.4	0.43	51.1	1.2	49.3	2.7	37.6	124.0
0.0080	1.4	0.30	51.1	0.7	51.9	2.4	88.1	106.4
0.0080	3.1	0.50	51.3	1.6	50.9	3.1	33.6	131.8
0.0080	2.9	0.37	51.3	1.5	47.9	3.7	118.9	180.6
0.0080	2.0	0.36	51.3	1.0	49.6	2.7	32.5	126.0
0.0080	2.0	0.60	51.3	1.0	52.5	1.7	105.6	62.2
0.0080	1.7	0.32	51.3	0.9	49.2	2.5	53.4	121.4
0.0080	1.7	0.38	51.4	0.9	49.9	2.2	23.7	99.3
0.0080	1.5	0.29	51.6	0.8	51.8	2.7	58.2	122.8
0.0081	1.9	0.28	51.7	1.0	60.1	3.9	407.6	144.3
0.0081	1.9	0.31	51.7	1.0	54.6	3.3	182.9	137.1
0.0081	1.5	0.27	51.7	0.8	57.0	3.2	284.2	126.8
0.0081	1.9	0.29	51.8	1.0	54.8	3.4	187.1	142.2
0.0081	2.1	0.65	52.2	1.1	52.0	1.6	44.2	58.6
0.0081	3.1	0.31	52.3	1.6	55.1	5.5	181.7	226.4
0.0081	2.0	0.39	52.3	1.0	53.0	2.6	82.4	110.1
0.0082	1.6	0.25	52.5	0.8	45.9	2.9	287.1	158.1
0.0082	3.7	0.69	52.5	1.9	52.9	2.8	68.8	93.6
0.0082	3.7	0.55	52.6	1.9	52.6	3.4	51.6	133.1
0.0082	2.8	0.53	52.6	1.5	54.3	2.8	129.9	107.2
0.0082	2.3	0.41	52.7	1.2	51.8	2.8	9.1	122.9
0.0083	1.9	0.50	53.2	1.0	54.1	2.0	91.7	78.8
0.0083	1.5	0.34	53.4	0.8	53.2	2.3	44.9	100.4
0.0083	2.8	0.50	53.4	1.5	53.5	2.9	57.1	114.6
0.0084	3.3	0.52	53.7	1.7	48.9	3.0	177.1	135.4
0.0084	2.0	0.43	54.2	1.1	53.1	2.4	5.3	99.8
0.0086	1.7	0.51	55.0	0.9	57.4	1.8	162.1	66.0
0.0086	1.8	0.39	55.2	1.0	53.7	2.4	13.0	103.4
0.0086	2.2	0.43	55.2	1.2	58.0	2.9	172.9	106.9
0.0086	2.4	0.41	55.3	1.3	56.7	3.2	115.9	123.4
0.0087	1.9	0.25	55.9	1.1	54.6	4.1	5.0	181.4
0.0087	1.3	0.52	55.9	0.7	55.3	1.4	27.8	52.3
0.0093	2.8	0.35	59.8	1.6	219.1	15.4	2720.2	120.9
0.0100	4.1	0.37	64.1	2.6	73.5	7.9	390.5	234.6
0.0101	6.7	0.58	64.9	4.4	110.7	12.1	1257.5	183.5
0.0108	3.1	0.34	69.3	2.1	70.8	6.3	120.1	203.8
0.0128	1.8	0.56	82.2	1.5	84.0	2.6	136.7	62.6
0.0135	1.7	0.50	86.4	1.5	85.5	2.8	62.0	70.4
0.0136	2.7	0.41	87.4	2.3	88.2	5.6	110.0	142.7
0.0137	4.1	0.56	87.5	3.6	88.0	6.2	102.5	145.2
0.0138	1.8	0.47	88.6	1.6	86.0	3.1	14.6	80.6
0.0139	1.3	0.36	89.2	1.2	90.3	3.1	120.4	79.2
0.0139	1.2	0.42	89.3	1.0	90.5	2.4	122.0	59.6
0.0140	2.3	0.48	89.7	2.1	91.4	4.2	136.0	99.0
0.0142	2.1	0.40	90.9	1.9	87.3	4.5	10.1	119.7
0.0142	2.5	0.46	90.9	2.3	91.3	4.7	104.0	114.0
0.0143	2.0	0.57	91.5	1.8	94.4	3.2	167.2	68.2

0.0143	4.8	1.00	91.7	4.3	568.2	20.7	3830.6	3.0
0.0143	1.7	0.36	91.8	1.5	94.0	4.2	150.3	101.0
0.0146	2.2	0.42	93.2	2.0	90.8	4.6	29.3	114.3
0.0151	4.1	0.74	96.6	3.9	98.7	5.2	149.9	87.4
0.0271	1.9	0.48	172.5	3.3	170.2	6.3	139.2	82.6
0.0273	2.4	0.46	173.4	4.1	174.2	8.3	185.3	106.8
0.0278	1.6	0.41	176.5	2.8	181.2	6.4	242.9	80.9
0.0279	2.9	0.51	177.3	5.1	173.8	9.2	126.8	117.3

0.0029	6.6	0.46	18.7	1.2	9.1	1.3	2161.0	494.8
0.0032	3.4	0.58	20.7	0.7	22.4	1.3	212.1	109.8
0.0033	5.1	0.75	21.3	1.1	21.8	1.5	75.2	105.3
0.0033	4.0	0.69	21.5	0.9	22.2	1.3	95.9	101.1
0.0034	1.6	0.57	21.7	0.4	22.3	0.6	92.8	56.7
0.0034	2.3	0.39	21.7	0.5	22.6	1.3	123.0	127.7
0.0034	3.7	0.78	21.7	0.8	22.1	1.0	64.5	69.6
0.0034	2.1	0.31	21.9	0.4	26.4	1.7	454.3	137.8
0.0034	1.6	0.47	22.0	0.3	22.8	0.8	116.4	69.5
0.0034	2.0	0.51	22.0	0.4	23.4	0.9	164.6	78.9
0.0034	2.6	0.39	22.2	0.6	24.8	1.6	282.1	142.3
0.0035	1.9	0.34	22.2	0.4	22.6	1.2	60.4	124.9
0.0035	2.0	0.64	22.2	0.4	22.4	0.7	47.1	57.2
0.0035	1.9	0.51	22.3	0.4	23.4	0.9	129.4	75.3
0.0035	4.0	0.81	22.4	0.9	25.3	1.2	308.9	65.0
0.0035	2.2	0.31	22.5	0.5	23.8	1.7	155.9	159.2
0.0035	2.5	0.51	22.6	0.6	21.6	1.0	89.2	101.5
0.0035	1.7	0.53	22.6	0.4	22.9	0.7	48.8	65.5
0.0035	1.8	0.67	22.6	0.4	22.8	0.6	37.4	47.2
0.0035	2.1	0.58	22.7	0.5	22.6	0.8	11.5	71.8
0.0035	2.1	0.47	22.8	0.5	23.0	1.0	42.2	92.7
0.0035	1.6	0.50	22.8	0.4	23.6	0.8	104.5	67.7
0.0036	3.2	0.18	22.9	0.7	42.0	7.1	1335.1	330.1
0.0036	3.0	0.73	22.9	0.7	23.4	0.9	72.1	65.9
0.0036	2.5	0.47	23.1	0.6	23.8	1.3	96.5	111.9
0.0036	1.4	0.54	23.1	0.3	23.5	0.6	66.3	52.2
0.0036	1.3	0.45	23.1	0.3	23.2	0.6	31.1	60.4
0.0036	1.7	0.51	23.1	0.4	23.7	0.8	78.9	69.1
0.0036	1.7	0.59	23.2	0.4	23.2	0.7	20.9	55.5
0.0036	2.9	0.35	23.3	0.7	22.2	1.9	86.1	194.0
0.0036	2.3	0.64	23.3	0.5	25.0	0.9	196.2	62.8
0.0036	1.9	0.51	23.3	0.4	23.8	0.9	79.3	73.9
0.0036	2.0	0.62	23.4	0.5	23.9	0.8	75.5	61.2
0.0037	2.0	0.59	23.5	0.5	23.7	0.8	41.6	64.1
0.0037	1.3	0.48	23.5	0.3	23.2	0.6	5.1	55.9
0.0037	2.8	0.72	23.6	0.7	24.0	0.9	69.0	65.0
0.0037	3.1	0.90	23.6	0.7	23.7	0.8	40.7	35.8

0.0037	3.4	0.77	23.6	0.8	23.9	1.0	52.3	67.3
0.0037	1.6	0.54	23.7	0.4	24.4	0.7	92.9	58.3
0.0037	3.5	0.22	23.8	0.8	50.8	7.8	1638.5	286.2
0.0037	2.2	0.35	23.9	0.5	23.2	1.5	48.9	144.8
0.0038	1.9	0.57	24.2	0.5	24.3	0.8	33.1	65.0
0.0038	3.1	0.54	24.3	0.8	22.4	1.3	176.1	122.1
0.0038	2.2	0.44	24.6	0.5	26.6	1.3	211.1	104.2
0.0039	3.1	0.69	25.4	0.8	26.6	1.2	138.0	76.3
0.0040	3.6	0.66	25.6	0.9	27.7	1.5	214.0	94.5
0.0040	2.0	0.69	25.7	0.5	26.1	0.7	58.6	49.3
0.0040	1.7	0.63	25.9	0.4	26.1	0.7	45.0	49.2
0.0040	1.7	0.61	26.0	0.4	27.1	0.8	124.4	53.0
0.0045	9.9	0.48	29.2	2.9	109.9	21.4	2676.8	300.4
0.0046	1.5	0.50	29.8	0.5	34.7	1.0	390.3	59.2
0.0048	1.2	0.48	30.9	0.4	32.1	0.8	121.2	50.4
0.0054	1.3	0.54	34.6	0.4	35.1	0.8	68.6	47.3
0.0068	2.1	0.84	43.5	0.9	43.9	1.1	65.8	33.0
0.0074	4.1	0.55	47.8	1.9	50.3	3.6	169.2	145.0
0.0075	2.4	0.45	47.9	1.1	47.7	2.5	36.7	113.2
0.0075	1.6	0.47	48.1	0.8	48.4	1.6	63.4	70.5
0.0075	3.4	0.40	48.1	1.6	42.5	3.6	262.2	199.3
0.0075	3.6	0.50	48.2	1.7	48.5	3.4	65.4	148.6
0.0075	2.0	0.46	48.4	1.0	50.5	2.2	152.5	91.7
0.0075	2.4	0.41	48.4	1.2	48.3	2.8	39.6	129.4
0.0075	2.8	0.30	48.5	1.4	49.3	4.5	86.9	213.8
0.0075	3.2	0.47	48.5	1.5	52.6	3.5	242.7	138.3
0.0076	2.3	0.36	48.6	1.1	47.2	3.0	25.0	145.4
0.0076	4.0	0.44	48.8	1.9	42.8	3.8	281.8	208.1
0.0076	2.6	0.43	48.8	1.3	51.3	3.1	169.2	128.7
0.0076	2.8	0.49	48.8	1.4	46.5	2.6	72.7	122.3
0.0076	3.5	0.49	48.9	1.7	49.5	3.4	77.9	147.6
0.0076	3.2	0.47	49.0	1.6	44.1	3.0	211.2	153.4
0.0076	2.8	0.46	49.0	1.4	46.2	2.8	94.6	133.3
0.0076	2.8	0.35	49.1	1.4	55.5	4.3	339.7	169.5
0.0077	3.2	0.51	49.2	1.6	50.5	3.1	113.2	128.5
0.0077	4.1	0.43	49.2	2.0	45.2	4.2	163.4	212.1
0.0077	3.0	0.43	49.3	1.5	49.6	3.4	63.5	151.0
0.0077	1.9	0.26	49.4	0.9	53.2	3.7	229.7	159.2
0.0077	2.7	0.45	49.5	1.3	53.3	3.1	229.3	124.1
0.0077	3.7	0.53	49.6	1.8	54.5	3.7	279.6	134.7
0.0077	2.8	0.35	49.6	1.4	38.4	3.0	617.2	200.5
0.0077	2.6	0.46	49.7	1.3	49.4	2.7	38.9	120.1
0.0077	2.0	0.39	49.7	1.0	50.0	2.5	63.6	111.8
0.0078	2.4	0.37	49.8	1.2	46.1	2.9	142.2	147.2
0.0078	2.2	0.36	49.8	1.1	47.3	2.8	76.1	137.2
0.0078	5.1	0.74	49.9	2.5	51.0	3.4	100.8	110.0
0.0078	2.4	0.50	49.9	1.2	49.1	2.3	7.6	100.8

0.0078	3.9	0.59	50.0	1.9	42.5	2.8	363.3	139.0
0.0078	1.7	0.25	50.0	0.9	49.9	3.3	44.2	157.5
0.0078	1.8	0.37	50.1	0.9	49.5	2.4	22.7	110.7
0.0078	2.1	0.36	50.3	1.0	48.9	2.8	20.2	131.2
0.0078	4.6	0.62	50.3	2.3	46.1	3.4	169.4	147.2
0.0079	2.9	0.46	50.5	1.5	47.3	2.9	112.5	139.4
0.0079	2.2	0.34	50.7	1.1	49.7	3.2	3.2	147.4
0.0079	1.8	0.41	50.8	0.9	51.1	2.1	64.8	92.9
0.0079	2.3	0.42	50.9	1.2	55.0	2.9	238.1	113.1
0.0081	2.2	0.36	52.0	1.1	55.5	3.3	210.3	134.2
0.0081	3.1	0.54	52.1	1.6	47.9	2.7	155.7	120.4
0.0081	3.4	0.22	52.1	1.8	122.2	17.7	1870.3	271.3
0.0081	2.8	0.48	52.2	1.5	52.6	3.0	72.9	122.0
0.0082	3.2	0.21	52.7	1.7	74.9	10.7	859.1	302.4
0.0083	2.7	0.14	53.2	1.4	100.3	17.9	1444.8	356.7
0.0086	4.0	0.87	55.0	2.2	52.2	2.3	72.4	55.5
0.0086	2.2	0.35	55.2	1.2	69.3	4.3	586.1	129.4
0.0090	3.3	0.32	57.9	1.9	52.3	5.2	193.6	240.5
0.0101	2.3	0.64	64.6	1.5	64.6	2.2	66.4	64.4
0.0106	2.6	0.59	68.1	1.7	71.5	3.0	186.7	82.4
0.0108	3.1	0.40	69.3	2.1	75.8	5.6	284.9	160.1
0.0799	2.6	0.91	495.3	12.5	497.3	11.3	506.5	26.4

0.0046	4.4	0.19	29.9	1.3	33.8	7.4	324.9	503.5
0.0050	3.0	0.33	32.4	1.0	33.6	3.1	118.2	207.3
0.0071	2.3	0.23	45.8	1.1	46.7	4.6	89.2	232.7
0.0072	9.7	0.21	46.1	4.5	49.1	22.3	201.9	1109.2
0.0072	13.7	0.29	46.1	6.3	64.5	29.5	811.5	997.9
0.0073	2.1	0.20	46.7	1.0	46.9	4.8	56.9	246.3
0.0074	9.0	0.23	47.8	4.3	48.1	18.3	65.3	933.0
0.0075	5.0	0.18	47.9	2.4	58.2	15.4	506.6	598.4
0.0076	6.4	0.33	48.6	3.1	45.9	8.6	-90.4	447.4
0.0076	7.7	0.14	48.7	3.7	38.1	20.3	-585.9	1558.7
0.0076	3.3	0.30	49.0	1.6	48.3	5.2	16.1	253.9
0.0077	3.6	0.16	49.5	1.8	47.1	10.2	-69.9	539.9
0.0078	17.6	0.33	49.9	8.8	61.9	31.7	556.5	1154.8
0.0079	2.0	0.16	50.6	1.0	51.6	6.3	101.0	292.9
0.0079	3.8	0.10	50.8	1.9	43.1	16.3	-368.9	1030.7
0.0079	1.6	0.36	50.9	0.8	52.2	2.2	115.7	95.1
0.0081	5.1	0.23	52.1	2.6	53.5	11.3	120.9	502.2
0.0083	14.4	0.52	53.4	7.7	64.1	17.3	485.7	534.3
0.0084	2.6	0.08	53.8	1.4	56.8	17.2	184.4	740.4
0.0086	5.6	0.18	54.9	3.1	63.5	19.5	399.7	712.3
0.0087	6.6	0.26	56.0	3.7	74.9	18.6	731.2	535.6
0.0098	2.9	0.18	62.6	1.8	61.3	9.6	11.5	383.8
0.0122	7.2	0.12	78.0	5.6	75.9	45.1	8.2	1624.3

0.0122	8.1	0.27	78.2	6.3	110.1	31.2	871.4	608.2
0.0123	9.5	0.25	78.9	7.4	90.3	33.0	402.5	854.9
0.0127	3.1	0.07	81.2	2.5	71.8	30.4	-232.6	1150.4
0.0127	10.7	0.25	81.4	8.7	68.7	28.0	-356.1	1094.3
0.0127	4.3	0.13	81.7	3.5	78.5	24.1	-18.1	782.5
0.0128	2.0	0.18	81.9	1.6	79.2	8.3	-0.5	257.3
0.0128	1.5	0.28	82.0	1.2	80.2	4.2	26.9	125.2
0.0128	9.6	0.39	82.1	7.8	120.5	28.1	964.6	470.7
0.0129	7.9	0.16	82.5	6.5	59.1	28.1	-810.4	1444.2
0.0129	3.3	0.22	82.6	2.7	84.2	12.1	129.9	345.5
0.0130	7.0	0.19	83.4	5.8	88.4	30.9	224.7	851.6
0.0131	5.4	0.17	83.9	4.5	79.8	25.0	-43.1	798.5
0.0132	5.1	0.17	84.4	4.3	76.9	22.0	-149.6	738.7
0.0132	7.6	0.42	84.4	6.3	83.2	14.2	49.2	387.4
0.0132	2.0	0.22	84.6	1.7	85.3	7.5	104.1	212.3
0.0133	2.2	0.08	84.9	1.9	77.6	21.2	-140.2	713.9
0.0133	4.6	0.12	85.2	3.9	54.4	21.0	NA	NA
0.0134	8.5	0.16	85.7	7.2	95.4	47.7	344.0	1250.2
0.0135	3.6	0.09	86.3	3.1	78.7	30.8	-147.5	1041.9
0.0135	3.1	0.15	86.4	2.7	98.6	19.8	403.5	472.0
0.0136	5.2	0.20	87.0	4.5	100.1	25.0	423.3	581.1
0.0136	5.5	0.29	87.1	4.8	81.8	14.8	-69.6	444.3
0.0136	3.6	0.21	87.1	3.1	73.6	12.5	-345.5	445.8
0.0137	4.0	0.31	87.8	3.5	88.7	11.3	112.2	298.9
0.0138	7.0	0.30	88.3	6.2	97.4	21.5	326.5	506.3
0.0138	1.1	0.64	88.5	0.9	90.0	1.4	130.1	29.9
0.0138	4.7	0.08	88.5	4.1	54.7	32.2	-1257.3	2050.4
0.0138	2.1	0.18	88.6	1.9	84.6	9.5	-28.5	279.7
0.0139	3.6	0.35	89.0	3.2	89.2	8.6	92.9	223.9
0.0139	4.4	0.68	89.2	3.9	91.2	5.7	144.4	111.7
0.0139	7.7	0.36	89.2	6.9	90.7	18.7	130.7	478.1
0.0139	6.9	0.11	89.2	6.1	79.6	49.7	-198.8	1798.8
0.0140	5.6	0.06	89.6	4.9	57.6	49.9	-1135.3	1658.1
0.0141	1.7	0.24	90.0	1.5	94.5	6.2	208.6	155.1
0.0141	3.7	0.14	90.4	3.3	77.1	19.1	-319.2	663.7
0.0141	13.0	0.38	90.5	11.7	96.4	31.8	244.9	756.0
0.0142	2.9	0.16	90.8	2.6	96.5	16.1	239.5	401.2
0.0144	4.7	0.09	92.3	4.3	65.0	31.1	-855.9	1490.3
0.0144	5.3	0.14	92.3	4.8	71.0	25.2	-598.4	1014.2
0.0144	4.6	0.17	92.4	4.2	89.6	23.0	17.2	645.1
0.0146	4.2	0.09	93.3	3.9	90.1	41.4	6.2	1214.7
0.0146	2.2	0.74	93.5	2.1	95.6	2.8	146.3	47.6
0.0146	2.9	0.54	93.7	2.7	93.9	4.8	99.0	105.7
0.0146	4.2	0.20	93.7	3.9	89.1	18.1	-33.6	508.0
0.0147	1.6	0.22	94.1	1.5	91.0	6.3	9.0	171.3
0.0149	4.0	0.12	95.1	3.8	73.0	24.3	-600.2	954.2
0.0149	4.0	0.27	95.6	3.8	108.1	14.8	391.9	312.7

0.0157	3.4	0.28	100.4	3.4	107.2	12.3	260.3	267.8
0.0169	2.0	0.25	108.0	2.2	106.8	8.2	81.7	185.8
0.0171	2.1	0.57	109.1	2.3	109.0	3.8	105.7	72.0
0.0218	2.3	0.72	138.8	3.2	141.1	4.3	180.0	52.4
0.0284	8.3	0.29	180.5	14.8	195.3	51.6	377.6	636.8
0.0285	6.2	0.19	181.1	11.1	176.3	52.5	113.2	767.0
0.0287	1.9	0.20	182.2	3.4	182.1	15.9	181.2	218.0
0.0293	3.5	0.20	185.9	6.5	168.4	26.9	-69.6	416.5
0.0293	4.6	0.34	185.9	8.4	200.7	24.8	378.8	289.6
0.0295	7.3	0.37	187.6	13.6	195.8	35.2	296.4	421.4
0.0303	0.6	0.09	192.2	1.2	195.7	12.5	237.6	160.9
0.0309	2.7	0.37	196.2	5.2	193.5	13.0	161.5	160.6
0.0314	2.1	0.19	199.3	4.1	193.2	19.5	119.3	257.5
0.0335	1.9	0.32	212.6	4.1	217.8	11.7	274.7	129.9
0.0341	2.5	0.21	216.3	5.4	227.3	24.1	342.8	262.7
0.0359	4.3	0.42	227.5	9.6	225.4	20.6	203.2	214.6
0.0461	3.7	0.97	290.7	10.4	296.7	9.7	344.3	20.7
0.0561	1.2	0.68	351.9	4.2	357.8	5.5	396.2	29.8
0.0562	2.3	0.62	352.4	7.8	351.6	10.9	346.5	65.6
0.0575	1.2	0.65	360.3	4.3	362.3	5.8	375.1	32.6
0.0579	1.1	0.53	362.7	3.9	363.7	6.4	370.2	39.7
0.0587	1.3	0.61	367.9	4.7	367.5	6.6	364.9	38.1
0.0589	2.5	0.72	368.9	9.1	375.4	11.0	415.8	53.8
0.0595	2.8	0.83	372.8	10.1	376.6	10.6	399.7	41.7
0.0609	2.6	0.87	381.0	9.5	378.1	9.3	360.5	32.6
0.0720	2.3	0.25	448.3	9.8	555.3	39.0	1022.3	178.9
0.0962	1.9	0.76	592.4	10.9	589.8	11.3	579.8	35.2
0.2003	1.5	0.99	1176.9	15.6	1175.2	10.2	1172.1	4.2

0.0049	3.3	0.24	31.6	1.0	30.5	4.0	-54.8	318.6
0.0054	2.3	0.19	34.6	0.8	32.0	3.9	-159.5	305.2
0.0059	1.3	0.22	38.2	0.5	38.3	2.1	45.7	133.4
0.0065	1.2	0.39	41.8	0.5	42.0	1.2	50.6	65.8
0.0071	13.2	0.21	45.3	6.0	40.2	24.7	-258.6	1710.9
0.0074	2.5	0.15	47.5	1.2	47.2	7.6	31.0	390.1
0.0074	5.9	0.26	47.5	2.8	44.9	9.8	-94.3	534.5
0.0075	2.3	0.10	48.0	1.1	54.0	12.2	327.7	528.9
0.0076	4.4	0.14	49.0	2.2	45.7	13.9	-125.7	774.0
0.0077	4.8	0.19	49.1	2.4	49.1	12.3	44.6	613.1
0.0077	4.5	0.09	49.3	2.2	30.4	14.8	NA	NA
0.0077	3.7	0.15	49.3	1.8	36.3	8.8	-757.7	697.1
0.0077	3.4	0.14	49.3	1.7	53.8	12.7	258.9	556.1
0.0078	2.4	0.28	50.1	1.2	49.0	4.2	-4.0	205.9
0.0078	4.0	0.15	50.3	2.0	42.0	10.8	-408.8	684.7
0.0079	6.0	0.17	50.7	3.0	49.3	16.6	-19.5	844.2
0.0080	1.5	0.32	51.1	0.7	52.8	2.4	133.0	103.6

0.0080	9.8	0.07	51.2	5.0	88.3	113.9	1261.2	340.2
0.0080	2.7	0.11	51.4	1.4	53.9	12.6	165.8	565.2
0.0080	3.3	0.13	51.6	1.7	50.0	12.3	-25.1	613.1
0.0081	2.1	0.46	51.8	1.1	54.7	2.4	182.9	91.3
0.0081	1.9	0.14	52.3	1.0	47.2	6.2	-205.0	337.4
0.0082	6.2	0.20	52.6	3.3	82.3	24.5	1059.7	626.1
0.0082	7.2	0.23	52.7	3.8	44.6	13.7	-370.1	804.2
0.0083	7.2	0.08	53.5	3.8	60.2	54.0	337.2	706.0
0.0083	2.3	0.26	53.5	1.2	57.4	5.0	219.9	201.2
0.0084	3.7	0.25	54.0	2.0	52.6	7.7	-7.5	353.8
0.0085	1.5	0.16	54.3	0.8	53.2	4.7	4.9	215.3
0.0085	1.9	0.08	54.3	1.0	54.2	13.1	46.1	598.8
0.0085	5.6	0.22	54.8	3.1	51.0	12.7	-125.1	621.0
0.0086	3.4	0.16	55.0	1.8	53.4	10.6	-20.5	493.0
0.0087	2.6	0.41	55.7	1.4	54.9	3.4	20.8	138.9
0.0088	3.4	0.12	56.2	1.9	59.4	16.1	191.1	654.3
0.0092	8.8	0.23	59.2	5.2	63.5	23.7	225.6	896.3
0.0095	5.4	0.22	61.0	3.3	66.7	15.9	276.7	558.9
0.0099	5.9	0.22	63.2	3.7	64.9	16.9	126.6	625.3
0.0101	6.9	0.15	65.0	4.5	61.9	27.3	-58.2	1145.8
0.0109	0.7	0.08	70.1	0.5	75.5	6.7	250.3	210.5
0.0114	5.1	0.14	72.9	3.7	69.6	25.2	-43.8	929.2
0.0120	10.3	0.35	77.0	7.9	101.0	28.1	710.6	592.6
0.0123	1.3	0.25	78.7	1.0	82.5	4.1	194.0	117.4
0.0123	10.0	0.20	78.9	7.8	70.9	33.7	-190.6	1269.1
0.0125	7.9	0.19	80.0	6.3	71.1	28.8	-218.9	1074.1
0.0125	2.8	0.66	80.2	2.2	82.1	3.3	136.5	75.0
0.0128	9.6	0.18	82.0	7.8	80.4	41.7	32.1	1362.7
0.0129	10.8	0.33	82.9	8.9	81.9	26.0	54.5	759.7
0.0130	10.3	0.11	83.1	8.5	47.0	42.1	NA	NA
0.0130	6.4	0.26	83.5	5.3	78.5	18.5	-71.4	583.3
0.0132	1.5	0.22	84.8	1.3	86.2	5.5	123.7	153.6
0.0133	2.4	0.21	85.1	2.1	83.6	9.2	40.8	267.5
0.0133	2.9	0.30	85.3	2.5	87.5	8.1	148.9	217.5
0.0133	9.0	0.13	85.3	7.6	78.8	53.8	-116.4	1988.3
0.0133	5.0	0.30	85.4	4.2	102.2	16.1	513.2	349.9
0.0134	2.0	0.22	85.5	1.7	75.3	6.4	-237.6	217.2
0.0134	3.1	0.16	85.7	2.7	90.5	17.1	219.2	454.0
0.0134	2.1	0.19	85.8	1.8	87.2	9.3	124.0	259.2
0.0134	9.8	0.04	86.0	8.4	169.7	381.3	1591.5	604.6
0.0134	4.0	0.13	86.0	3.4	80.2	24.1	-88.3	776.7
0.0135	3.4	0.16	86.2	2.9	90.1	17.8	196.2	478.2
0.0136	1.8	0.06	86.8	1.5	75.7	20.3	-262.4	714.1
0.0136	1.5	0.23	87.0	1.3	88.1	5.6	115.8	151.5
0.0138	13.2	0.49	88.2	11.6	114.6	29.3	704.4	507.7
0.0138	1.8	0.21	88.2	1.6	89.1	7.1	112.8	192.9
0.0141	5.1	0.17	90.0	4.5	70.5	20.3	-550.9	804.0

0.0141	4.6	0.33	90.4	4.1	101.3	13.3	365.1	293.7
0.0142	1.5	0.17	90.6	1.3	93.4	7.8	164.6	203.2
0.0142	3.3	0.16	91.1	3.0	90.8	18.4	84.1	499.7
0.0143	11.3	0.19	91.4	10.3	102.7	57.9	372.6	1430.4
0.0144	7.2	0.28	92.3	6.6	89.6	21.7	18.6	590.4
0.0145	1.3	0.26	92.6	1.2	89.8	4.4	15.6	118.2
0.0145	2.2	0.22	93.0	2.0	89.3	8.6	-10.4	237.3
0.0149	4.2	0.18	95.6	4.0	82.7	18.6	-273.8	592.3
0.0153	5.7	0.16	97.6	5.5	94.9	32.3	28.6	866.4
0.0155	6.1	0.18	98.9	6.0	99.7	31.2	117.8	780.0
0.0157	3.3	0.19	100.2	3.2	122.0	19.5	569.7	365.2
0.0158	13.9	0.49	101.0	14.0	130.4	35.1	705.5	540.4
0.0161	3.2	0.16	102.9	3.3	84.3	15.8	-414.6	508.6
0.0167	1.3	0.23	106.9	1.4	111.3	6.2	206.4	133.6
0.0168	2.7	0.22	107.6	2.9	115.3	13.2	278.9	270.7
0.0188	1.3	0.34	120.2	1.6	120.6	4.5	129.5	87.3
0.0285	3.9	0.18	181.1	7.1	169.6	33.9	11.5	518.6
0.0299	5.4	0.15	189.6	10.1	161.3	54.8	-237.7	943.4
0.0301	1.3	0.32	191.2	2.5	188.0	7.3	148.5	94.2
0.0321	0.6	0.25	203.6	1.2	201.4	4.5	176.6	56.1
0.0321	1.7	0.23	203.7	3.5	196.2	13.2	107.8	169.9
0.0381	2.0	0.21	241.2	4.8	249.0	21.2	323.9	214.0
0.0607	1.4	0.73	380.0	5.1	378.4	6.0	369.1	29.3
0.0616	1.7	0.70	385.6	6.5	380.5	7.9	349.1	40.0
0.2055	3.1	0.91	1204.8	34.2	1187.3	24.0	1155.7	28.0
0.1945	1.9	0.27	1145.9	20.4	1151.7	49.0	1162.8	135.8
0.1982	1.4	0.47	1165.5	15.2	1181.9	21.1	1212.0	52.6
0.2353	2.7	0.88	1362.0	33.7	1455.1	24.3	1593.7	28.3
0.3532	1.5	0.94	1949.8	25.7	1980.1	14.1	2011.9	9.5
0.3827	1.4	0.94	2088.7	24.9	2116.5	13.2	2143.6	8.8
0.5600	3.1	1.00	2866.7	72.8	3056.4	30.5	3183.6	3.7

0.0045	3.0	0.21	29.2	0.9	30.5	4.4	133.7	340.8
0.0046	9.4	0.20	29.3	2.7	31.3	14.6	187.5	1137.6
0.0053	2.0	0.10	33.8	0.7	33.3	6.8	2.7	498.4
0.0054	12.5	0.64	34.5	4.3	36.6	7.0	171.8	354.0
0.0062	1.7	0.30	40.1	0.7	40.2	2.3	47.8	131.8
0.0063	1.1	0.11	40.4	0.4	43.3	4.2	203.3	230.8
0.0064	2.3	0.24	41.4	0.9	43.0	4.0	133.1	218.2
0.0065	1.2	0.16	41.8	0.5	42.0	3.0	52.4	171.8
0.0066	5.3	0.30	42.2	2.2	47.3	8.1	317.6	381.0
0.0066	1.7	0.35	42.7	0.7	41.2	2.0	-44.4	112.1
0.0067	10.0	0.19	43.3	4.3	54.5	28.4	576.6	1226.6
0.0069	1.8	0.24	44.2	0.8	42.8	3.1	-36.2	177.4
0.0073	5.1	0.35	47.0	2.4	50.0	7.2	196.0	321.1
0.0074	11.7	0.30	47.4	5.5	60.6	22.8	618.2	824.0

0.0074	14.8	0.22	47.8	7.0	66.0	43.1	790.4	1566.8
0.0075	2.1	0.11	48.1	1.0	47.4	8.4	12.4	435.4
0.0076	4.4	0.11	48.5	2.1	41.0	15.8	-381.6	1048.1
0.0076	5.1	0.12	49.0	2.5	39.5	16.4	-509.8	1168.4
0.0077	0.7	0.29	49.3	0.4	49.7	1.3	69.3	59.2
0.0077	11.5	0.12	49.3	5.7	76.5	71.8	1039.1	#VALUE!
0.0077	4.1	0.15	49.4	2.0	43.9	11.9	-245.6	700.7
0.0077	3.9	0.47	49.4	1.9	52.4	4.2	190.8	170.1
0.0077	9.1	0.09	49.5	4.5	29.0	28.1	-1464.1	0.0
0.0077	6.7	0.39	49.6	3.3	53.4	8.9	228.0	364.8
0.0077	3.9	0.48	49.7	1.9	58.0	4.5	416.4	158.2
0.0077	3.5	0.12	49.7	1.7	47.9	13.5	-44.9	709.0
0.0078	12.8	0.00	50.0	6.4	707.7	#NUM!	NA	NA
0.0079	6.6	0.33	50.5	3.3	66.0	12.8	673.0	406.3
0.0079	3.5	0.21	50.6	1.7	60.7	9.9	480.5	365.8
0.0079	3.3	0.20	50.6	1.7	59.9	9.8	447.0	369.1
0.0079	2.8	0.18	50.8	1.4	45.7	6.8	-215.3	376.2
0.0080	3.4	0.25	51.1	1.7	53.9	7.0	183.2	301.6
0.0080	1.6	0.25	51.3	0.8	52.0	3.2	82.7	147.0
0.0080	2.6	0.25	51.4	1.3	48.0	4.8	-119.5	246.4
0.0080	4.0	0.14	51.4	2.0	43.0	12.1	-403.0	757.9
0.0080	6.2	0.10	51.4	3.2	46.2	26.8	-217.4	1612.6
0.0081	1.4	0.16	51.8	0.7	53.9	4.6	146.8	204.8
0.0081	2.7	0.12	51.9	1.4	55.9	12.3	234.2	523.0
0.0081	4.7	0.39	52.0	2.4	49.2	5.9	-85.3	276.5
0.0082	1.5	0.16	52.6	0.8	51.3	4.5	-11.2	213.4
0.0083	5.6	0.35	53.1	3.0	51.9	8.0	-5.6	358.6
0.0085	5.3	0.13	54.8	2.9	49.0	19.1	-224.7	1028.4
0.0086	6.1	0.25	55.0	3.4	44.7	10.5	-475.8	624.5
0.0087	1.6	0.19	55.9	0.9	54.1	4.4	-24.3	197.2
0.0095	14.4	0.38	60.7	8.7	75.8	27.8	582.3	788.5
0.0096	3.2	0.18	61.3	2.0	56.2	9.6	-155.8	433.3
0.0097	3.0	0.62	62.3	1.9	61.0	2.9	10.7	92.2
0.0103	4.9	0.10	66.1	3.2	54.4	25.5	-436.3	1322.3
0.0119	5.7	0.13	76.0	4.3	99.4	42.3	705.7	990.1
0.0124	12.2	0.00	79.1	9.6	#NUM!	#NUM!	NA	NA
0.0125	11.0	0.13	80.2	8.8	90.7	72.6	375.0	2373.7
0.0128	8.2	0.27	81.7	6.6	100.1	28.5	562.1	639.6
0.0129	5.9	0.19	82.5	4.8	66.4	19.5	-481.9	805.5
0.0129	4.1	0.13	82.7	3.3	76.0	22.6	-129.8	772.6
0.0132	5.4	0.22	84.6	4.5	83.9	19.4	62.9	567.1
0.0133	11.3	0.27	85.2	9.5	62.8	25.8	-726.8	1184.2
0.0134	5.1	0.26	85.7	4.4	93.1	17.8	287.0	445.4
0.0134	5.6	0.10	85.9	4.8	72.1	39.9	-365.3	1594.5
0.0134	3.0	0.37	86.1	2.6	91.5	7.2	234.2	177.4
0.0135	1.5	0.26	86.4	1.3	85.5	4.8	61.4	134.0
0.0136	2.8	0.23	86.8	2.4	86.6	10.4	82.1	289.4

0.0136	9.4	0.25	87.2	8.1	83.7	30.0	-14.3	901.0
0.0137	6.3	0.19	87.5	5.5	80.7	25.8	-116.1	823.2
0.0137	1.8	0.32	87.5	1.6	91.0	4.9	185.2	123.7
0.0139	5.6	0.20	88.7	5.0	95.4	25.6	266.2	643.1
0.0139	4.2	0.26	88.9	3.7	95.0	14.8	250.9	365.5
0.0139	9.3	0.11	88.9	8.2	76.9	63.1	-282.9	2736.9
0.0139	3.7	0.11	89.1	3.2	83.2	27.4	-80.9	856.0
0.0139	1.3	0.18	89.1	1.2	92.8	6.5	189.0	167.7
0.0139	6.8	0.21	89.2	6.1	113.3	35.6	653.7	715.9
0.0140	5.3	0.24	89.7	4.7	91.6	19.8	140.9	521.1
0.0141	4.9	0.16	90.0	4.4	95.2	28.5	229.0	731.2
0.0142	7.3	0.18	91.1	6.6	85.0	33.2	-81.2	1014.2
0.0145	1.7	0.49	93.1	1.6	90.8	3.0	29.4	73.0
0.0146	3.5	0.33	93.4	3.2	90.1	9.1	4.9	239.9
0.0147	3.8	0.21	94.1	3.6	96.6	16.6	159.8	413.8
0.0147	4.1	0.18	94.2	3.8	98.0	21.4	192.0	528.7
0.0147	3.5	0.27	94.3	3.3	78.2	9.7	-388.4	323.9
0.0147	1.6	0.09	94.3	1.5	89.0	15.5	-51.6	445.1
0.0148	4.2	0.21	94.5	4.0	89.5	17.2	-41.6	481.9
0.0150	1.4	0.35	96.2	1.3	95.8	3.6	86.2	87.7
0.0152	3.0	0.51	97.2	2.9	100.5	5.7	178.3	119.2
0.0153	1.6	0.45	97.6	1.6	97.4	3.4	92.5	76.6
0.0157	2.0	0.38	100.2	2.0	103.4	5.1	176.9	111.5
0.0160	2.7	0.25	102.1	2.8	121.4	12.4	516.9	231.5
0.0204	2.4	0.80	130.0	3.0	128.6	3.6	102.0	42.5
0.0206	1.4	0.52	131.6	1.9	133.8	3.5	173.8	55.4
0.0234	0.9	0.11	149.2	1.3	154.0	11.8	229.0	190.6
0.0280	5.6	0.71	178.0	9.9	174.3	12.7	124.3	130.4
0.0281	3.5	0.18	178.8	6.2	167.2	30.1	6.2	465.7
0.0330	1.5	0.36	209.1	3.2	204.8	7.9	156.4	92.4
0.0335	2.8	0.92	212.7	5.8	213.5	5.8	222.9	26.8
0.0344	1.2	0.57	217.9	2.7	222.5	4.3	271.4	40.9
0.0550	0.7	0.27	345.3	2.4	352.4	7.9	399.4	57.4
0.0564	1.2	0.49	353.9	4.1	352.9	7.1	346.0	46.9
0.0569	1.6	0.30	356.7	5.6	355.1	15.9	344.6	114.8
0.0570	2.0	0.66	357.4	6.9	358.6	9.2	366.1	51.4
0.0583	0.7	0.52	365.0	2.4	363.0	3.9	349.9	24.6
0.0822	5.1	0.92	509.3	25.1	506.5	22.3	494.1	49.1
0.1105	2.2	0.97	675.6	14.2	672.6	11.3	662.4	12.6
0.1312	2.6	0.44	794.9	19.1	815.1	32.6	870.7	108.3
0.2290	2.2	0.82	1329.3	26.4	1399.3	20.4	1507.6	29.4
0.5005	1.4	0.83	2616.1	30.9	2625.1	16.3	2632.1	16.1

0.0064	3.5	0.21	41.3	1.4	47.8	7.6	388.3	357.3
0.0065	15.7	0.20	41.7	6.5	93.8	69.4	1766.0	1706.8
0.0066	2.2	0.22	42.7	0.9	41.6	4.2	-21.9	243.0

0.0067	1.9	0.19	42.7	0.8	40.7	3.9	-78.5	234.2
0.0067	3.2	0.21	42.9	1.4	45.7	6.7	192.7	344.4
0.0067	1.7	0.26	42.9	0.7	43.9	2.8	94.4	146.7
0.0067	1.6	0.22	43.2	0.7	46.4	3.3	214.2	163.3
0.0069	2.8	0.62	44.6	1.2	44.6	1.9	42.7	83.7
0.0071	16.4	0.32	45.6	7.4	59.0	28.9	643.3	1086.6
0.0072	11.1	0.04	46.2	5.1	101.6	256.0	1734.1	602.1
0.0072	2.3	0.21	46.3	1.1	43.0	4.5	-138.5	259.2
0.0072	8.2	0.23	46.4	3.8	44.6	15.8	-49.1	882.8
0.0072	6.4	0.09	46.5	3.0	34.0	23.0	-776.4	2176.7
0.0073	12.1	0.10	46.6	5.6	65.4	78.9	824.0	592.3
0.0073	7.1	0.08	46.8	3.3	23.0	20.5	NA	NA
0.0073	7.8	0.14	47.2	3.7	50.2	28.2	197.4	1440.5
0.0074	6.3	0.28	47.4	3.0	57.4	12.6	496.2	484.4
0.0074	10.2	0.06	47.5	4.8	65.6	112.8	786.6	981.0
0.0074	17.1	0.09	47.7	8.1	59.8	110.6	576.2	1264.9
0.0074	5.6	0.16	47.7	2.7	44.7	15.7	-116.1	898.0
0.0074	9.9	0.15	47.8	4.7	47.5	29.9	35.0	1697.4
0.0074	13.4	0.19	47.8	6.4	30.0	20.4	-1244.5	713.9
0.0075	5.7	0.04	48.0	2.7	91.7	118.7	1461.7	205.3
0.0075	3.4	0.13	48.0	1.6	35.9	8.8	-713.9	698.5
0.0075	4.0	0.09	48.2	1.9	56.2	23.3	411.5	992.1
0.0075	7.6	0.20	48.2	3.7	38.4	14.7	-540.6	1060.0
0.0075	13.9	0.10	48.3	6.7	100.1	128.0	1622.6	86.7
0.0075	11.1	0.17	48.3	5.4	43.2	28.4	-236.1	1874.8
0.0075	5.5	0.14	48.4	2.7	53.2	19.8	271.5	895.0
0.0076	7.4	0.21	48.8	3.6	61.3	20.7	579.9	760.4
0.0076	7.5	0.17	48.9	3.7	48.5	20.7	32.0	1075.5
0.0076	13.5	0.07	49.0	6.6	-44.4	-88.3	NA	NA
0.0076	5.7	0.14	49.1	2.8	48.6	19.0	26.4	983.0
0.0076	8.9	0.35	49.1	4.3	53.8	13.3	267.2	553.2
0.0077	3.1	0.18	49.1	1.5	49.9	8.4	87.1	406.7
0.0077	5.2	0.13	49.3	2.5	38.6	15.7	-582.4	1150.8
0.0077	7.3	0.06	49.3	3.6	50.2	60.0	94.7	1159.7
0.0077	3.6	0.24	49.5	1.8	45.3	6.7	-170.2	368.6
0.0077	4.2	0.21	49.5	2.1	39.5	7.6	-529.7	518.5
0.0077	2.3	0.20	49.5	1.1	53.7	6.0	244.5	257.5
0.0077	5.1	0.19	49.5	2.5	56.4	15.1	361.8	621.6
0.0077	3.5	0.19	49.6	1.7	46.0	8.2	-137.1	448.3
0.0077	3.1	0.26	49.6	1.5	51.3	5.9	130.8	270.4
0.0077	4.0	0.09	49.6	2.0	54.6	23.8	281.4	1067.0
0.0077	6.5	0.16	49.6	3.2	38.1	15.2	-636.8	1137.2
0.0077	9.7	0.21	49.7	4.8	42.3	19.6	-354.9	1255.3
0.0077	11.1	0.40	49.7	5.5	67.0	17.8	737.9	541.4
0.0078	8.1	0.27	49.8	4.0	47.0	13.5	-89.6	706.1
0.0078	3.5	0.20	49.8	1.7	46.5	8.0	-117.6	426.5
0.0078	2.3	0.54	49.9	1.1	51.8	2.1	144.2	82.8

0.0078	1.7	0.15	49.9	0.8	47.8	5.3	-53.3	272.6
0.0078	4.6	0.21	49.9	2.3	46.3	9.9	-137.3	531.9
0.0078	1.9	0.17	50.0	1.0	51.8	5.8	139.1	267.8
0.0078	13.9	0.11	50.0	6.9	51.8	61.2	135.4	1105.8
0.0078	1.8	0.58	50.1	0.9	51.3	1.6	109.1	60.4
0.0078	2.7	0.18	50.1	1.3	48.1	7.0	-50.1	359.7
0.0078	6.4	0.14	50.2	3.2	42.9	19.1	-345.8	1216.1
0.0078	4.9	0.15	50.2	2.5	43.2	14.3	-333.7	880.1
0.0078	5.3	0.11	50.2	2.6	44.1	20.4	-278.9	1253.4
0.0078	7.2	0.22	50.3	3.6	48.9	15.8	-19.3	799.7
0.0078	2.9	0.42	50.4	1.5	51.1	3.5	87.5	150.8
0.0079	4.6	0.18	50.5	2.3	50.5	12.7	52.4	611.7
0.0079	10.5	0.03	50.5	5.3	145.4	475.1	2251.6	427.0
0.0079	8.0	0.39	50.5	4.0	49.0	9.7	-21.5	453.3
0.0079	11.2	0.15	50.5	5.6	40.8	29.2	-500.5	2207.8
0.0079	8.2	0.23	50.5	4.1	45.5	15.5	-212.8	871.2
0.0079	13.9	0.37	50.8	7.0	89.2	32.1	1297.9	699.0
0.0079	9.6	0.25	50.8	4.8	58.1	21.8	371.7	870.7
0.0079	4.6	0.24	50.9	2.3	51.5	9.4	81.6	432.9
0.0080	14.6	0.29	51.2	7.5	54.8	26.9	217.1	1183.4
0.0080	4.6	0.21	51.3	2.3	46.1	10.0	-219.1	552.4
0.0080	2.2	0.41	51.5	1.1	50.9	2.7	22.3	118.7
0.0080	9.2	0.21	51.6	4.7	56.9	23.8	289.1	998.5
0.0081	3.2	0.09	51.8	1.6	30.8	11.2	NA	NA
0.0081	7.0	0.24	51.9	3.6	60.7	17.5	424.2	658.0
0.0081	7.6	0.16	52.0	4.0	51.2	23.1	17.0	1151.9
0.0082	10.5	0.22	52.5	5.5	60.6	28.7	392.6	1127.6
0.0082	3.7	0.31	52.6	1.9	58.4	6.7	304.9	255.6
0.0082	2.9	0.29	52.6	1.5	56.7	5.5	233.8	222.0
0.0083	12.8	0.10	53.2	6.8	70.9	89.2	717.9	710.9
0.0083	11.3	0.19	53.5	6.0	59.7	35.2	319.8	1488.8
0.0083	14.4	0.39	53.6	7.7	85.4	30.2	1100.5	698.9
0.0084	4.6	0.33	53.7	2.4	62.6	8.4	416.0	292.3
0.0084	5.7	0.13	54.1	3.1	54.5	23.6	72.3	1097.3
0.0085	1.7	0.15	54.4	0.9	58.3	6.4	218.7	258.7
0.0085	16.8	0.07	54.7	9.1	-93.9	-225.8	NA	NA
0.0086	6.7	0.25	55.1	3.7	58.8	15.4	213.9	615.1
0.0086	6.1	0.25	55.2	3.4	56.0	13.4	87.7	570.3
0.0088	3.9	0.06	56.2	2.2	43.4	27.7	-616.7	1968.8
0.0088	13.6	0.24	56.2	7.6	56.5	30.5	72.3	1371.1
0.0088	5.9	0.25	56.5	3.3	68.6	15.6	512.2	505.4
0.0092	12.8	0.12	59.3	7.6	47.7	48.8	-502.1	1493.7
0.0133	6.8	0.22	85.0	5.7	97.2	28.6	406.6	687.0
0.0136	1.7	0.26	87.0	1.4	87.6	5.3	103.6	145.6
0.0137	2.3	0.42	87.4	2.0	87.9	4.5	100.5	115.6
0.0138	1.3	0.54	88.6	1.1	90.0	2.0	127.2	46.3
0.0143	3.7	0.22	91.5	3.4	95.8	15.3	203.2	381.6

0.0144	10.7	0.87	92.4	9.8	97.4	11.4	220.7	138.7
--------	------	------	------	-----	------	------	-------	-------

0.0033	5.0	0.16	21.2	1.0	23.3	7.1	243.7	711.8
0.0033	5.4	0.21	21.5	1.2	31.9	7.9	907.5	512.3
0.0033	10.5	0.19	21.5	2.3	18.6	10.0	-348.7	1468.0
0.0034	4.5	0.12	21.7	1.0	18.6	6.6	-374.6	952.9
0.0034	4.0	0.22	21.8	0.9	26.8	4.9	501.1	402.0
0.0034	6.0	0.22	22.1	1.3	22.1	6.0	26.1	655.2
0.0034	5.1	0.20	22.2	1.1	23.2	6.0	136.4	606.5
0.0034	5.2	0.30	22.2	1.2	22.1	3.8	13.1	403.1
0.0035	5.1	0.30	22.2	1.1	23.6	3.9	165.7	376.0
0.0035	7.6	0.32	22.3	1.7	24.0	5.6	204.6	518.5
0.0035	3.7	0.12	22.3	0.8	23.0	7.0	92.5	744.9
0.0035	3.8	0.11	22.4	0.8	18.0	5.9	-533.2	897.5
0.0035	1.7	0.11	22.4	0.4	21.8	3.3	-43.5	374.1
0.0035	7.3	0.17	22.4	1.6	22.7	9.3	59.0	1013.4
0.0035	8.3	0.26	22.4	1.9	32.0	10.1	827.4	661.6
0.0035	2.4	0.09	22.5	0.5	19.8	5.1	-296.1	672.1
0.0035	3.4	0.09	22.5	0.8	19.0	7.4	-396.1	1059.1
0.0035	3.7	0.16	22.5	0.8	23.2	5.3	95.9	548.3
0.0035	3.3	0.11	22.5	0.7	24.2	7.2	196.7	710.6
0.0035	5.2	0.18	22.5	1.2	21.9	6.2	-42.5	697.9
0.0035	11.3	0.17	22.6	2.5	19.6	12.6	-333.1	1819.0
0.0035	3.9	0.18	22.6	0.9	26.0	5.5	353.3	482.0
0.0035	6.3	0.15	22.6	1.4	22.9	9.9	54.8	1071.6
0.0035	3.1	0.07	22.6	0.7	14.5	6.8	NA	NA
0.0035	6.5	0.27	22.6	1.5	23.9	5.7	149.7	555.5
0.0035	5.6	0.30	22.6	1.3	20.3	3.8	-244.7	458.3
0.0035	10.3	0.25	22.7	2.3	21.5	8.9	-109.8	1028.7
0.0035	5.0	0.30	22.7	1.1	22.2	3.7	-37.0	391.5
0.0035	6.5	0.17	22.8	1.5	22.0	8.1	-56.8	912.8
0.0035	4.5	0.26	22.8	1.0	22.8	3.9	26.5	404.8
0.0035	6.8	0.37	22.8	1.5	19.6	3.6	-361.3	444.8
0.0035	2.4	0.17	22.8	0.5	24.3	3.4	178.5	330.4
0.0035	3.5	0.23	22.8	0.8	27.2	4.1	434.1	333.5
0.0035	3.1	0.07	22.8	0.7	20.3	8.9	-268.9	1173.4
0.0035	5.2	0.24	22.8	1.2	20.4	4.4	-257.0	546.8
0.0036	4.5	0.35	22.9	1.0	27.3	3.4	432.5	267.6
0.0036	2.6	0.12	22.9	0.6	23.8	5.3	118.6	528.9
0.0036	4.9	0.15	22.9	1.1	27.5	8.7	450.4	717.4
0.0036	4.7	0.11	22.9	1.1	24.7	10.6	196.1	1050.4
0.0036	5.1	0.12	23.0	1.2	15.3	6.6	-1076.4	1349.1
0.0036	7.0	0.23	23.0	1.6	25.4	7.8	263.4	713.5
0.0036	3.8	0.13	23.0	0.9	23.2	6.9	40.5	732.5
0.0036	4.3	0.24	23.0	1.0	24.1	4.3	132.6	412.6
0.0036	9.9	0.37	23.1	2.3	20.9	5.5	-221.9	628.4

0.0036	4.3	0.19	23.1	1.0	24.5	5.4	167.7	515.3
0.0036	3.5	0.14	23.2	0.8	23.3	5.9	38.5	619.9
0.0036	4.4	0.13	23.3	1.0	19.3	6.6	-457.3	924.7
0.0036	3.8	0.13	23.3	0.9	21.5	6.4	-182.4	754.3
0.0036	6.2	0.33	23.4	1.4	25.7	4.7	250.5	401.0
0.0037	5.0	0.16	23.5	1.2	20.0	6.2	-380.6	816.5
0.0037	7.6	0.44	23.5	1.8	25.1	4.3	178.9	364.5
0.0037	4.7	0.13	23.5	1.1	25.9	9.2	250.7	847.8
0.0037	4.2	0.12	23.5	1.0	22.7	8.2	-68.6	919.8
0.0037	6.8	0.34	23.6	1.6	31.7	6.2	698.5	398.9
0.0037	5.2	0.25	23.6	1.2	21.5	4.4	-202.7	511.1
0.0037	7.0	0.21	23.7	1.6	30.7	10.0	625.5	712.9
0.0038	4.8	0.13	24.3	1.2	29.7	10.9	487.3	841.9
0.0038	4.4	0.19	24.4	1.1	21.1	4.9	-337.3	604.0
0.0038	8.1	0.20	24.7	2.0	32.8	13.4	674.1	903.8
0.0038	6.5	0.16	24.7	1.6	38.6	15.4	1018.4	843.5
0.0038	6.4	0.05	24.8	1.5	74.6	90.4	2272.3	367.6
0.0039	6.0	0.21	25.2	1.5	39.1	11.1	1004.9	587.4
0.0039	3.2	0.19	25.3	0.8	27.1	4.5	189.4	383.5
0.0039	3.2	0.20	25.3	0.8	26.7	4.3	155.1	376.5
0.0065	2.6	0.11	42.0	1.1	47.8	10.7	347.4	520.9
0.0066	6.5	0.29	42.1	2.7	38.2	8.4	-199.7	545.3
0.0066	6.5	0.29	42.4	2.7	47.4	10.4	307.0	493.5
0.0067	2.9	0.25	43.2	1.2	48.1	5.4	298.5	253.1
0.0067	2.6	0.13	43.3	1.1	48.1	9.3	292.0	451.5
0.0068	3.0	0.16	43.4	1.3	41.1	7.7	-92.9	465.7
0.0068	2.0	0.22	43.6	0.9	41.6	3.6	-74.8	212.8
0.0068	1.2	0.10	43.6	0.5	42.6	5.0	-11.4	290.3
0.0068	3.5	0.07	43.6	1.5	37.4	19.3	-343.7	1438.3
0.0068	1.0	0.18	43.7	0.4	40.9	2.3	-116.8	136.7
0.0068	3.7	0.35	43.7	1.6	43.5	4.4	29.5	234.9
0.0068	2.0	0.17	43.9	0.9	47.8	5.6	250.2	271.8
0.0068	1.9	0.11	43.9	0.8	41.3	7.0	-108.0	426.4
0.0068	3.0	0.19	44.0	1.3	41.0	6.3	-129.8	382.5
0.0068	1.3	0.15	44.0	0.6	43.8	3.6	32.4	197.0
0.0068	1.6	0.19	44.0	0.7	43.1	3.5	-7.8	199.8
0.0069	2.1	0.19	44.1	0.9	44.2	4.7	52.8	255.9
0.0069	3.3	0.15	44.1	1.4	42.4	9.1	-51.7	531.3
0.0069	5.4	0.14	44.1	2.4	37.1	14.5	-396.5	1063.2
0.0069	1.8	0.17	44.2	0.8	45.9	4.6	137.0	240.0
0.0069	1.6	0.19	44.2	0.7	45.0	3.6	89.6	192.4
0.0069	3.0	0.21	44.2	1.3	48.9	6.7	284.3	317.3
0.0069	4.2	0.30	44.3	1.9	58.3	8.0	681.3	288.3
0.0069	3.6	0.19	44.3	1.6	41.9	7.8	-94.1	460.5
0.0069	2.0	0.26	44.4	0.9	45.3	3.5	95.2	182.3
0.0069	3.0	0.24	44.4	1.3	44.3	5.5	40.2	295.6
0.0069	7.6	0.54	44.6	3.4	50.5	6.9	341.1	266.9

0.0069	0.8	0.14	44.6	0.3	44.3	2.4	26.0	132.1
0.0070	2.7	0.18	44.6	1.2	43.4	6.3	-23.8	356.2
0.0070	1.8	0.12	44.9	0.8	47.7	7.3	187.1	363.6
0.0070	1.5	0.13	45.2	0.7	52.0	5.8	380.5	254.0
0.0070	3.8	0.16	45.2	1.7	48.6	11.5	218.8	560.9
0.0071	2.3	0.09	45.4	1.1	48.4	12.1	199.9	601.3
0.0077	4.2	0.18	49.6	2.1	48.7	11.4	6.2	576.6
0.0078	1.3	0.20	50.2	0.6	50.1	3.1	47.2	148.4
0.0080	9.8	0.05	51.2	5.0	112.4	227.8	1738.4	383.4
0.0131	3.3	0.11	84.1	2.8	67.5	19.3	-487.4	791.8
0.3582	5.2	1.00	1973.4	89.2	1935.1	45.6	1894.3	8.9

Best age	±	Conc
(Ma)	(Ma)	(%)

21.6	0.5	NA
45.8	1.2	NA
46.4	1.5	NA
47.2	1.1	NA
47.3	0.9	NA
47.4	1.8	NA
47.5	0.8	NA
47.5	1.4	NA
47.5	1.4	NA
47.6	1.3	NA
47.7	0.9	NA
47.8	0.7	NA
48.0	1.1	NA
48.1	1.8	NA
48.1	0.9	NA
48.1	0.8	NA
48.2	1.1	NA
48.2	0.9	NA
48.5	1.0	NA
48.6	1.1	NA
48.7	1.4	NA
48.7	1.0	NA
49.0	1.4	NA
49.1	1.2	NA
49.1	1.0	NA
49.1	1.0	NA
49.1	0.9	NA
49.2	0.9	NA
49.2	1.2	NA
49.2	1.5	NA
49.4	1.3	NA
49.4	1.2	NA
49.5	0.9	NA
49.5	0.8	NA
49.6	1.5	NA
49.7	1.1	NA
49.7	1.1	NA
49.8	1.3	NA
49.8	1.0	NA
49.9	1.4	NA

49.9	2.0	NA
50.0	0.9	NA
50.0	0.9	NA
50.1	1.0	NA
50.1	0.9	NA
50.2	0.8	NA
50.3	2.0	NA
50.4	1.2	NA
50.4	2.3	NA
50.5	1.2	NA
50.5	0.9	NA
50.6	1.8	NA
50.6	1.9	NA
50.9	1.2	NA
51.0	1.1	NA
51.1	0.8	NA
51.5	0.8	NA
51.6	1.2	NA
51.7	1.8	NA
51.8	1.1	NA
51.8	1.1	NA
51.8	0.9	NA
51.8	1.8	NA
52.0	1.3	NA
52.1	0.8	NA
52.3	1.1	NA
52.4	1.1	NA
52.5	1.3	NA
52.5	2.1	NA
53.4	1.0	NA
54.1	1.2	NA
55.0	0.7	NA
55.5	2.3	NA
56.6	2.2	NA
56.8	1.1	NA
57.4	1.4	NA
58.2	1.1	NA
58.3	1.2	NA
58.3	2.1	NA
59.1	0.8	NA
59.1	1.3	NA
59.3	1.1	NA
59.3	1.6	NA
59.5	1.3	NA
59.6	1.6	NA
59.7	1.8	NA
59.8	1.3	NA

59.9	1.1	NA
59.9	1.5	NA
60.0	1.4	NA
60.4	0.9	NA
60.6	1.1	NA
61.3	1.5	NA
61.5	1.5	NA
61.6	0.9	NA
61.8	1.5	NA
62.5	1.5	NA
62.9	1.6	NA
63.7	1.2	NA
64.7	2.4	NA
65.9	1.3	NA
66.4	1.3	NA
66.9	0.9	NA
68.1	1.2	NA
89.4	1.4	NA
91.7	2.6	NA
151.1	4.3	NA
157.0	4.5	NA
183.1	3.4	NA

23.2	0.4	NA
44.9	1.2	NA
45.4	1.0	NA
46.0	1.1	NA
46.8	0.8	NA
46.8	1.0	NA
46.9	0.7	NA
47.0	0.8	NA
47.0	0.8	NA
47.2	1.0	NA
47.3	1.0	NA
47.4	1.6	NA
47.7	1.2	NA
47.9	1.0	NA
48.0	1.2	NA
48.2	1.3	NA
48.2	1.8	NA
48.3	0.7	NA
48.3	1.3	NA
48.4	1.4	NA
48.4	1.8	NA
48.5	1.4	NA
48.5	1.1	NA

48.5	1.0	NA
48.6	1.1	NA
48.6	1.1	NA
48.7	1.2	NA
48.9	1.2	NA
48.9	1.1	NA
49.0	1.1	NA
49.1	1.1	NA
49.1	1.0	NA
49.1	1.1	NA
49.1	0.9	NA
49.2	1.1	NA
49.2	1.7	NA
49.2	0.8	NA
49.3	1.0	NA
49.3	1.4	NA
49.3	0.9	NA
49.3	1.0	NA
49.3	1.0	NA
49.3	1.1	NA
49.4	0.9	NA
49.4	1.0	NA
49.4	1.1	NA
49.5	1.0	NA
49.5	1.2	NA
49.7	0.9	NA
49.8	1.1	NA
49.8	1.0	NA
49.9	1.1	NA
50.0	0.9	NA
50.0	1.4	NA
50.1	0.9	NA
50.1	0.7	NA
50.1	1.4	NA
50.1	1.3	NA
50.2	1.1	NA
50.3	1.2	NA
50.4	1.2	NA
50.5	1.1	NA
50.5	1.5	NA
50.5	1.0	NA
50.6	1.5	NA
50.6	1.1	NA
50.6	1.0	NA
50.6	0.9	NA
50.9	1.0	NA
51.0	0.7	NA

51.1	1.2	NA
51.2	0.7	NA
51.3	0.8	NA
51.4	1.1	NA
51.8	1.1	NA
51.9	1.3	NA
52.2	0.9	NA
52.3	1.4	NA
52.3	0.8	NA
52.8	0.8	NA
52.8	1.1	NA
53.1	1.2	NA
53.4	0.8	NA
53.8	1.9	NA
55.9	0.9	NA
56.5	1.0	NA
56.7	1.4	NA
56.7	1.7	NA
62.6	3.7	NA
67.8	2.3	NA
71.3	1.7	NA
80.2	1.0	NA
83.4	2.6	NA
84.0	2.8	NA
84.4	1.8	NA
85.9	1.4	NA
86.1	1.9	NA
89.2	1.3	NA
89.3	1.8	NA
89.7	1.6	NA
89.7	1.8	NA
90.5	1.2	NA
91.8	2.1	NA
148.9	2.5	NA
156.7	1.7	NA
171.9	4.9	NA
174.6	4.1	NA

23.8	0.7	NA
44.0	0.8	NA
45.4	0.8	NA
46.0	1.1	NA
46.0	1.0	NA
46.4	1.5	NA
46.7	0.6	NA
46.7	0.9	NA

46.8	1.1	NA
47.1	0.9	NA
47.4	0.9	NA
47.8	1.2	NA
48.0	1.6	NA
48.1	1.4	NA
48.3	1.2	NA
48.3	0.9	NA
48.5	1.0	NA
48.8	0.8	NA
48.8	0.7	NA
48.9	1.1	NA
48.9	1.8	NA
49.0	1.2	NA
49.0	0.8	NA
49.1	1.1	NA
49.2	1.1	NA
49.2	2.1	NA
49.2	0.7	NA
49.2	0.8	NA
49.2	1.5	NA
49.5	1.0	NA
49.5	0.8	NA
49.6	1.4	NA
49.7	1.1	NA
49.7	0.8	NA
49.7	1.5	NA
49.7	0.7	NA
49.8	1.0	NA
49.9	2.3	NA
49.9	0.7	NA
49.9	1.3	NA
50.0	1.2	NA
50.0	1.1	NA
50.1	1.0	NA
50.1	1.4	NA
50.2	1.1	NA
50.3	1.5	NA
50.4	0.8	NA
50.5	0.8	NA
50.6	0.9	NA
50.6	1.1	NA
50.7	1.8	NA
50.7	1.4	NA
50.7	0.9	NA
50.8	1.3	NA
51.0	1.3	NA

51.1	1.2	NA
51.1	0.7	NA
51.3	1.6	NA
51.3	1.5	NA
51.3	1.0	NA
51.3	1.0	NA
51.3	0.9	NA
51.4	0.9	NA
51.6	0.8	NA
51.7	1.0	NA
51.7	1.0	NA
51.7	0.8	NA
51.8	1.0	NA
52.2	1.1	NA
52.3	1.6	NA
52.3	1.0	NA
52.5	0.8	NA
52.5	1.9	NA
52.6	1.9	NA
52.6	1.5	NA
52.7	1.2	NA
53.2	1.0	NA
53.4	0.8	NA
53.4	1.5	NA
53.7	1.7	NA
54.2	1.1	NA
55.0	0.9	NA
55.2	1.0	NA
55.2	1.2	NA
55.3	1.3	NA
55.9	1.1	NA
55.9	0.7	NA
59.8	1.6	NA
64.1	2.6	NA
64.9	4.4	NA
69.3	2.1	NA
82.2	1.5	NA
86.4	1.5	NA
87.4	2.3	NA
87.5	3.6	NA
88.6	1.6	NA
89.2	1.2	NA
89.3	1.0	NA
89.7	2.1	NA
90.9	1.9	NA
90.9	2.3	NA
91.5	1.8	NA

91.7	4.3	NA
91.8	1.5	NA
93.2	2.0	NA
96.6	3.9	NA
172.5	3.3	NA
173.4	4.1	NA
176.5	2.8	NA
177.3	5.1	NA

18.7	1.2	NA
20.7	0.7	NA
21.3	1.1	NA
21.5	0.9	NA
21.7	0.4	NA
21.7	0.5	NA
21.7	0.8	NA
21.9	0.4	NA
22.0	0.3	NA
22.0	0.4	NA
22.2	0.6	NA
22.2	0.4	NA
22.2	0.4	NA
22.3	0.4	NA
22.4	0.9	NA
22.5	0.5	NA
22.6	0.6	NA
22.6	0.4	NA
22.6	0.4	NA
22.7	0.5	NA
22.8	0.5	NA
22.8	0.4	NA
22.9	0.7	NA
22.9	0.7	NA
23.1	0.6	NA
23.1	0.3	NA
23.1	0.3	NA
23.1	0.4	NA
23.2	0.4	NA
23.3	0.7	NA
23.3	0.5	NA
23.3	0.4	NA
23.4	0.5	NA
23.5	0.5	NA
23.5	0.3	NA
23.6	0.7	NA
23.6	0.7	NA

23.6	0.8	NA
23.7	0.4	NA
23.8	0.8	NA
23.9	0.5	NA
24.2	0.5	NA
24.3	0.8	NA
24.6	0.5	NA
25.4	0.8	NA
25.6	0.9	NA
25.7	0.5	NA
25.9	0.4	NA
26.0	0.4	NA
29.2	2.9	NA
29.8	0.5	NA
30.9	0.4	NA
34.6	0.4	NA
43.5	0.9	NA
47.8	1.9	NA
47.9	1.1	NA
48.1	0.8	NA
48.1	1.6	NA
48.2	1.7	NA
48.4	1.0	NA
48.4	1.2	NA
48.5	1.4	NA
48.5	1.5	NA
48.6	1.1	NA
48.8	1.9	NA
48.8	1.3	NA
48.8	1.4	NA
48.9	1.7	NA
49.0	1.6	NA
49.0	1.4	NA
49.1	1.4	NA
49.2	1.6	NA
49.2	2.0	NA
49.3	1.5	NA
49.4	0.9	NA
49.5	1.3	NA
49.6	1.8	NA
49.6	1.4	NA
49.7	1.3	NA
49.7	1.0	NA
49.8	1.2	NA
49.8	1.1	NA
49.9	2.5	NA
49.9	1.2	NA

50.0	1.9	NA
50.0	0.9	NA
50.1	0.9	NA
50.3	1.0	NA
50.3	2.3	NA
50.5	1.5	NA
50.7	1.1	NA
50.8	0.9	NA
50.9	1.2	NA
52.0	1.1	NA
52.1	1.6	NA
52.1	1.8	NA
52.2	1.5	NA
52.7	1.7	NA
53.2	1.4	NA
55.0	2.2	NA
55.2	1.2	NA
57.9	1.9	NA
64.6	1.5	NA
68.1	1.7	NA
69.3	2.1	NA
495.3	12.5	97.8

29.9	1.3	NA
32.4	1.0	NA
45.8	1.1	NA
46.1	4.5	NA
46.1	6.3	NA
46.7	1.0	NA
47.8	4.3	NA
47.9	2.4	NA
48.6	3.1	NA
48.7	3.7	NA
49.0	1.6	NA
49.5	1.8	NA
49.9	8.8	NA
50.6	1.0	NA
50.8	1.9	NA
50.9	0.8	NA
52.1	2.6	NA
53.4	7.7	NA
53.8	1.4	NA
54.9	3.1	NA
56.0	3.7	NA
62.6	1.8	NA
78.0	5.6	NA

78.2	6.3	NA
78.9	7.4	NA
81.2	2.5	NA
81.4	8.7	NA
81.7	3.5	NA
81.9	1.6	NA
82.0	1.2	NA
82.1	7.8	NA
82.5	6.5	NA
82.6	2.7	NA
83.4	5.8	NA
83.9	4.5	NA
84.4	4.3	NA
84.4	6.3	NA
84.6	1.7	NA
84.9	1.9	NA
85.2	3.9	NA
85.7	7.2	NA
86.3	3.1	NA
86.4	2.7	NA
87.0	4.5	NA
87.1	4.8	NA
87.1	3.1	NA
87.8	3.5	NA
88.3	6.2	NA
88.5	0.9	NA
88.5	4.1	NA
88.6	1.9	NA
89.0	3.2	NA
89.2	3.9	NA
89.2	6.9	NA
89.2	6.1	NA
89.6	4.9	NA
90.0	1.5	NA
90.4	3.3	NA
90.5	11.7	NA
90.8	2.6	NA
92.3	4.3	NA
92.3	4.8	NA
92.4	4.2	NA
93.3	3.9	NA
93.5	2.1	NA
93.7	2.7	NA
93.7	3.9	NA
94.1	1.5	NA
95.1	3.8	NA
95.6	3.8	NA

100.4	3.4	NA
108.0	2.2	NA
109.1	2.3	NA
138.8	3.2	NA
180.5	14.8	NA
181.1	11.1	NA
182.2	3.4	NA
185.9	6.5	NA
185.9	8.4	NA
187.6	13.6	NA
192.2	1.2	NA
196.2	5.2	NA
199.3	4.1	NA
212.6	4.1	NA
216.3	5.4	NA
227.5	9.6	NA
290.7	10.4	NA
351.9	4.2	NA
352.4	7.8	NA
360.3	4.3	NA
362.7	3.9	NA
367.9	4.7	NA
368.9	9.1	NA
372.8	10.1	NA
381.0	9.5	NA
448.3	9.8	43.9
592.4	10.9	102.2
1172.1	4.2	100.4

31.6	1.0	NA
34.6	0.8	NA
38.2	0.5	NA
41.8	0.5	NA
45.3	6.0	NA
47.5	1.2	NA
47.5	2.8	NA
48.0	1.1	NA
49.0	2.2	NA
49.1	2.4	NA
49.3	2.2	NA
49.3	1.8	NA
49.3	1.7	NA
50.1	1.2	NA
50.3	2.0	NA
50.7	3.0	NA
51.1	0.7	NA

51.2	5.0	NA
51.4	1.4	NA
51.6	1.7	NA
51.8	1.1	NA
52.3	1.0	NA
52.6	3.3	NA
52.7	3.8	NA
53.5	3.8	NA
53.5	1.2	NA
54.0	2.0	NA
54.3	0.8	NA
54.3	1.0	NA
54.8	3.1	NA
55.0	1.8	NA
55.7	1.4	NA
56.2	1.9	NA
59.2	5.2	NA
61.0	3.3	NA
63.2	3.7	NA
65.0	4.5	NA
70.1	0.5	NA
72.9	3.7	NA
77.0	7.9	NA
78.7	1.0	NA
78.9	7.8	NA
80.0	6.3	NA
80.2	2.2	NA
82.0	7.8	NA
82.9	8.9	NA
83.1	8.5	NA
83.5	5.3	NA
84.8	1.3	NA
85.1	2.1	NA
85.3	2.5	NA
85.3	7.6	NA
85.4	4.2	NA
85.5	1.7	NA
85.7	2.7	NA
85.8	1.8	NA
86.0	8.4	NA
86.0	3.4	NA
86.2	2.9	NA
86.8	1.5	NA
87.0	1.3	NA
88.2	11.6	NA
88.2	1.6	NA
90.0	4.5	NA

90.4	4.1	NA
90.6	1.3	NA
91.1	3.0	NA
91.4	10.3	NA
92.3	6.6	NA
92.6	1.2	NA
93.0	2.0	NA
95.6	4.0	NA
97.6	5.5	NA
98.9	6.0	NA
100.2	3.2	NA
101.0	14.0	NA
102.9	3.3	NA
106.9	1.4	NA
107.6	2.9	NA
120.2	1.6	NA
181.1	7.1	NA
189.6	10.1	NA
191.2	2.5	NA
203.6	1.2	NA
203.7	3.5	NA
241.2	4.8	NA
380.0	5.1	NA
385.6	6.5	NA
1155.7	28.0	104.3
1162.8	135.8	98.5
1212.0	52.6	96.2
1593.7	28.3	85.5
2011.9	9.5	96.9
2143.6	8.8	97.4
3183.6	3.7	90.0

29.2	0.9	NA
29.3	2.7	NA
33.8	0.7	NA
34.5	4.3	NA
40.1	0.7	NA
40.4	0.4	NA
41.4	0.9	NA
41.8	0.5	NA
42.2	2.2	NA
42.7	0.7	NA
43.3	4.3	NA
44.2	0.8	NA
47.0	2.4	NA
47.4	5.5	NA

47.8	7.0	NA
48.1	1.0	NA
48.5	2.1	NA
49.0	2.5	NA
49.3	0.4	NA
49.3	5.7	NA
49.4	2.0	NA
49.4	1.9	NA
49.5	4.5	NA
49.6	3.3	NA
49.7	1.9	NA
49.7	1.7	NA
50.0	6.4	NA
50.5	3.3	NA
50.6	1.7	NA
50.6	1.7	NA
50.8	1.4	NA
51.1	1.7	NA
51.3	0.8	NA
51.4	1.3	NA
51.4	2.0	NA
51.4	3.2	NA
51.8	0.7	NA
51.9	1.4	NA
52.0	2.4	NA
52.6	0.8	NA
53.1	3.0	NA
54.8	2.9	NA
55.0	3.4	NA
55.9	0.9	NA
60.7	8.7	NA
61.3	2.0	NA
62.3	1.9	NA
66.1	3.2	NA
76.0	4.3	NA
79.1	9.6	NA
80.2	8.8	NA
81.7	6.6	NA
82.5	4.8	NA
82.7	3.3	NA
84.6	4.5	NA
85.2	9.5	NA
85.7	4.4	NA
85.9	4.8	NA
86.1	2.6	NA
86.4	1.3	NA
86.8	2.4	NA

87.2	8.1	NA
87.5	5.5	NA
87.5	1.6	NA
88.7	5.0	NA
88.9	3.7	NA
88.9	8.2	NA
89.1	3.2	NA
89.1	1.2	NA
89.2	6.1	NA
89.7	4.7	NA
90.0	4.4	NA
91.1	6.6	NA
93.1	1.6	NA
93.4	3.2	NA
94.1	3.6	NA
94.2	3.8	NA
94.3	3.3	NA
94.3	1.5	NA
94.5	4.0	NA
96.2	1.3	NA
97.2	2.9	NA
97.6	1.6	NA
100.2	2.0	NA
102.1	2.8	NA
130.0	3.0	NA
131.6	1.9	NA
149.2	1.3	NA
178.0	9.9	NA
178.8	6.2	NA
209.1	3.2	NA
212.7	5.8	NA
217.9	2.7	NA
345.3	2.4	NA
353.9	4.1	NA
356.7	5.6	NA
357.4	6.9	NA
365.0	2.4	NA
509.3	25.1	103.1
675.6	14.2	102.0
794.9	19.1	91.3
1507.6	29.4	88.2
2632.1	16.1	99.4

41.3	1.4	NA
41.7	6.5	NA
42.7	0.9	NA

42.7	0.8	NA
42.9	1.4	NA
42.9	0.7	NA
43.2	0.7	NA
44.6	1.2	NA
45.6	7.4	NA
46.2	5.1	NA
46.3	1.1	NA
46.4	3.8	NA
46.5	3.0	NA
46.6	5.6	NA
46.8	3.3	NA
47.2	3.7	NA
47.4	3.0	NA
47.5	4.8	NA
47.7	8.1	NA
47.7	2.7	NA
47.8	4.7	NA
47.8	6.4	NA
48.0	2.7	NA
48.0	1.6	NA
48.2	1.9	NA
48.2	3.7	NA
48.3	6.7	NA
48.3	5.4	NA
48.4	2.7	NA
48.8	3.6	NA
48.9	3.7	NA
49.0	6.6	NA
49.1	2.8	NA
49.1	4.3	NA
49.1	1.5	NA
49.3	2.5	NA
49.3	3.6	NA
49.5	1.8	NA
49.5	2.1	NA
49.5	1.1	NA
49.5	2.5	NA
49.6	1.7	NA
49.6	1.5	NA
49.6	2.0	NA
49.6	3.2	NA
49.7	4.8	NA
49.7	5.5	NA
49.8	4.0	NA
49.8	1.7	NA
49.9	1.1	NA

49.9	0.8	NA
49.9	2.3	NA
50.0	1.0	NA
50.0	6.9	NA
50.1	0.9	NA
50.1	1.3	NA
50.2	3.2	NA
50.2	2.5	NA
50.2	2.6	NA
50.3	3.6	NA
50.4	1.5	NA
50.5	2.3	NA
50.5	5.3	NA
50.5	4.0	NA
50.5	5.6	NA
50.5	4.1	NA
50.8	7.0	NA
50.8	4.8	NA
50.9	2.3	NA
51.2	7.5	NA
51.3	2.3	NA
51.5	1.1	NA
51.6	4.7	NA
51.8	1.6	NA
51.9	3.6	NA
52.0	4.0	NA
52.5	5.5	NA
52.6	1.9	NA
52.6	1.5	NA
53.2	6.8	NA
53.5	6.0	NA
53.6	7.7	NA
53.7	2.4	NA
54.1	3.1	NA
54.4	0.9	NA
54.7	9.1	NA
55.1	3.7	NA
55.2	3.4	NA
56.2	2.2	NA
56.2	7.6	NA
56.5	3.3	NA
59.3	7.6	NA
85.0	5.7	NA
87.0	1.4	NA
87.4	2.0	NA
88.6	1.1	NA
91.5	3.4	NA

92.4	9.8	NA
------	-----	----

21.2	1.0	NA
21.5	1.2	NA
21.5	2.3	NA
21.7	1.0	NA
21.8	0.9	NA
22.1	1.3	NA
22.2	1.1	NA
22.2	1.2	NA
22.2	1.1	NA
22.3	1.7	NA
22.3	0.8	NA
22.4	0.8	NA
22.4	0.4	NA
22.4	1.6	NA
22.4	1.9	NA
22.5	0.5	NA
22.5	0.8	NA
22.5	0.8	NA
22.5	0.7	NA
22.5	1.2	NA
22.6	2.5	NA
22.6	0.9	NA
22.6	1.4	NA
22.6	0.7	NA
22.6	1.5	NA
22.6	1.3	NA
22.7	2.3	NA
22.7	1.1	NA
22.8	1.5	NA
22.8	1.0	NA
22.8	1.5	NA
22.8	0.5	NA
22.8	0.8	NA
22.8	0.7	NA
22.8	1.2	NA
22.9	1.0	NA
22.9	0.6	NA
22.9	1.1	NA
22.9	1.1	NA
23.0	1.2	NA
23.0	1.6	NA
23.0	0.9	NA
23.0	1.0	NA
23.1	2.3	NA

23.1	1.0	NA
23.2	0.8	NA
23.3	1.0	NA
23.3	0.9	NA
23.4	1.4	NA
23.5	1.2	NA
23.5	1.8	NA
23.5	1.1	NA
23.5	1.0	NA
23.6	1.6	NA
23.6	1.2	NA
23.7	1.6	NA
24.3	1.2	NA
24.4	1.1	NA
24.7	2.0	NA
24.7	1.6	NA
24.8	1.5	NA
25.2	1.5	NA
25.3	0.8	NA
25.3	0.8	NA
42.0	1.1	NA
42.1	2.7	NA
42.4	2.7	NA
43.2	1.2	NA
43.3	1.1	NA
43.4	1.3	NA
43.6	0.9	NA
43.6	0.5	NA
43.6	1.5	NA
43.7	0.4	NA
43.7	1.6	NA
43.9	0.9	NA
43.9	0.8	NA
44.0	1.3	NA
44.0	0.6	NA
44.0	0.7	NA
44.1	0.9	NA
44.1	1.4	NA
44.1	2.4	NA
44.2	0.8	NA
44.2	0.7	NA
44.2	1.3	NA
44.3	1.9	NA
44.3	1.6	NA
44.4	0.9	NA
44.4	1.3	NA
44.6	3.4	NA

44.6	0.3	NA
44.6	1.2	NA
44.9	0.8	NA
45.2	0.7	NA
45.2	1.7	NA
45.4	1.1	NA
49.6	2.1	NA
50.2	0.6	NA
51.2	5.0	NA
84.1	2.8	NA
1894.3	8.9	104.2

Sample	206/238 Age (% 2-sigma)	206/207 Age (% 2-sigma)
1KS-408	0.9	1
1KS-754	1.4	1
2KS-188	1.1	0.8
3KS-105	1	0.9
1XK-10	1.1	0.8
1XK-313	1	0.7
2XK-47	0.9	0.9
1DK-19	1.4	not enough old grains
1DK-246	0.9	0.7

Section	Correction	Red Chert	Green Chert	Black Chert	Quartzite	Green Lithi	Brown SS	White SS	Red Sandst
1KS30	1KS30	0	0	0	0	0	0	0	0
1KS300	1KS300				5			4	
1KS670	1KS670								
3KS4	3KS4								
1YZ70	1YZ70	39	39	16	1			18	
1YZ120	1YZ120	40	25					23	
1YZ280	1YZ280	26	27		3			28	
1DK10	1DK10				3				
1DK210	1DK210				1	1			
1DK700	1DK700	16	10		3	14		5	
1XK260	1XK260	4	7	2	21				
1XK680	1XK680	50	11	7	12	10	14		

Serpentiniz	Limestone	Volcanic	Basalt	qtz vein	Granite	Siltstone	phyllite	Gabbro
	0	16		0	0	85	0	
		105				114		
		100						
		100						
		14					4	
		18						
	1	26		6				
	7	34		2		65		
	2	35		10		65		
2	1	30				2		
		50				12		
		20						

Sample ID	Qm	Qp	Qpt	Qss	Silt	K	P	
1KS-79	190	39	4				1	130
1KS-367	69	17	2					68
1KS-754	93	49					1	72
2KS-183	74	35					4	89
2KS-11	174	135			1			94
1YZ-34	146	74	1					15

Phyllite	Schist	Lv.Lath	Lv.microliti	Lv.felsic	Lv.vitric	Lv.mafic	Shale/mud	Chert
1			7	2	56			7
		8		115	118	7	4	32
				100	90	5	6	26
3	1	8		81	108		5	29
				13	20	1	1	4
1				12	149		7	27

Black Chert Musc	Chlorite	Biotite	Tourm	CaCO3	PRX	Serp	Chalcedony
	5		2			7	1
			3			1	3
		3	3		1		
	3					6	
	1	4	2				
1	5	7	2			3	

Other	Total	Comments Qt (qm+qp	Qt+c (Qt + F	L total	Qt+c norm: F Normaliz
	450	233	240	131	79 53.33333 29.11111
	450	88	120	68	254 27.14932 15.38462
1	450	142	168	73	209 37.33333 16.22222
4	450	109	138	93	210 31.29252 21.08844
	450	310	314	94	42 69.77778 20.88889
	450	221	248	15	186 55.23385 3.340757

Ltotal normalized	Qm	Lt	F	Qmnormal	F normalized	Lt normalized	Ls	
17.55556		190	86	131	46.68305	32.18673	21.13022	7
57.46606		69	294	68	16.00928	15.77726	68.21346	40
46.44444		93	235	73	23.19202	18.20449	58.60349	33
47.61905		74	248	93	17.83133	22.40964	59.75904	34
9.333333		174	46	94	55.41401	29.93631	14.64968	5
41.42539		146	214	15	38.93333	4	57.06667	35

Lv	Lm	Lm (norma Lv (normali Ls (normalized)		
65	6	7.692308	83.33333	8.974359
248	5	1.706485	84.64164	13.65188
195	0	0	85.52632	14.47368
197	4	1.702128	83.82979	14.46809
34	0	0	87.17949	12.82051
161	2	1.010101	81.31313	17.67677